2013

Polymer damage mitigation--predictive lifetime models of polymer insulation degradation and biorenewable thermosets through cationic polymerization for self-healing applications

Peter Raymond Hondred
Iowa State University

Polymer damage mitigation—predictive lifetime models of polymer insulation degradation and biorenewable thermosets through cationic polymerization for self-healing applications

by

Peter Raymond Hondred

A dissertation submitted to the graduate faculty

in partial fulfillment of the requirements for the degree of

DOCTOR OF PHILOSOPHY

Major: Materials Science and Engineering

Program of Study Committee:
Michael R. Kessler, Major Professor
Nicola Bowler
Mufit Akinc
Xiaoli Tan
Malika Jefferies-El

Iowa State University

Ames, Iowa

2013

TABLE OF CONTENTS

LIST OF TABLES

LIST OF FIGURES

ACKNOWLEDGEMENTS

I want to begin by thanking my major professor, Dr. Michael R. Kessler, for his guidance throughout my graduate studies. His technical expertise and his encouragement were extremely important to my success. I would also like to thank Dr. Nicola Bowler, Dr. Mufit Akinc, Dr. Malika Jefferies-EL, and Dr. Xiaoli Tan for serving on my advisory committee. A special thank you is to be given to Dr. Nicola Bowler and Dr. Sungho Yoon for their help and suggestions during the early stages of my research.

This thesis is composed of two research projects. The first project was supported by NASA and the second was supported by the NSF as well as by assistance from the NSF GK12 fellowship. The funding from these agencies was vital in development of this work as well as the testing/experiments involve herein. The wire insulation degradation work was funded under cooperative agreement NNX07AU54A. The biopolymers for self-healing applications were funded through Dr. Kessler's prestigious NSF Career Award.

I would like to thank Symbi, Iowa State's NSF GK12 program, for both their monetary support and for providing me with the opportunity to sharpen my communication skills while helping out with 8^{th} grade science classes. Additionally, I want to thank Tim Weida and Debbie Victor for welcoming me into their 8^{th} grade classes as well as providing support and encouragement. I would furthermore, like to thank the Meredith 8^{th} grade class of 2012 and the McCombs class of 2013 for allowing me to participate in their classrooms for a year. These experiences will leave a lasting impression with me as I look back at the fun and educational times we had.

I would additionally like to thank the graduate students, postdoctoral researchers, and undergraduate students from the Polymer Composite Research Group for helpful discussions, creative ideas, technical expertise, and their friendship. Dr. Prashanth Bad, Dr. Xia Sheng, Dr. Tim Mauldin, Eliseo De Leon, Danny Vennerberg, Mitch Rock, Amy Bauer, Tom Garrison among others helped made work both a productive and enjoyable experience. I would also like to thank Josh Heyer and Josh Mangler for their assistance during the summer months producing samples and running experiments.

Finally, I want to thank my lovely wife, Carissa, for her unwavering love, steadfast support, unyielding patience, and complete confidence in me throughout my academic career. Her love and encouragement along the way is more than I could ask for and as a small token of my appreciation for all she had done for me, I dedicate this thesis work to her.

ABSTRACT

Over the past 50 years, the industrial development and applications for polymers and polymer composites has become expansive [1]. However, as with any young technology, the techniques for predicting material damage and resolving material failure are in need of continued development and refinement. This thesis work takes two approaches to polymer damage mitigation—material lifetime prediction and spontaneous damage repair through self-healing while incorporating bio-renewable feedstock. First, material lifetime prediction offers the benefit of identifying and isolating material failures before the effects of damage results in catastrophic failure. Second, self-healing provides a systematic approach to repairing damaged polymer composites, specifically in applications where a hands-on approach or removing the part from service are not feasible.

With regard to lifetime prediction, we investigated three specific polymeric materials—polytetrafluoroethylene (PTFE), poly(ethylene-alt-tetrafluoroethylene) (ETFE), and Kapton. All three have been utilized extensively in the aerospace field as a wire insulation coating. Because of the vast amount of electrical wiring used in aerospace constructions and the potential for electrical and thermal failure, this work develops mathematical models for both the thermal degradation kinetics as well as a lifetime prediction model for electrothermal breakdown. Isoconversional kinetic methods, which plot activation energy as a function of the extent of degradation, present insight into the development each kinetic model. The models for PTFE, ETFE, and Kapton are one step,

[1] Osswald, T. A.; Menges, G. Materials Science of Polymers for Engineers. Cincinatti: Hanser Gardner, (2003) 16.

consecutive three-step, and competitive and consecutive five-step respectively. Statistical analysis shows that an n^{th} order autocatalytic reaction best defined the reaction kinetics for each polymer's degradation.

Self-healing polymers arrest crack propagation through the use of an imbedded adhesive that reacts when cracks form. This form of damage mitigation focuses on repairing damage before the damage causes a failure in the polymer's function. In this work, the healing agent (adhesive) is developed using bio-renewable oils instead of solely relying on petroleum based feedstocks. Several bio-renewable thermosetting polymers were successfully prepared from tung oil through cationic polymerization for the use as the healing agent in self-healing microencapsulated applications. Modifications to both the monomers in the resin and the catalyst for polymerization were made and the subsequent changes to mechanical, thermal, and structural properties were identified. Furthermore, compressive lap shear testing was used to confirm that the adhesive properties would be beneficial for self-healing applications. Finally, scanning electron microscopy of the crack plane was used to study the fracture mechanism of the crack.

CHAPTER 1: GENERAL INTRODUCTION

1.1 Introduction

While natural polymers—tree sap, tar, shellac, animal shells and horns—have been available throughout history, it was not until World War II that synthetic polymers and the subsequent polymer industry began to rapidly expand. Chemical modifications to natural polymers were occurring as early as late 1800s with such inventions as vulcanized rubber. In the early 1900s synthetic polymers and fibers such as Bakelite (1909) and Rayon (1911) were developed. However, World War II brought about a depletion of natural resources such as silk, wool, and latex which required the invention of synthetic materials such as nylon, polyethylene, acrylic, and many more polymers. Over the past 60 years, the polymer industry has continued to expand rapidly to provide products with applications in nearly every commercial field with a concurrent rapid infusion of synthetic polymers into everyday life. As a result, the need for understanding the process of polymer damage and mitigating it becomes imperative. The work described in this thesis investigates two main types of damage that are common in polymers—thermal degradation and mechanical stress cracking.

First, polymers are often susceptible to degradation (mechanical, structural, electrical, and other properties) due to elevated temperatures for extended periods of time. Through thermogravimetric analysis, a material's degradation, or mass loss, can be calculated as a function of temperature. Using this data, kinetic models can predict the degradation patterns for different thermal environments. Additionally, these kinetic models can be integrated with models of other physical changes such as electrical breakdown to build a comprehensive

lifetime prediction model based on multiple environmental variables. In this work, both thermal degradation via thermogravimetric analysis and electrical breakdown via dielectric rigidity analysis were investigated to provide kinetic models for thermal degradation and lifetime predictive models for aerospace wiring.

Second, polymers under external stimuli such as thermal cycling or mechanical loading often fail because of microcracking that propagates through the material ultimately leading to large cracks and structural failure. To prevent large cracks from causing material failure, a biomimetic concept called self-healing can be implemented to arrest microcrack growth in its infancy. Currently, the field of self-healing materials relies exclusively on encapsulated healing agents derived from petroleum products due to the stringent set of requirements for a successful healing agent. In this work, new biorenewable materials derived from tung oil are investigated as potential alternatives as the healing agent in self-healing applications. These tung oil based polymers have demonstrated the necessary good mechanical and adhesive properties while at the same time dramatically reducing the need for petroleum products.

1.2 Dissertation Organization

This work is organized into multiple main chapters, with each being a manuscript that has been published or is being prepared for submission to scholarly journals. Chapter 1 is a general introduction which provides the background and motivation associated with the work done in the subsequent chapters. Chapters 2 through 4 cover the work on thermal degradation. Chapter 2 involves thermogravimetric analysis of polytetrafluoroethylene

(PTFE) and poly(ethylene-alt-tetrafluoroethylene) (ETFE) to develop kinetic models representing thermal degradation of each polymer. This chapter covers the theory behind kinetic modeling and the governing differential equation for the rate of degradation. Furthermore, this chapter discusses how both isoconversional kinetics and model-based kinetics provide insight into the overall kinetic model. Chapter 3 covers thermal degradation kinetic modeling similar to Chapter 2, but the kinetic modeling is for a polyimide commercially known as Kapton. In addition, this chapter uses mass spectroscopy and FTIR to analyze off gasses of the thermal degradation of Kapton to look at the mechanisms for degradation as a validation of the kinetic model. Chapter 4 then builds on the kinetic model in Chapter 3 to offer a lifetime predictive model for Kapton under electrical and thermal loadings. This chapter then discusses the relationships between electrical life theory and thermogravimetric theory.

Chapters 5 and 6 cover the research on biorenewable materials derived from tung oil for the suitability of it being used as the healing agent in self-healing applications. Chapter 5 investigated the changes to the thermal, mechanical, and adhesive properties of tung oil based thermosets when varied with a tung oil methyl ester. This chapter also investigates crosslink density of the thermosets using NMR to determine the components incorporated into the three-dimensional network and with transmission electron microscopy to determine material morphology. Moreover, scanning electron microscopy shows the mode of failure for the tung oil thermosets when used as an adhesive. Chapter 6 discusses the use of various catalysts for the cationic polymerization of tung oil based thermosets. The various catalysts are rare earth triflates, salts formed out of the rare earth metals in the periodic table. This

chapter investigates the same material properties important to self-healing that are discussed in Chapter 5.

The last chapter in the dissertation, Chapter 7, provides conclusions that flow from the work previously discussed, while additionally offering recommendations for future research to pursue. Following Chapter 7, are Appendix A and B which discusses the educational work supported by the NSF GK12 fellowship. These appendices investigate the impact a graduate research student can have on eighth grade middle school science students. Appendix A evaluates knowledge gain by middle school students who participated in specific classroom demonstrations involving polymer science. The eighth grade students were assessed on their understanding of polymers prior to the demonstration and again afterwards to determine if they exhibited a significant improvement scientific knowledge and interest. Appendix B discusses the attitude of middle school students toward having a graduate research student in their classroom. Their attitudes were determined through small focus groups with students from the eighth grade classroom.

1.3 Thermal Degradation Kinetics and Lifetime Prediction Modeling of Wire Insulations

1.3.1 Motivation and Literature Review

Previous conventional wisdom that aerospace wire insulation failures such as cracks, fraying, and degradation are atypical and harmless has proven to be a costly liability exhibited in the tragic accidents of Swissair 111 (Nova Scotia, 1998) and TWA 800 (Long Island, NY 1996) [1]. These accidents have been attributed to damaged wiring insulation

caused by degradation, cracking, and fraying; a problem for many miles of wire buried deep within their structures. For example a single F18C/D contains 11 miles of wiring alone [2].

The accidents mentioned above focused the attention of several federal agencies on finding methods to locate aircraft wiring faults [3]. Simplistic solutions, i.e., visually inspecting wires, fail to adequately provide protection from insulation failure. A more difficult method, time domain reflectometry (TDR), has proven to accurately identify potential failure locations in wires, but has proven extremely difficult to use. TDR utilizes a short rise time pulse along the conductor and monitors for any reflections back to the source due to discontinuities in the wire [4-6].Another method, high voltage testing, has been shown to find very small faults but the high cost of the method is prohibitive and additionally it cannot be used on fueled aircrafts [4-6]. In an effort to find a practical solution, both economically and functionally, frequency domain reflectometry, mixed signal reflectometry, sequence time domain reflectometry, and capacitance sensors are all being pursued [7-12]. All these methods, while containing their own faults, have shown promise.

The vast amount of wire in each aerospace application necessitates an extremely time consuming inspection in order to investigate all the wires. To reduce the work load, this thesis offers insight into the degradation kinetics as well as the voltage breakdown lifetime prediction for common wire insulation. Once wires are characterized, targeted inspections can focus on troubled areas and offer a more effective inspection regime for the time allotted in each plane. With a better understanding of thermal degradation kinetics and voltage breakdown values, work has been done to use capacitive sensors for measuring complex permittivity of planar and cylindrical structures in an effort to isolate wire failures [13].

As the aerospace industry matures, hundreds of failures are being discovered in typical aircrafts. Consequently, it is imperative to understand the cause of the failures. However, despite the importance of understanding the mechanisms and kinetics of wire degradation under various thermal, environmental, and mechanical loadings, no systematic studies has been reported on the thermal degradation kinetics of typical wire insulation materials. Therefore, this work attempts to elucidate the kinetic models for degradation in several common polymers used in wire insulation and provide a connection to lifetime predictive models for voltage breakdown.

1.3.2 Theory

Chemical and physical changes in polymer systems, including but not limited to degradation, crystallization, and curing, are triggered by external stimuli such as the environment's temperature [14]. A major concern for polymer systems is the long term viability of the material and the magnitude of the degradation due to the thermal loads the system experiences. Trying to determine the degradation kinetics of the polymer system can be difficult since these changes often are not discrete and the mechanisms are complex and overlapping.

When modeling these chemical and physical changes, the governing differential equation has the following form:

$$\frac{dr}{dt} = K(T) \cdot f(r) \tag{1}$$

where dr/dt is the rate of chemical or physical change, $K(T)$ is the temperature-dependent rate constant, and $f(r)$ corresponds to the reaction model [15]. The temperature-dependent rate constant is commonly described by the Arrhenius equation:

$$K(T) = A \cdot e^{\frac{-E}{RT}} \tag{2}$$

where *R* is the universal gas constant, *E* is the activation energy, and *A* is a pre-exponential factor [16].

Under the governing equation above, thermal degradation, a solid-state transformation, can be written as the product of two functions, one part depending on temperature T and the other depending on the fraction transformed α:

$$\frac{d\alpha}{dt} = K(T) \cdot f(\alpha) \tag{3}$$

where α represents the degree of degradation [17].

Thermogravimetric analysis (TGA) measures the degree of degradation (as measured by mass loss) with respect to time (*t*) and temperature (*T*) [18]. The degree of degradation (α) can be defined as:

$$\alpha = f(t,T) = 1 - \frac{wt\%}{100} \tag{4}$$

where *wt%* is the relative mass obtained directly from the TG experiment.

When heating at a constant rate, the equation can be redefined to eliminate the time-dependence by dividing through the differential equation by the heating rate:

$$\frac{d\alpha}{dT} = \frac{A}{\beta} \cdot e^{\frac{-E}{RT}} \cdot f(\alpha) \tag{5}$$

where $\beta = dT/dt$ is the heating rate [19].

Derivative thermograms (DTG) and isoconversional analysis techniques, which provide information about how activation energy changes with the degree of degradation, provide the number of steps and elucidate the type of mechanism in the formulation of mathematical kinetic models of these insulation materials. The DTG provides insight into the minimum number of reaction steps. A Friedman analysis, which is the first step in the isoconversional method, contains information on the activation energy. This analysis can also indicate the speed of each reaction step—accelerated, normal, or retarded. Through the direction of the isoconversional method, the degradation kinetics for each insulation material was mathematically modeled and the fittings are presented below in Figure 1. Table 1, the model steps and statistical fit, show the variability and complexity in the degradation kinetics of PTFE, ETFE and Kapton.

During the onset of degradation, catastrophic failure due to subsequent short-circuiting of electrical wiring insulation may result. Therefore, it is our goal to correlate the degradation mechanism and model predictions to dielectric breakdown through life theory and TG theory as seen in the work by Toop [15]. Through the use of the TG model activation energies and the failure voltage, the weight loss life prediction can be correlated to the electrical breakdown voltage as seen in equation 5 [15]:

$$log\, T_f = \left(\frac{E_\alpha}{2.303R\theta}\right) + log\, \frac{E_\alpha p(x_f)}{\beta R} \tag{6}$$

where T_f is failure time, E_α is activation energy, R is the gas constant, θ is the absolute temperature, $p(x_f)$ is empirical correlation, and β is the heating rate.

1.3.3 Research Objective

In this work, thermal degradation characterization of typical aerospace wire insulations, PTFE, ETFE, and Kapton, involves scanning thermogravimetric analysis (TGA) in an oxygenated environment at multiple heating rates. Kinetic parameters used to characterize the degradation are determined from the scanning thermograms. Previous studies have documented the thermal decomposition of the plastics used [20-24]. Here, fluoropolymers and polyimides were investigated for their mass loss as a function of temperature both isothermally and dynamically. However, unlike previous studies, we utilize a systematic process to develop a kinetic model to describe the degradation process.

Two basic approaches exist to developing a kinetic model for thermal degradation—isoconversional kinetics and model based kinetics [25,26]. Advanced isoconversional kinetics, or model-free kinetics, are developed from the work of Friedman and Ozawa-Flynn-Wall and the concept hinges on the premise that the mechanism for degradation is not required [19,27]. Instead by varying the activation energy, the general governing equation can represent the unknown mechanism. Model based kinetics, however, intend to describe the process through a series of mechanisms each containing its own activation energy in the process [17]. In this work, we marry the two techniques by utilizing information gained by the isoconversional method to define the kinetic models.

After the kinetic models were developed for the aerospace wire insulation, this work investigated the use of integrating the kinetic model with voltage breakdown data to develop a lifetime predictive model for Kapton where both the voltage and temperature can be defined. This portion of the work followed the work done by D. Toop, who concluded that chemical and physical changes can both be represented by the same governing differential

equation and consequently combined to provide a single lifetime prediction for a given temperature and voltage [15]. It is our hope that these kinetic models and lifetime models will provide the necessary information for improving the safety of aerospace wires.

1.4 Biorenewable Polymers for Self-healing Application

1.4.1 Motivation

The field of polymer science is rapidly expanding at a time when the feedstock traditional used for high performance synthetic polymers is uncertain [28]. Petroleum reserves, a traditional fossil feedstock for synthetic polymers, are predicted to run dry in roughly 80 years and yet a viable replacement has not been fully realized [28]. With this uncertainty, new polymers from alternative and renewable feedstocks have significant potential to impact the economy and the environment.

Much research has gone into exploring the possibility of carbohydrates, starches, and proteins as replacement feedstocks. However, other potential feedstocks for producing high molecular weight polymers have not been studied nearly as extensively— such feedstocks would be fats and oils. Oils such as those from soybean are biodegradable and readily available in bulk quantities. Additionally, these vegetable oils are one of the most abundant and inexpensive renewable resources available [29,30]. With this notion, research by Larock and Kessler has shown that vegetable oils have a great potential for an alternative feedstock for polymerization [31,32]. The unsaturation in the vegetable oils offers target reaction sites for synthesis through cationic polymerization or ring opening metathesis by adding functional groups to the unsaturation [33-37]. These high molecular weight polymers have

mechanical properties that mirror petroleum based materials and therefore are an excellent alternative to traditional polymers [33].

While the field of renewable feedstocks for polymerization has grown rapidly in recent years, high performance polymers are still primarily developed from petroleum due to the stringent requirements for the bulk material properties. Unlike most renewable feedstocks, vegetable oils can provide the bulk material properties to substitute for petroleum. Additionally, the range of oils contain varying levels of unsaturation and consequently reactivity and crosslinking varies resulting in a large spread in material properties—important for a materials choice in applications.

In this work, the area of self-healing polymers is the focus. Self-healing application further pursue ways to minimize the polymer industry's impact on the environment by autonomously repairing damaged parts instead of fabricating replacement parts. Self-healing polymers, specifically the healing agent, have been almost exclusively developed from petroleum based materials due to the extensive requirements for a successful healing agent. Polymers from vegetable oils offer mechanical properties required for self-healing and would reduce the need for petroleum products in a technology almost exclusively based on fossil fuels. This work focuses on utilizing biorenewable feedstocks, vegetable oils, as the healing agent in self-healing applications and thereby compounding the benefits to the environment and the limited energy supply available.

1.4.2 Literature Review

Discussed below are the pathways for preparing thermosetting bio-polymer networks polymerized from agricultural oils as well as the results demonstrated from these systems. The oils, or triglyceride, contain three fatty acid connected together by a glycerin bond. Each fatty acid is composed of a carbon chain length of 16 to 18 carbons with a varying amount of carbon-carbon double bonds randomly located along the length of the chain. These polymers have been created using two reaction types, cationic and ring opening metathesis polymerization (ROMP), where the unsaturation in the oil is the targeted reaction site. The various fatty acids in common agricultural oils can be seen in Table 1-1.

Table 1-1. Fatty acids found in common agricultural oils.

Fatty acid	[#C: #DB*]	Canola	Corn	Linseed	Olive	Soybean	Tung	Fish
Palmitic	16:0	4.1	10.9	5.5	13.7	11.0	—	—
Stearic	18:0	1.8	2.0	3.5	2.5	4.0	4	—
Oleic	18:1	60.9	25.4	19.1	71.1	23.4	8	18.2
Linoleic	18:2	21.0	59.6	15.3	10.0	53.3	4	1.10
Linolenic	18:3	8.8	1.2	56.6	0.6	7.8	—	0.99
α-elaeostearic acid	—	—	—	—	—	—	84.0	—
Average #DB/triglyceride	—	3.9	4.5	6.6	2.8	4.6	7.5	3.6

*#C : number of carbon atoms in chain and #DB : number of double bonds in that chain

ROMP has proven a successful area of research in preparing rigid thermosets from modified vegetable oils. The first step involves modifying the unsaturation in the oils with ring strained molecules such as cyclopentadiene using a Diels-Alder reaction. This process

partially norbornenylizes the triglyceride. When using cyclopentadiene as the ring strained molecule, the product can be purchased from Cargill Inc. as Dilulin™ [38]. ROMP is not directly effective with unsaturation and therefore the unsaturation must first be norbornenylized to successfully polymerize the oils.

When mixed with various co-monomers, the ring strain in the norbornene groups reacts in the presence of the ROMP catalyst and creates a three dimensional cross-linked network. Kessler et al has shown renewable polymers based on Dilulin and other custom made monomers from agricultural oil have high modulus and glass transition temperatures [39-41]. In fact, increasing crosslinking density with a crosslinking agent (CL) has provided a glass transition temperature of 127 °C and a thermal stability up to 400 °C [41].

While ROMP materials from vegetable oils bring promise, thermosets from cationic polymerization have shown similar potential. Cationic polymerization is a chain growth polymerization process that requires a cationic initiator to transfer charge to the monomer to initiate growth. Often the initiator of choice is a Lewis acid such as boron trifluoride. A cationic polymerization process of a general vegetable oil with co-monomers initiated with a common Lewis acid can be seen in Figure 1-1.

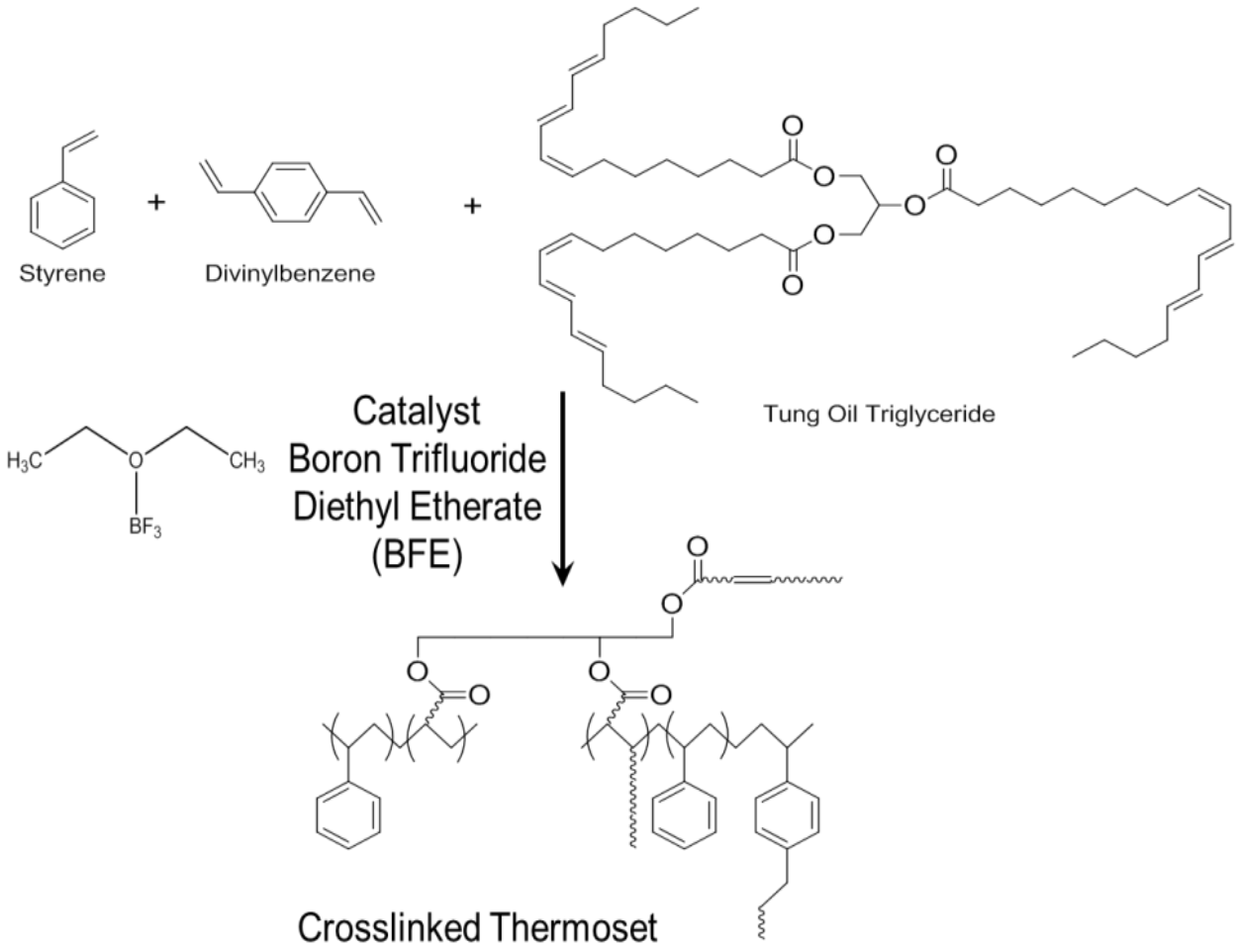

Figure 1-1. Crosslinked thermoset obtained throuch cationic polymerization of agricultural oil, styrene, and divinylbenzene

Material properties for various soybean oil blended with styrene and divinylbenzene obtain excellent room temperature modulus from 6×10^6 to 2×10^9 and glass transition temperatures from 0 to 105 °C [42-46]. Additionally, these materials have shown excellent dampening properties which would be beneficial for preventing failure due to vibration due to their segmental inhomogeneities during crosslinking [47,48].

By manipulating the ratio of co-monomers, oils and fillers, the degree of crosslinking and mechanical properties can be controlled. The extensive variation in fatty acids of agricultural oils offers a broad range of material properties which are tunable by modifying the composition of monomers. Recent formulas have provided biomaterials ranging from tough and ductile to very soft rubbers to very hard and brittle polymers.

This research interest is in self-healing applications; specifically, targeting a microencapsulation technique for self-healing applications [49]. Microencapsulation involves creating micron size capsules filled with liquid monomer. When a microcrack ruptures the capsules that are imbedded in the polymer matrix, the liquid monomer flows into the crack and reacts with a catalyst also imbedded in the polymer. The reaction creates a new polymer layer that acts as an adhesive to "glue" or "heal" the polymer back to its original structural integrity. This biomimetic concept is based on the way cuts heal in nature. When utilizing these polymers in self-healing applications, several stringent requirements are necessary. These requirements include but are not limited to: low viscosity, low volatility, good wetting properties, minimal diffusion through composite matrix, fast reaction kinetics, good adhesive strength, and good mechanical properties of the resulting polymer.

The first portion of these requirements—low viscosity, low volatility, good wetting properties, and minimal diffusion—highlight the need for the healing agent to quickly flow into the microcrack, to fill the microcrack and to stay in the microcrack until the polymerization process has taken place. The second portion of requirements—fast reaction kinetics, good adhesive strength, and good mechanical properties—are necessary to quickly and effectively repair the damaged polymer.

With regard to the first set of requirements, agricultural oils have several properties ideal for self-healing. First, these oils are have low volatility and are stable up to 300 °C in some cases [45]. Second, triglycerides are larger molecules and consequently do not easily diffuse in to other polymer matrices. The final two properties, viscosity and wettability, are easily addressed by blending with co-monomers. Whereas oils are known for higher viscosity and poor wettability, co-monomers exist with low viscosity and excellent wettability. They thus can provide a homogenous solution with uniform low viscosity and good wettability.

The next set of requirements to focus on are the polymerization properties of the healing agent and the material properties of the resulting polymer. Work on the cationic polymerization of soybean oil, styrene, and divinylbenzene has shown extremely fast reaction kinetics such that cure is achieved within two minutes [50]. As mentioned above, Kessler and Larock have shown that agricultural oils have shown good mechanical properties when polymerized. Additionally, the range of mechanical properties that these oils provide offers excellent opportunities to tailor the mechanical properties of the healing agent to closely mirror that of the polymer matrix for ideal compatibility between the two polymers. Given the benefits agricultural oils hold for self-healing and the added benefit of the rapid reaction kinetics from cationic polymerization, the marriage vegetable oils and self-healing applications has promise.

1.4.3 Research Objective

With the cationic polymerization of agricultural oils for the use as a healing agent in self-healing applications chosen, this work focuses on the bulk characterization of new

monomer blends. These blends will be tested for their physical, mechanical, and adhesive properties to validate further pursuit of self-healing applications.

The α-elaeostearic fatty acid is extremely reactive to cationic polymerization because the three unsaturated are conjugated and based on Table 1-1, tung oil is predominantly comprised of α-elaeostearic acid. Additionally, Larock has shown tung oil based polymers have fast reaction kinetics and good mechanical properties [51].

Two variations will be made to the polymers developed from tung oil. First, a methyl ester derived from the tung oil will be added as a co-monomer to vary the mechanical properties. The co-monomers include tung oil, tung oil methyl ester, styrene, and divinylbenzene. The methyl ester is substituted in for the tung oil to vary the final crosslink density and subsequent mechanical properties. This reaction will be run with a traditional Lewis acid catalyst, boron trifluoride diethyl etherate. Since most Lewis acids are susceptible to moisture in the air, the initiator requires a constant inert environment—which is difficult for processing. With this constraint in mind, the second variation is with the initiator. A series of rare earth triflates are investigated as potential initiators that would ease processing because these triflates are not air sensitive like most Lewis acids. A series of triflates will be used to polymerize tung oil based thermosets and their resulting thermo-mechanical properties are compared.

In all cases, the thermo-mechanical properties of the resulting polymers will be tested through thermogravimetric analysis and dynamic mechanical analysis. Variations in glass transition temperature, thermal stability, and crosslink density is analyzed based on the changes to the monomer composition. The thermosets will be tested in compressive lapshear

to determine the adhesive properties of the material. Further analysis of the fracture surface through scanning electron microscope will elucidate the mechanism of failure.

1.5 References

[1] Furse, C.; Haupt, R. Down to the wire. IEEE Spectrum. February 2001. 34-39.

[2] Furse, C. et al. "A critical comparison of reflectometry methods for location of wiring faults." Smart Structures and Systems, vol 2. No. 1 (2006) 25-46

[3] NSTC, "Review of federal programs for wire system safety," White house report. Nov. 2000

[4] Waddoups, B. "Analysis of reflectometry for detection of chafed aircraft wiring insulation", MS Thesis, Utah State University, Logan, Utah. 2001

[5] Schmidt, M. "Use of TDR for cable testing", MS Thesis, Utah State University, Logan, Utah. 2002

[6] Jani, A. "Location of small frays using TDR," MS Thesis, Utah State University, Logan, Utah, 2003

[7] Furse, C. et al. "Frequency domain reflectometry for on board testing of aging aircraft wiring," IEEE Transactions Electromagnetic Compatibility, 306-315, May 2003

[8] Chung, Y. C. et al. "Application of phase detection frequency domain reflectometry for locating faults in an F-18 flight control harness," IEEE Transactions Electromagnetic Compatibility. 47(2), 327-334. 2005

[9] Tsai, P.; Lo, C.; Chung, Y.C.; and Furse, C. "Mixed signal reflectometer for location of faults on aging wiring," IEEE Sensor Journal, 5(6), 1479-1482. 2005

[10] Furse, C.; Smith, P.; Safavi, M.; and Lo, C. “Feasibility of spread spectrum sensors for location of Arcs on live wires,” IEEE Sensors Journal, 5(6), 1445-1450. 2005

[11] Furse, C. et al. “Spread spectrum censors for critical fault location on live wire networks,” Journal of Structural Control Health Monitoring, 12(3/4), 257-267. 2005

[12] Chung, Y. C.; Amarnath, N.; Furse, C. “Capacitance and Inductance Sensors for Open and Short Ends Circuit Wire Faults Detection,” IEEE Transactions Instrument and Measurement 58(8), 2495-2502 (2009)

[13] Chen, T.; Bowler, N.; Bowler, J. “Analysis of Arc-Electrode Capacitive Sensors for Characterization of Dielectric Cylindrical Rods,” IEEE Transactions on Instrumentation and Measurement. Vol 61. No. 1, Jan. 2012.

[14] Vyazovkhin, S.; Sbirrazzuoli N. “Isoconversional Kinetic Analysis of Thermally Stimulated Processes in Polymers” Macromolecular Rapid Communications. Vol 27. No. 18. 1515-1532 (2006)

[15] D. Toop, IEEE Transactions on Electrical Insulation, 1971, 2–14.

[16] S. Vyazovkin. Kinetic concepts of thermally stimulated reactions in solids: a view from a historical perspective, International Review in Physical Chemistry 2000; 19(1):45-60.

[17] M.E. Brown, D. Dollimore, A.K. Galewey. Reactions in the Solid State, Comprehensive Chemical Kinetics, Vol. 22, Elsevier, Amsterdam.

[18] D. W. Levi, L. Reich, H.T. Lee. Degradation of Polymers by Thermal Gravimetric Techniques, Polymer Engineering and Science 1965, 5(3):135-141.

[19] H. L. Friedman, Kinetics of thermal degradation of char-forming plastics from thermogravimetry. J. Polym. Sci, Part C, Polymer Symposium (6PC), 183 (1964).

[20] B. Baker Jr. and D. Kasprzak, Thermal degradation of commercial fluoropolymers in air, Polymer Degradation and Stability, 1993, Vol 42, 181-188.

[21] A. Prasad and R. Singh, Thermal decomposition kinetics of a commercial fluoropolymer, Materials Research Bulletin, 1995, Vol 30, 1407-1412.

[22] H. Schild, Application of TGA/FTIR to the thermal degradation mechanism of tetrafluoroethylene–propylene copolymers, J. Polymer Science: Part A, 1993, Vol 31, 1629-1632.

[23] R. A. Dine-Hart, D.B.V. Parker, and W.W. Wright, "Oxidative Degradation of a Polyimide Film", Brit. Polym. J., Vol. 3, pp. 222-236, 1971.

[24] A. C. Lua, and J. Su, "Isothermal and non-isothermal pyrolysis kinetics of Kapton® polyimide", Polym. Degrad. Stab., Vol. 91, pp. 144-153, 2006.

[25] S. Vyazovkin, J. Comp. Chem. 2001, 22, 179.

[26] M.E. Brown, D. Dollimore, A.K. Galewey. Reactions in the Solid State, Comprehensive Chemical Kinetics, Vol. 22, Elsevier, Amsterdam.

[27] T. J. Ozawa, J. Therm. Anal. 1970, 2, 301; J. H. Flynn, Thermochim. Acta 1997, 300, 83.

[28] Chiellini, E.; Cinelli, P.; Corti, A. "Developments and Future Trends For Environmentally Degradable Plastics," in Renewable Resources and Renewable Energy: A Global Challenge. Edited by Graziani, M; Fornasiero, P. Boca Raton, FL: CRC Press (2007) 63.

[29] M. A. R. Meier, J. O. Metzger, U. S. Schubert, Chem. Soc. Rev. 2007, 36, 1788.

[30] E. W. Eckey, ‘‘Vegetable Fats and Oils’’, ACS Monograph Series, Reinhold Publishing Co., New York 1954

[31] Larock, R. C.; Li, F. Thermosetting Polymers from Cationic Copolymerization of Tung Oil: Synthesis and Characterization, J. Appl. Polym. Sci. 2000, 78, 1044.

[32] D. D. Andjelkovic, Y. Lu, M. R. Kessler, R. C. Larock: Novel Rubbers from Cationic Copolymerization of Soybean Oils and Dicyclopentadiene. II. Mechanical and Damping Properties, Macromolecular Materials and Engineering. 2009; 294, 472-483

[33] Larock, R. C.; Li, F. “Thermosetting Polymers from Cationic Copolymerization of Tung Oil: Synthesis and Characterization,” J. Appl. Polym. Sci. 2000, 78, 1044.

[34] Li, F.; Perrenoud, A.; Larock, R. C. “Thermophysical and Mechanical Properties of Novel Polymers Prepared by the Cationic Copolymerization of Fish Oils, Styrene and Divinylbenzene,” Polymer 2001, 42, 10133.

[35] Li, F.; Hasjim, J.; Larock, R. C. “Synthesis, Structure, Thermophysical and Mechanical Properties of New Polymers Prepared by the Cationic Copolymerization of Corn Oil, Styrene and Divinylbenzene,” J. Appl. Polymer Sci. 2003, 90, 1830-1838.

[36] Henna, P.; Larock, R. C.; Kessler, M. “Fabrication and Properties of Vegetable Oil-Based Glass Fiber Composites by Ring Opening Metathesis Polymerization,” Macromol. Mater. Eng. 2008, 293, 979-990.

[37] Henna, P.; Larock, R. C.; Kessler, M. “Fabrication and Properties of Vegetable Oil-Based Glass Fiber Composites by Ring Opening Metathesis Polymerization,” Macromol. Mater. Eng. 2008, 293, 979-990.

[38] Chen, J.; Soucek, M. D.; Simonsick, W. J.; Cilikay, R. W. “Synthesis and Photopolymerization of Norbornyl Epoxidized Linseed Oil,” Polymer 43 (2002) 5379.

[39] Sheng, X.; Lee, J. K.; Kessler; M. R. “The Influence of Cross-link Density on the Properties of ROMP Thermosets,“ Polymer 50 (2009) 1264.

[40] Sheng, X.; Kessler, M. R.; Lee, J. K. “The Influence of Cross-linking Agents on Ring-Opening Metathesis Polymerized Thermosets,” J. Therm. Anal. Calor. 89 (2007) 459.

[41] Mauldin, T. C.; Haman, K.; Sheng, X.; Henna, P.; Larock, R. C.; Kessler, M. R. “Ring- Opening Metathesis Polymerization of a Modified Linseed Oil with Varying Levels of Crosslinking,“ J Polym, Sci. A1. 46 (2008) 6851.

[42] Li, F.; Larock, R. C. “New Soybean Oil-Styrene-Divinylbenzene Thermosetting Copolymers. II: Dynamic Mechanical Properties,” J. Polym. Sci., Part B: Polym. Phys. 38 (2000) 2721.

[43] Li, F.; Larock, R. C. “New Soybean Oil-Styrene-Divinylbenzene Thermosetting Copolymers. III. Tensile Stress- Strain Behavior,” J. Polym. Sci., Part B: Polym. Phys. 39 (2001) 60.

[44] Li, F.; Hanson, M.; Larock, R. C. “Soybean Oil-Divinylbenzene Thermosetting Polymers: Synthesis, Structure, Properties and their Relationships,” Polymer 42 (2001) 1567.

[45] Li, F.; Larock, R. C. “New Soybean Oil-Styrene-Divinylbenzene Thermosetting Copolymers. I. Synthesis and Characterization,” J. Appl. Polym. Sci. 80 (2001) 658.

[46] Li, F.; Larock, R. C. “New Soybean Oil-Styrene-Divinylbenzene Thermosetting Copolymers. VI. Time-Temperature-Transformation Cure Diagram and the Effect of Curing Conditions on the Thermosets Properties,” Polym. Int. 52 (2002) 126.

[47] Li, F.; Larock, R. C. “New Soybean Oil-Styrene-Divinylbenzene Thermosetting Polymers. IV. Good Damping Properties,” Polym. Adv. Tech. 13 (2002) 436.

[48] Lu, Y., Larock, R. C. “Novel Polymeric Materials from Vegetable Oils and Vinyl Monomers: Preparation, Properties, and Applications,” ChemSusChem 2 (2009) 136.

[49] T. C. Mauldin, M. R. Kessler : Self-healing Polymers and Composites, International Materials Reviews. 2010, 55(6), 317-346

[50] Badrinarayanan, P.; Lu, Y.; Larock, R. C.; Kessler, M. R. “Cure Characterization of Soybean Oil-Styrene-Divinylbenzene Thermosetting Copolymers,“ J. of Appl. Polym. Sci. 113 (2009) 1042.

[51] Li, F.; Larock, R. Thermosetting Polymers from Cationic Copolymerization of Tung Oil: Synthesis and Characterization. Journal of Applied Polymer Science. 78(5) 1044-1056. (2000)

CHAPTER 2: DEGRADATION KINETICS OF POLYTETRAFLUOROETHYLENE (PTFE) AND POLY(ETHYLENE-ALT-TETRAFLUOROETHYLENE) (ETFE)

A paper published in *High Performance Polymer*

Peter R. Hondred[1], Sungho Yoon[1, 2], Nicola Bowler[1], and Michael R. Kessler[1]*

2.1 Abstract

This paper studies the degradation kinetics of two fluorocarbon based polymers, polytetrafluoroethylene (PTFE) and poly(ethylene-alt-tetrafluoroethylene) (ETFE), commonly used in coatings, solid lubricants, and wiring insulation. During the onset of degradation, these polymers may fail in their desired function, with associated monetary or human cost. This work examines the degradation kinetics of PTFE and ETFE by applying thermogravimetric analysis. Results from an isoconversional method, where activation energy is represented as a function of the extent of degradation, are used to develop kinetic models describing their degradation. A statistical analysis to evaluate the accuracy and validity of the implemented kinetic models is presented and it is found that an nth-order, single-step autocatalytic reaction model best describes PTFE degradation whereas a consecutive three-step autocatalytic reaction model best describes degradation of ETFE.

2.2 Introduction

Fluoropolymers are often selected for particular applications because of their high thermal stability. These materials may degrade, however, under prolonged exposure to

extreme temperatures. In electrical insulation applications, degradation results in a vulnerability to dielectric breakdown and electrical failure. Catastrophic failures in aerospace equipment have been attributed to arc tracking and damaged insulation [1]. Likewise, coatings and solid lubricants release toxic chemicals when degraded at elevated temperatures. Cookware with non-stick coatings carry warnings never to heat up while empty, for this very reason [2].

PTFE, commercially known as Teflon®, is a high-performance thermoplastic polymer from tetrafluoroethylene. The specific structure of PTFE can be seen in Figure 2-1a. ETFE, commercially known as Tefzel®, is a high-performance thermoplastic copolymer from equal parts ethylene and tetrafluoroethylene, which is copolymerized so that an alternating structure is obtained [3]. The specific structure of ETFE can be seen in Figure 2-1b.

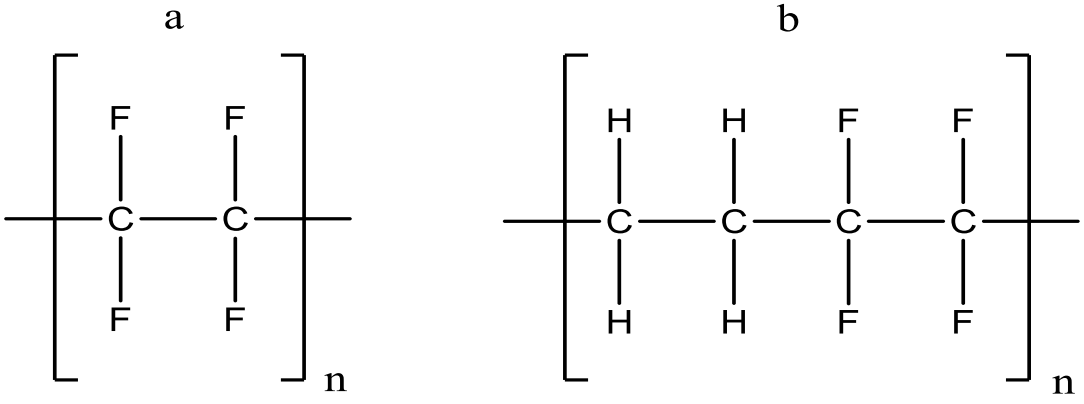

Figure 2-1. The chemical structure of (a) tetrafluoroethylene and (b) ethylene-tetrafluoroethylene.

PTFE and ETFE are versatile polymers used for many applications and, as a result, they have been studied extensively. Advanced thermal analysis techniques have been used to measure the transformation energetics, specific heat, thermal expansion, viscoelastic

properties, thermal diffusivity and thermal conductivity of PTFE [4]. In the case of ETFE, isothermal mass loss rate by thermogravimetric analysis (TGA) and differential scanning calorimetry (DSC) have been documented [5-7]. In addition, effects of thermal and electrical stress on the breakdown behavior of ETFE have been reported by Hammoud et al [1]. Accompanying the push to extend aircraft service life, there is a need to develop accurate and predictive kinetic models of polymer degradation with respect to its thermal history.

The most common tool for analyzing polymer degradation is TGA. TGA measures the degree of degradation (as indicated by mass loss) with respect to time (t) and temperature (T) [8]. The degree of degradation (α) can be defined as:

$$\alpha = f(t,T) = 1 - \frac{wt\%(t,T)}{100} \tag{1}$$

where $wt\%(t,T)$ is the instantaneous relative mass obtained directly from the TGA experiment.

TGA experiments capturing the polymer degradation at different heating rates provide data that can be used to obtain degradation kinetic parameters, such as activation energy, for various reaction models. In this work, PTFE and ETFE are analyzed by TGA conducted in air, to investigate their degradation in an oxidative environment. Friedman analysis and Ozawa-Flynn-Wall analysis are used to elucidate reaction types such as autocatalytic degradation. These analyses utilize isoconversional mass loss trend lines to calculate activation energy. The slopes of the trend lines provide insight into the reaction types. Several common reactions are compared, and a statistical evaluation provides a basis

for determining the quality of fit with the experimental data. In both PTFE and ETFE, autocatalytic reaction models fit the data best.

2.3 Materials & Preparation

PTFE polymer was purchased from DuPont under the product name Teflon® as sheets of 1 mm thickness. The PTFE samples were cleaned prior to experimental testing with a Kim Wipe and ethanol to remove any oils or dusts on the sample that might affect the weight and degradation of the material. Each test sample was punched from the purchased sheet using a circular punch, ensuring reproducible sample weight and shape. The PTFE samples were circular discs with diameter 3.5 ± 0.1 mm and mass 25 ± 2 mg.

The ETFE polymer was purchased from DuPont as Tefzel® Grade 750 for wire and cable applications. Tefzel Grade 750 is modified slightly in composition to provide an ETFE polymer with higher upper temperature capability for thermal stability and mechanical toughness to protect wires due to thermal exposure or mechanical wear [3]. Tefzel was received as small (2.5 mm) thermoplastic pellets. For testing, ETFE was injection-molded into 62.5 mm diameter × 1-mm-thick disks. To relieve residual stress that resulted from the injection molding process, the disks were annealed between two stainless steel plates at 60°C for 2 hours. The ETFE was cleaned and circular samples punched as described for PTFE. The ETFE sample masses were 8.7 ± 0.2 mg. To reduce sample-to-sample variability due to non-uniformity in the disk due to the injection molding process, all samples were punched from the third of the disk farthest from the injection point.

2.4 Methods

A thermogravimetric analyzer, model Q50 from TA Instruments (New Castle, DE), was used for the TGA experiments. Experiments on PTFE were conducted from room temperature to 700 °C at five different ramp rates: 2, 5, 10, 20 and 30 °Cmin^{-1}. Experiments on ETFE were conducted from room temperature to 600 °C at seven ramp rates: 0.5, 1, 2, 5, 10, 20 and 30 °Cmin^{-1}. Under the controlled environments of the TGA instrument, the samples were degraded in an air atmosphere using a balanced purge gas flow rate of 40 mL/min and a sample purge gas flow rate of 60 mL/min. Samples were placed on a platinum pan during the degradation process. Kinetic analysis was performed with the Netzsch Thermokinetics 2 program (version 2004.05) and standard statistical and plotting programs.

2.5 Kinetic Modeling

In degradation kinetics, the degree of degradation, equation (1), varies from 0 (no mass loss) to 1 (total mass loss). When modeling, the rate of degradation is assumed to depend separately on T and α, such that the governing differential equation has the following form:

$$\frac{d\alpha}{dt} = K(T)f(\alpha) \tag{2}$$

where $d\alpha/dt$ is the rate of degradation, $K(T)$ is the temperature-dependent rate constant, and $f(\alpha)$ corresponds to the reaction model [9]. In degradation kinetics, the Arrhenius equation describes the temperature-dependent rate constant by:

$$K(T) = Ae^{-E/RT} \tag{3}$$

where R is the universal gas constant, E is the activation energy, and A is a pre-exponential factor [10].

The time-dependence of the governing equation may be eliminated by heating at a constant rate, whereby equation (2) can be rewritten in the following temperature-dependent form:

$$\frac{d\alpha}{dT} = \frac{A}{\beta} e^{-E/RT} f(\alpha) \tag{4}$$

and $\beta = dT/dt$ is the heating rate [11].

The kinetic parameters (A and E) can be obtained by applying the the time-independent rate equation, through linear transformation, such that:

$$ln\left(\frac{d\alpha/_{dt}}{f(\alpha)}\right) = ln\left(\frac{A}{\beta}\right) - \frac{E}{RT}. \tag{5}$$

Equation (5) follows the linear form $y = a_0 + a_1 x$ (with $x = 1/T$) and optimal fit of the kinetic parameters is determined using multiple linear regressions.

In traditional chemical kinetics, the activation energy expressed in the Arrhenius equation is treated as a constant for a particular mechanism, being the minimum energy required for the reaction. On the other hand, a model-free isoconversional method allows for varying kinetic parameters by assuming both the activation energy and pre-exponential factor

are a function of the degree of degradation [12]. The differential isoconversional method, or Friedman's method, is a well-known technique that obtains the activation energy by plotting the logarithmic form of the rate equation for each heating rate:

$$ln\left[\beta_i\left(\frac{d\alpha}{dt}\right)_{\alpha,i}\right] = ln\left(A_\alpha f(\alpha)\right) - \frac{E_\alpha}{RT_{\alpha,i}} \quad (6)$$

where subscript α indicates a particular degree of degradation and i indicates a particular heating rate [12].

The activation energy at each degree of degradation is calculated with linear regression from a plot of $ln\left[\beta_i(d\alpha/dt)_{\alpha,i}\right]$ versus $1/T_{\alpha,i}$ across all of the heating rates tested. Similar to the Friedman method, kinetic parameters can also be calculated by the Ozawa-Flynn-Wall integral isoconversional method [13,14].

In a model fitting method, the differential equation assumes constant activation energy and pre-exponential factor [9]. By utilizing aspects of the model-free isoconversional method to glean additional information, improvements to the model fit approach can be realized.

Expanding the kinetic analysis from a single-step reaction to a consecutive multistep reaction, the differential equations are as follows:

$$\frac{da}{dt} = -f(a,b)A_1e^{-E_1/RT} \quad (7)$$

$$\frac{db}{dt} = -\frac{da}{dt} - f(b,c)A_2e^{-E_2/RT} \quad (8)$$

$$c = 1 - a - b = \alpha \tag{9}$$

where the reaction follows an A → B → C model [15]. The rate of reaction for the degradation from A → B (step 1) is given by da/dt. The rate of reaction for the degradation from B → C (step 2) is given by db/dt. In these equations, (7) to (9), a, b, and c represent concentrations in chemical kinetics and A, B and C represent degradation states where state A corresponds to $a = 1$, $b = 0$ and $c = 0$, state B corresponds to $a = 0$, $b = 1$ and $c = 0$, and state C corresponds to $a = 0$, $b = 0$ and $c = 1$. The degradation follows chemical kinetics, where step 2 follows step 1. As soon as the product of step 1 (denoted b) starts to form, however, step 2 may begin. Therefore, the product of one step can be used in the next step of the reaction before all the reactant in the first step is depleted.

2.6 Results and Discussion

Degradation was observed in TGA scans for PTFE and ETFE at relatively high temperatures; above approximately 450 and 350 °C, respectively, as shown in Figure 2-2. Like most fluoropolymers, both PTFE and ETFE are extremely stable at intermediate temperatures. The onset of degradation increases with increasing heating rate and involves a rapid and complete degradation. From the TGA curves, the variation between the temperatures of the degradation onset points provides insight into the reaction model. The uniform separation between the temperatures of the degradation onset points for the PTFE degradation curves, Figure 2-2a, is indicative of a single-step degradation process. For ETFE, Figure 2-2b, the separation between the temperatures of the degradation onset points

increases as the heating rate increases. This indicates a consecutive step reaction model, with more than one step. (On the other hand, a decreasing separation between the degradation onset points as the heating rate increases would indicate a competitive reaction model.)

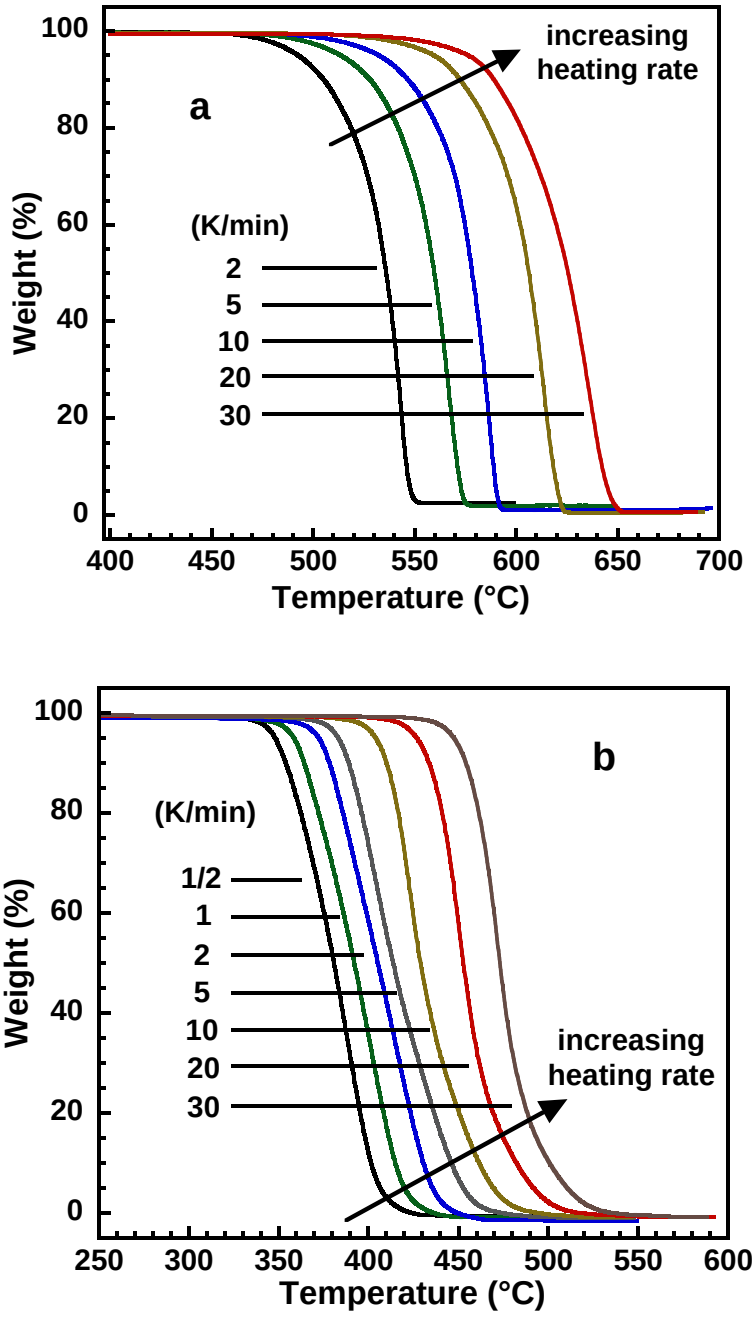

Figure 2-2. TGA curves for (a) PTFE and (b) ETFE at various heating rates.

The derivative of the weight with respect to temperature provides clearer insight into the mechanisms of degradation. For a specific heating rate, the number of peaks in the derivative thermogram (DTGA) represents the minimum number of reaction steps involved. By varying the heating rates, the degradation steps can be separated and isolated. Figure 2-3a shows the DTGA curves of PTFE. One dominant peak is observed for the five heating rates. A single-step reaction was analyzed based on the single dominant DTGA peak. A shoulder is present to the high-temperature side of the dominant peak in the DTGA data but exhibits negligible influence on the accuracy of fit of the single-step reaction model. Several two-step models (both competitive and consecutive) were tested, however, no significant improvement was found and often times, the modeled result fit worse than the single step reaction. For ETFE, it is clearly seen in Figure 2-3b at heating rate of 2 K/min that there are two distinct peaks. At slow heating rates, the reaction is dominated by a specific mechanism. As the heating rate increases, however, this dominant mechanism is replaced with an alternative mechanism which becomes dominant at higher heating rates. It can be deduced, therefore, that a minimum of two degradation steps exist in the degradation of ETFE.

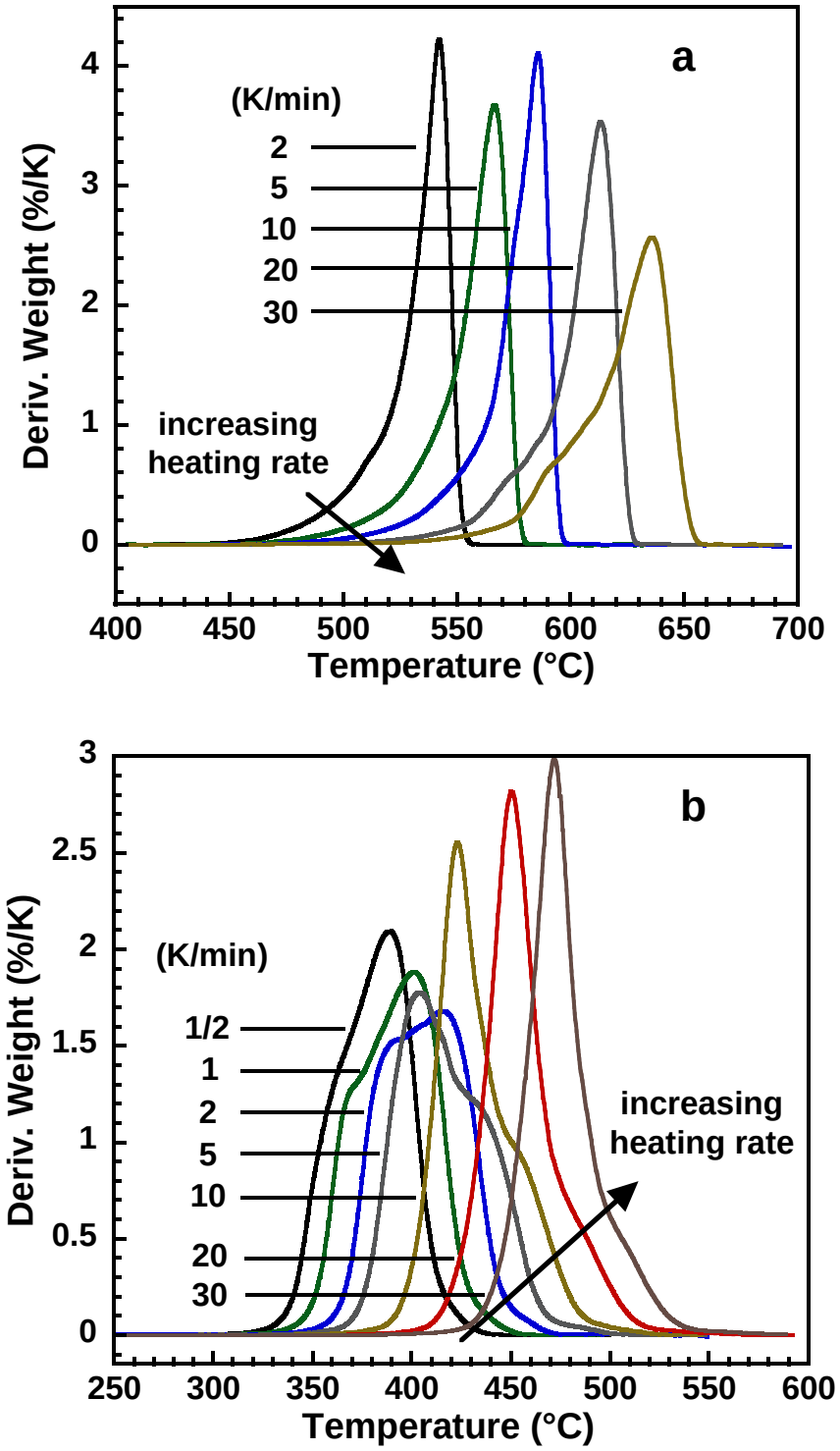

Figure 2-3. DTGA curves for (a) PTFE and (b) ETFE.

Building on the preliminary qualitative analysis of the thermograms made above, a Friedman analysis based on equation (6), shown in Figure 2-4, provides information about multi-step processes during the reaction and also offers insight into the type of reaction step. As for the DTGA plots, the number of peaks appearing in the plot indicates the minimum number of reaction steps occurring during degradation. For PTFE there is one dominant peak and for ETFE there are two overlapping peaks seen in Figure 2-4. Therefore a single-step reaction is again evident in the case of degradation of PTFE, and a multi-step reaction for ETFE.

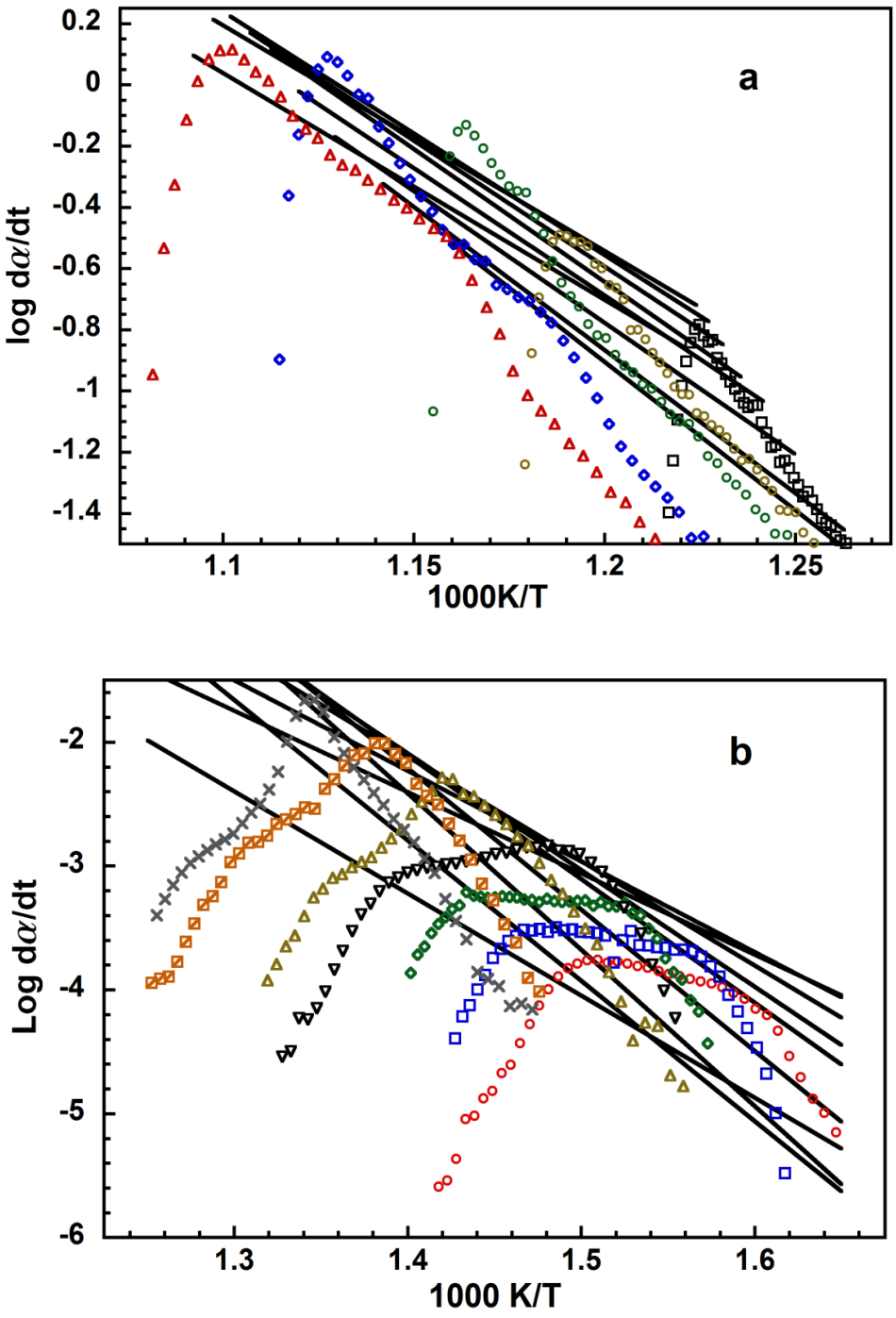

Figure 2-4. Friedman Analysis, equation 6, for (a) PTFE and (b) ETFE.

The type of the reaction can also be determined by comparing the slope of the constant fractional mass loss trend line to the slope of each peak at the beginning of the reaction step [16]. Comparing the slope of the fractional mass loss trend line to the slope of the constant heating rate data at each peak, specifically the linear portion to the low temperature (right) side of each peak, a reaction type can be identified. Comparing the relative magnitude of each negative slope defines the reaction type: normal, accelerated, and retarded. For both PTFE and ETFE, the first peaks all show acceleration as evidenced by the fact that the slope of the peak is steeper than the mass loss trend line. This is supposed due to autocatalysis. In the case of autocatalysis, the generic governing differential equation, presented in equation (2), should have reaction model, $f(\alpha)$, such that:

$$f(\alpha) = (1-\alpha)^n(1 + K_{cat}X)\ , \tag{9}$$

where n represents the reaction order, K_{cat} represents the autocatalysis constant, and X represents the step of the reaction [17].

From the Friedman analysis as well as the Ozawa-Flynn-Wall analysis, activation energy as a function of fractional mass loss can be obtained [12-14]. For the Friedman analysis, the activation energy is proportional to the slope of the isoconversional trendlines. Equation (6), from which the Friedman plot is built, has the general format of a line and the slope in that equation is a function of activation energy. Similarly, activation energy and pre-exponential factors can be calculated with Ozawa-Flynn-Wall analysis; however, this method requires the use of an integral approach as opposed to the derivative approach of the Friedman analysis. For PTFE, the plot of the activation energy with respect to the amount of

degradation, shown in Figure 2-5, again confirms the single-step autocatalytic reaction by presenting generally declining activation energy as mass loss increases. Activation energy developed from Friedman analysis presents activation energies declining from approximately 130 to 70 kJ/mol, as mass loss increases.

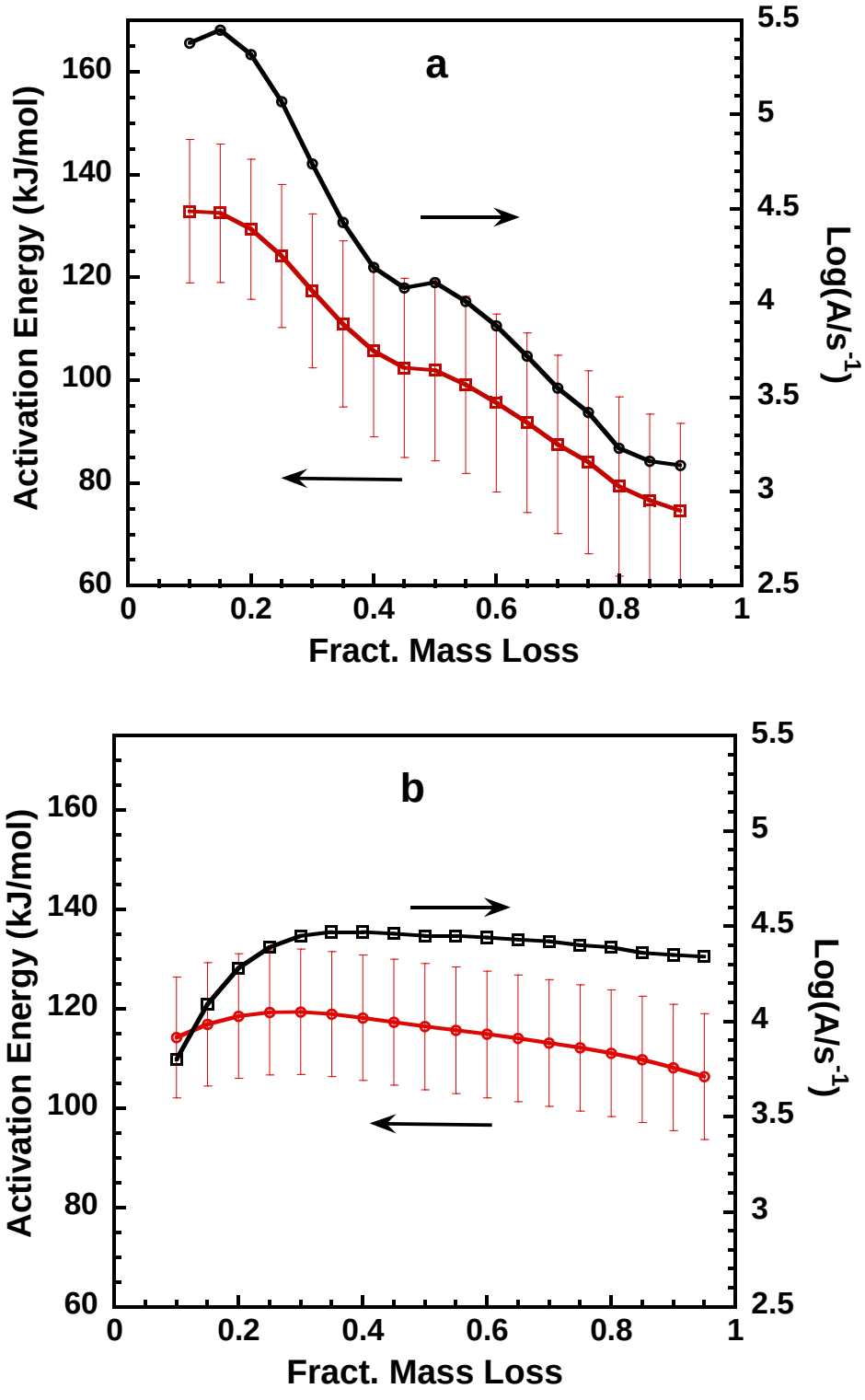

Figure 2-5. PTFE activation energy from (a) Friedman Analysis and (b) Ozawa-Flynn-Wall Analysis

The plot of the activation energy for ETFE with respect to the fractional mass loss confirms the hypothesized multistep reaction by displaying fluctuating activation energy, as shown in Figure 2-6. This characteristic indicates an overlap of multiple reactions. Activation energy developed from Friedman analysis presents activation energies between 140 kJ/mol and 210 kJ/mol.

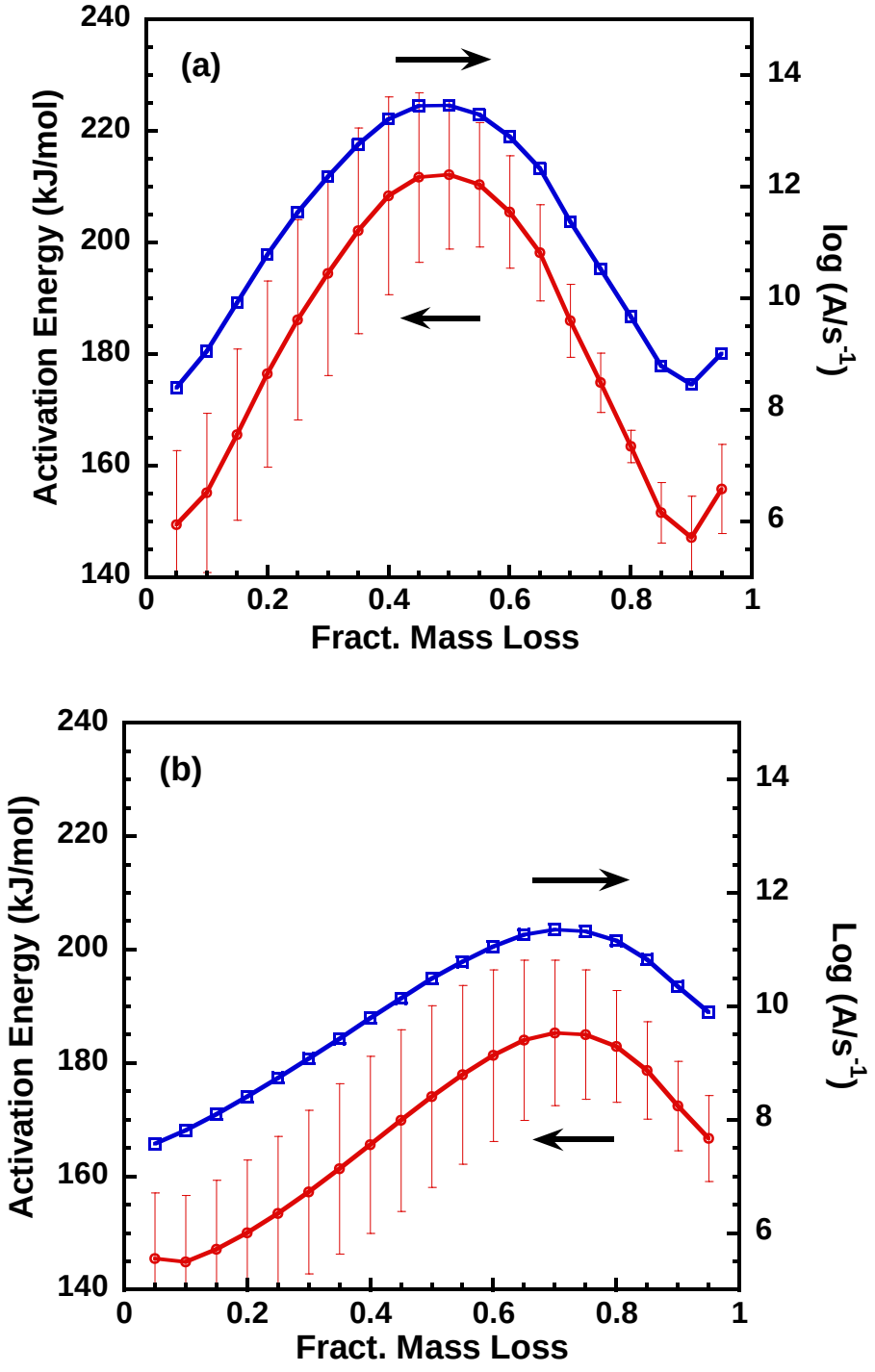

Figure 2-6. ETFE activation energy from (a) Friedman Analysis and (b) Ozawa-Flynn-Wall Analysis

2.7 PTFE Model

The TGA curves, DTGA curves, Friedman Analysis, and activation energies indicate that an nth order, single-step autocatalytic kinetic model is most appropriate to represent the thermal degradation of PTFE. Comparing the nth order, single-step autocatalytic reaction with other single-step reactions, an F-test shows that this reaction model fits the data best. See Table 2-1 for an F-test comparison and a schematic representation of the different models. The F-test is a statistical test used to compare models that have been fit to experimental data sets. The F-test identifies the best model fit of the population for which the data was sampled by testing the residual variances of the individual models against one another. The equation is as follows:

$$F_{exp}(f_1, f_r) = \frac{\sum_{j=1}^{S}\sum_{k=1}^{N_s}\left(Y_{jk}-\hat{Y}_{jk}(model_1)\right)^2 / f_1}{\sum_{j=1}^{S}\sum_{k=1}^{N_s}\left(Y_{jk}-\hat{Y}_{jk}(model_r)\right)^2 / f_r} \tag{10}$$

or:

$$F-test = \frac{lack-of-fit\ sum\ of\ squares/degrees\ of\ freedom}{pure-error\ sum\ of\ squares/degrees\ of\ freedom} \tag{11}$$

where f_1 is the degree of freedom for model 1 and f_r is the degree of freedom for the reference model. Typically the model with the lowest deviation, the best fit, is chosen as the reference model and, therefore, $F_{exp} = 1$ for that case. $F_{critical}$ is determined as the critical value from the F-distribution, for a confidence level of 95%. If F_{exp} is smaller than $F_{critical}$,

there is no statistical difference between models which satisfy that condition. If, however, F_{exp} is larger than $F_{critical}$ then there is a statistically significant difference in the ability of the models to describe the degradation curves.

Table 2-1. Comparative performance of various kinetic reaction models in describing thermal degradation of PTFE. $F_{critical}$ = 1.10. The n values for the nth order and nth order with autocatalysis are n = 0.83, 0.74 respectively.

Reaction Model	$f(\alpha)$	F_{exp}
First Order	$(1-\alpha)$	7.21
Second Order	$(1-\alpha)^2$	19.34
n^{th} Order	$(1-\alpha)^n$	1.17
n^{th} Order with Autocatalysis	$(1-\alpha)^n(1+K_{cat}X)$	1.0

The model fitted data and the kinetic parameters are plotted in Figure 2-7. Additionally other multistep reactions were tested in order to support this choice of an nth order, single-step autocatalytic reaction. In all cases, the models provided negligible improvement or in many cases decreased results.

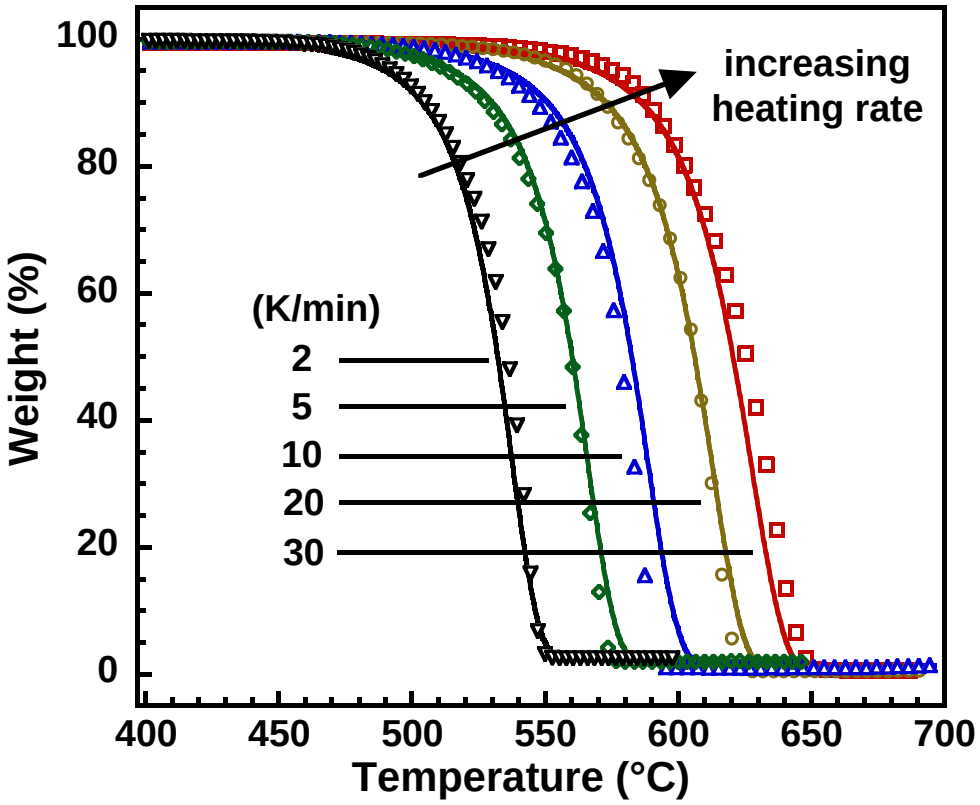

Figure 2-7. The best fit to TGA data for PTFE degradation in air, described by an nth-order, single-step autocatalytic reaction model. In the plot, the curves represent the model predictions and the symbols represent the experimental data. The activation energy is 169.0 kJ/mol, Log (A1/s^{-1}) is 7.25, reaction order is 0.74, and Log (Kcat) is 1.16.

2.8 ETFE Model

From analysis of the data for ETFE, a three-step consecutive model was deduced to be the most appropriate. The best three-step consecutive reaction model fit to the data is presented in Figure 2-8, with corresponding model parameters presented in Table 2-2. The activation energy for the first step in the final model is the same as the activation for the two-step fit of the slow thermograms. This means that the first step of the final model is the

deciding step for the initial part of the degradation reaction. The second step is a secondary process for that deciding step. This secondary process is responsible for large temperature separation of the degradation onset points at high heating rates in Figure 2-2b. This second step, a coupling step, should not be considered separately from the first step. The third step in the three-step consecutive model is responsible for the second DTGA peak, i.e. the final stage of the degradation process for both the slow and fast heating rates.

Comparing the three-step consecutive reaction to three-step competitive reactions, an F-test shows that the consecutive reaction fits the data better. Results of the F-test comparison and a schematic representation of the different models is given in Table 2-3.

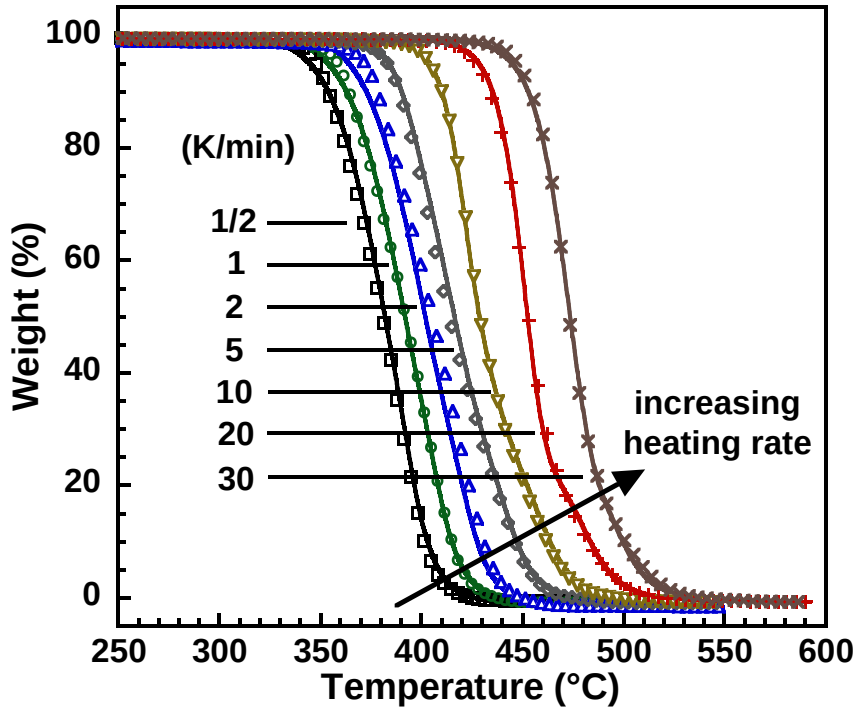

Figure 2-8. The best fit to TGA data for ETFE degradation in air, described by a consecutive three-step autocatalytic reaction model. In the plot, the curves represent the model predictions and the symbols represent the experimental data. The parameters for the model can be seen in Table 2-2.

Table 2-2. Reaction parameters describing a consecutive three-step autocatalytic reaction model for ETFE.

	Activation Energy (kJ/mol)	Log (A_1/s^{-1})	Reaction Order	Log (K_{cat})
Step 1	247.25	16.55	1.48	-0.59
Step 2	0.03	-3.50	0.74	2.34
Step 3	123.03	6.38	1.37	0.63

Table 2-3. Comparative performance of various kinetic reaction models in describing thermal degradation of ETFE. $F_{critical}$ = 1.02.

Consecutive Reaction	Competitive Reaction 1	Competitive Reaction 2	Competitive Reaction 3
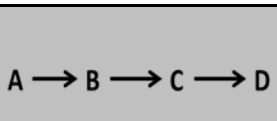	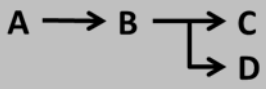	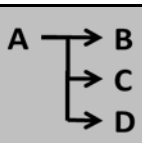	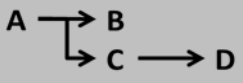
1.0	**1.78**	**11.69**	**57.24**

Finally, a two-step consecutive reaction model was applied to data for the two slowest and two fastest heating rates. The model fit of the slow heating rate DTGA revealed a poor fit at the end of the reaction and this difference between model and experimental data indicated the need for an additional step, again supporting the choice of a three-step model.

2.9 Conclusions

This work analyzes the degradation of PTFE and ETFE in an air environment by applying distinct reaction models. Kinetic models were developed through analysis of the TGA curves, the DTGA curves, the Friedman plot, and activation energies. For PTFE, an nth-order, single step autocatalytic reaction model was discovered to be most appropriate.

For ETFE, a consecutive three-step autocatalytic reaction model was designated. Additionally, the DTGA curves provide the required minimum modular steps for the reaction. For PTFE and ETFE the minimum steps were one and two steps, respectively. The Friedman analysis provided confirmation of the minimum reaction steps while further addressing the type of reaction rates, for which autocatalytic was shown appropriate for both materials. For PTFE, the statistical F-test shows enough information was collected to develop an accurate kinetic model. However, for ETFE a two-step model was not detailed enough to predict the entire degradation curve. By modeling the derivative of the slow heating rate, the deviation of the model at the final degradation step indicated need for an additional step as well as the lack of continuity between parameters for the slow heating rate model and the fast heating rate model. Consequently, a three-step consecutive reaction model with each step governed by an nth-order autocatalytic reaction model was chosen. The model, governed by autocatalysis, was compared to several multistep reaction models with competitive and consecutive steps to provide statistical confidence in the model fit.

2.10 Acknowledgements

This work was funded by NASA under cooperative agreement NNX07AU54A.

2.11 References

[1] C. Furse, R. Haupt. Down to the Wire. IEEE Spectrum, 2001. p. 34-39.

[2] Dupont. *Safety of Teflon non-sticks.* Retrieved September 14, 2011. http://www2.dupont.com/Teflon/en_US/products/safety/key_questions.html#

[3] Richard Arhart, DuPont employee, personal communications.

[4] J. Blumm, A Lindemann, M. Meyer, C. Strasser, Characterization of PTFE Using Advanced Thermal Analysis Technique, *International Journal of Thermophysics*, 2010, 1919-1927.

[5] B. Baker Jr. and D. Kasprzak, Thermal degradation of commercial fluoropolymers in air, Polymer Degradation and Stability, 1993, Vol 42, 181-188.

[6] A. Prasad and R. Singh, Thermal decomposition kinetics of a commercial fluoropolymer, Materials Research Bulletin, 1995, Vol 30, 1407-1412.

[7] H. Schild, Application of TGA/FTIR to the thermal degradation mechanism of tetrafluoroethylene–propylene copolymers, J. Polymer Science: Part A, 1993, Vol 31, 1629-1632.

[8] D. W. Levi, L. Reich, H.T. Lee. Degradation of Polymers by Thermal Gravimetric Techniques, Polymer Engineering and Science 1965, 5(3):135-141.

[9] M.E. Brown, D. Dollimore, A.K. Galewey. Reactions in the Solid State, Comprehensive Chemical Kinetics, Vol. 22, Elsevier, Amsterdam.

[10] S. Vyazovkin. Kinetic concepts of thermally stimulated reactions in solids: a view from a historical perspective, International Review in Physical Chemistry 2000; 19(1):45-60.

[11] H. L. Friedman, Kinetics of thermal degradation of char-forming plastics from thermogravimetry. J. Polym. Sci, Part C, Polymer Symposium (6PC), 183 (1964).

[12] H. Friedman. Kinetics of Thermal Degradation of Char-forming Plastics from Thermo-gravimetry. Applications to a Phenol Plastic. J Polym Sci 1963; 6C:183-195.

[13] T. Ozawa. A New Method of Analyzing Thermogravimetric Data, Bull Chem Soc Jpn 1965; 38(11):1881-1886.

[14] J.H. Flynn, L.A. Wall. General Treatment of the Thermogravimetry of Polymers. J Res Natl Bur Stand 1966; 70a(6):487-523.

[15] J. Opfermann and E. Kaisersberger, An advantageous variant of the Ozawa-Flynn-Wall analysis. Thermochim. Acta, 1992, Vol 203, 167-175.

[16] P. Hondred, S. Yoon, N. Bowler, E. Moukhina, M. Kessler. Degradation Kinetics of Polyimide Film. High Performance Polymers 2011, Vol 23 Number 4. 335-342

[17] Netzsch Thermokinetics (v. 2004.05) 2004. (Program Help).

CHAPTER 3: DEGRADATION KINETICS OF POLYIMIDE FILM

A paper published in *High Performance Polymer*

Peter R. Hondred[1], Sungho Yoon[1,2], Nicola Bowler[1], Elena Moukhina[3] and Michael R. Kessler[1]

3.1 Introduction

Kapton, a high performance polymer, is utilized in a wide variety of applications because of its exceptional material properties such as thermal stability and mechanical strength. Kapton is a commercially-available polyimide polymer developed by DuPont. It is the product of a condensation reaction from Pyromellitic Dianhydride and oxydianiline in Dimethylacetamide [1]. As a high performance polymer, Kapton film synthesis involves casting a heavily solvent-laden solution in a drum and pulling it through a low temperature oven to remove the solvent and then through a high temperature oven to convert the precursor film, polyamic acid, into the inert polyimide film. This technique is required because Kapton behaves like a thermoset in the sense that, once it is formed, it no longer can be melt-processed [1]. The fully formed Kapton does not have a melting point and once formed into the polyimide film remains as a film. The specific structure of Kapton is shown in Figure 3-1.

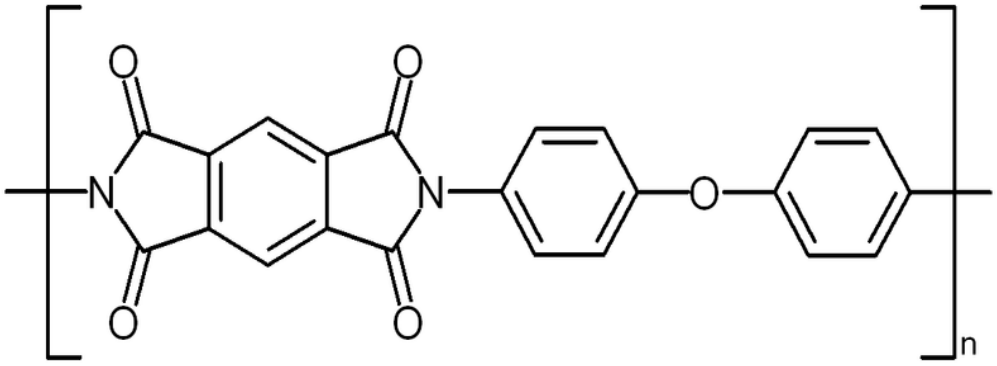

Figure 3-1. The chemical structure of Kapton

Kapton is a long-established polymer and consequently has been studied extensively, especially for aerospace applications. Thermal decomposition kinetics by thermogravimetry (TG), differential scanning calorimetry (DSC), and Dynamic Mechanical Analysis (DMA) have all been documented [2-5]. In addition, the effect of oxidative degradation on the crosslinking of Kapton has been reported by Dine-Hart et al. [6]. Likewise, Aik Chong Lua et al. investigated isothermal and non-isothermal pyrolysis of Kapton in nitrogen gas [7]. As the problem of degradation continues to plague Kapton and other polymers in aerospace wire insulation applications, there is a need to develop accurate and predictive kinetic models of the polymer degradation with respect to its thermal history.

The most common tool for analyzing polymer degradation is thermogravimetry (TG). TG measures the degree of degradation (as measured by mass loss) with respect to time (t) and temperature (T) [8]. The degree of degradation (α) for the case of total decomposition with zero rest mass can be defined as:

$$\alpha = f(t,T) = 1 - \frac{wt\%}{100} \tag{1}$$

where $wt\%$ is the relative mass obtained directly from the TG experiment.

TG experiments capturing the polymer degradation at different heating rates provide data that can be used to obtain degradation kinetic parameters, such as activation energy, for various reaction models. In this work, Kapton is analyzed by TG in an air environment to investigate the degradation in oxidative environments. Through the use of isoconversional kinetics, the advanced model mechanisms are identified. A mathematical model representing degradation is developed with an excellent statistical fit to the experimental TG data and is used to compare isothermal data. Finally, Fourier Transformed Infrared (FTIR) analysis and Mass Spectroscopy (MS) analysis of the exit gases identifies the breakdown components of Kapton to verify the complex degradation of Kapton.

3.2 Materials & Preparation

The Kapton polymer studied here was purchased from DuPont as Kapton HN thin film, 125-μm thick. It is a general purpose film recommended for applications that experience a wide range of temperatures while still maintaining an excellent balance of properties. Sample materials were stored in a desiccant dry box to reduce unwanted exposure to humidity. Each test sample was punched out of the film using a circular punch, 5 mm in diameter, ensuring reproducible sample weight and shape. The sample masses were 3.6 ± 0.5 mg.

3.3 Methods

A thermogravimetric analyzer, model Q50 from TA Instruments (New Castle, DE), was used for all of the TG experiments. The experiments were conducted from room temperature to 900 °C at five separate ramp rates: 2, 5, 10, 20, and 30 $Kmin^{-1}$. Under the controlled environment of the TG instrument, the samples were degraded in an air

atmosphere using a balanced purge gas flow rate of 40 mL/min and a sample purge gas flow rate of 60 mL/min. Samples were placed on a platinum pan during the degradation process. Kinetic analysis was performed with the Netzsch Thermokinetics 2 program (version 2004.05) and standard statistical and plotting programs. Further study was conducted through evolved gas analysis, a technique utilizing MS and FTIR on exit gases from the TG experiments, to verify the degradation breakdown components and paths.

3.4 Kinetic Modeling

In degradation kinetics, the degree of degradation (Eqn. 1) varies from 0 (no mass loss) to 1 (complete mass loss). When modeling, two separate functions are assumed; $K(T)$ and $f(\alpha)$, such that the governing differential equation has the following form:

$$\frac{d\alpha}{dt} = K(T)f(\alpha) \tag{2}$$

where $d\alpha/dt$ is the rate of degradation, $K(T)$ is the temperature-dependent rate constant, and $f(\alpha)$ corresponds to the reaction model [9]. The temperature-dependent rate constant is commonly described by the Arrhenius equation:

$$K(T) = A\, e^{-E/RT} \tag{3}$$

where R is the universal gas constant, E is the activation energy, and A is a pre-exponential factor [10].

When heating at a constant rate, Eqn. 2 can be redefined to eliminate the time-dependence by dividing through by the heating rate:

$$\frac{d\alpha}{dT} = \frac{A}{\beta} f(\alpha)\, e^{-E/RT} \tag{4}$$

where $\beta = dT/dt$ is the heating rate.

Through linear transformation, the kinetic parameters (A and E) can be obtained by the time-independent rate equation:

$$ln\left(\frac{d\alpha/_{dT}}{f(\alpha)}\right) = ln\left(\frac{A}{\beta}\right) - \frac{E}{RT} \quad (5)$$

Eqn. 5 follows the linear form $y = a_0 + a_1 x$ (with $x = 1/T$) and optimal fit of the kinetic parameters is determined using linear regression. By calculating these parameters through linear regression at several different mass losses, the variation in the kinetic parameters as a function mass loss is determined.

In one approach for kinetic degradation modeling, constant activation energy and pre-exponential factors are assumed [10]. The model-free isoconversional method allows for varying kinetic parameters by assuming both the activation energy and pre-exponential factor are a function of the degree of degradation [11]. Freidman's method, a well-known technique, obtains the activation energy by plotting the logarithmic form of the rate equation for each heating rate:

$$\ln\left[\beta_i \left(\frac{d\alpha}{dT}\right)_{\alpha,i}\right] = \ln\left(A_\alpha\, f(\alpha)\right) - \frac{E_\alpha}{RT_{\alpha,i}} \quad (6)$$

where the subscripts α and i represent the value at a particular degree of degradation and the data from the given heating rate experiment, respectively [12]. The activation energy at each degree of degradation is calculated with linear regression from a plot of $ln\left[\beta_i\,(d\alpha/dT)_{\alpha,i}\right]$ versus $1/T_{\alpha,i}$ across all of the heating rates tested. The Friedman plot not only provides confirmation of the multi-step processes during the reaction but also provides insight into the type of reaction steps. The type of reaction can be determined by comparing the slope of the constant fractional mass loss trend line to the slope of the constant heating rate data at each peak. The peak slope specifically refers to the slope of the linear portion to the right side of

each peak. Comparing the relative magnitude of each negative slope, three types of reactions are defined: normal, accelerated, and retarded. A normal reaction corresponds to slopes of equal magnitude in both the fractional mass loss trend line and the peak slope of the constant heating rate data—Figure 3-2(A). An accelerated reaction corresponds to a steeper peak slope in the constant heating rate data compared to the fractional mass loss trend line—Figure 3-2(B). A retarded reaction corresponds to a steeper fractional mass loss trend line compared to the peak slope in the constant heating rate data—Figure 3-2(C). Similar to the Friedman method, kinetic parameters can also be calculated by the Ozawa and Flynn-Wall integral isoconversional method [12,13].

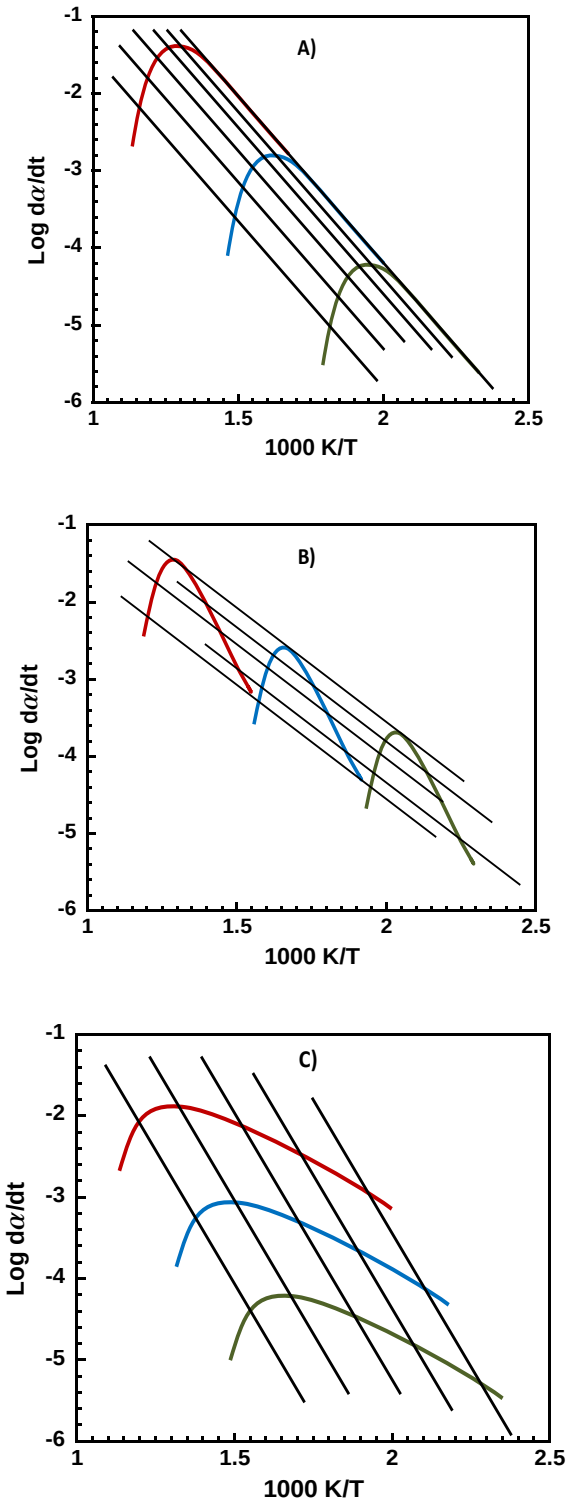

Figure 3-2. Friedman plot for a single step (A) normal reaction, (B) accelerated reaction, and (C) retarded reaction.

Expanding the kinetic analysis from a single-step reaction to a multistep reaction, the differential equations are separated based on each step of the reaction. The overall degree of degradation is constructed as follows:

$$\alpha = 1 - \sum_j w_j a_j \tag{7}$$

where α is the total fractional mass loss, a_j is fractional mass loss of a specific reaction step, w_j is the contribution of a specific reaction step into total mass loss, and j represents the given reaction step [14]. The sum of the contributions of all steps is equal to 1:

$$\sum_j w_j = 1 \tag{8}$$

Each fractional mass loss of a specific reaction step can be written as an individual differential equation modeling the degradation of the reaction step such as [14]:

$$\frac{d(a_j \rightarrow a_{j+1})}{dt} = A_j \, e^{-E_j/RT} \, f(a_j, a_{j+1}) \tag{9}$$

The rate of reaction for a degradation from A → B (step 1) is given by $d(a_1 \rightarrow a_2)/dt$. The rate of reaction for the degradation from B → C (step 2) is given by $d(a_2 \rightarrow a_3)/dt$. The rate of reaction for the degradation from C → D (step 3) is given by $d(a_3 \rightarrow a_4)/dt$. In this format of differential equations the values a_1, a_2, a_3 and a_4 are the formal concentrations of the formal substances A, B, C, and D. A is the educt, B is the product of the first step and educt for the second step, C is the product of the second step and the educt for the third step, and D is the product of the third step which is the final product of the whole process. Each value of a_i changes from 0 to 1. The initial state corresponds to a_1=1, a_2=0, a_3=0 and a_4=0, and final state D corresponds to a_1=a_2=a_3=0, and a_4=1. If the reaction steps are completely separated, then the intermediate state after the first step

corresponds to a_1=0, a_2=1 and a_3=a_4=0 and the intermediate state right after the second step corresponds to a_1=a_2=0, a_3=1 and a_4=0. The degradation continues to follow the analogy of chemical kinetics, where step 2 follows step 1, step 3 follows step 2, but may occur before complete conversion of A to B.

3.5 Results & Discussion

The TG scans for five different heating rates began at room temperature and the data can be seen in Figure 3-3. Like most polyimides, Kapton is extremely stable at intermediate temperatures [1]. The onset of degradation increases with increasing heating rate and involves a rapid and complete degradation. The derivative of the weight with respect to temperature provides better insight into the mechanism of degradation. For a specific heating rate, the number of peaks in the derivative thermograms (DTG) represents the minimum number of reaction steps involved. By varying the heating rates, the degradation steps can be separated and isolated. At higher heating rates, for Kapton, the reaction mechanisms can be separated for better kinetic model understanding. Figure 3-4 shows the DTG curves. The peaks of the DTG help to determine the reaction steps. Based on the DTG curves below, heating at 30 $K \cdot min^{-1}$, a minimum of three reaction steps, or three peaks, can be seen.

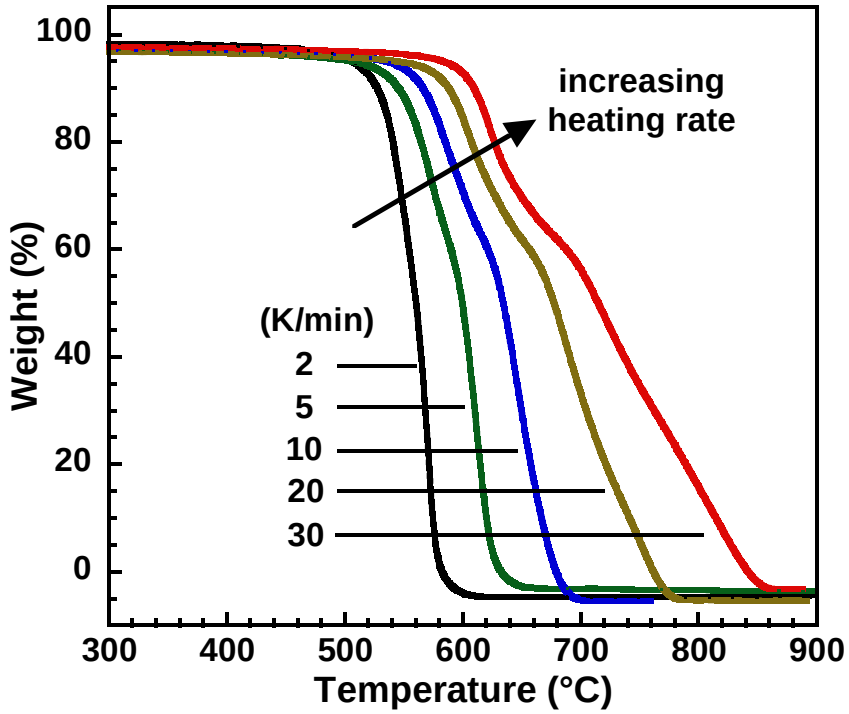

Figure 3-3. TG curves broaden as the rate increases from 2 to 30 K·min^{-1}.

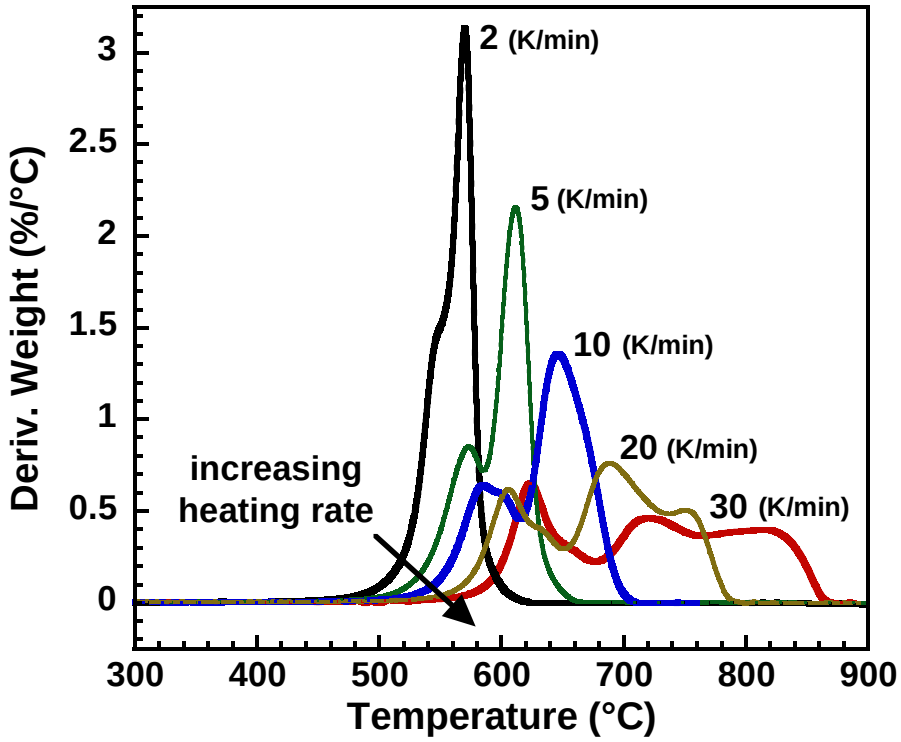

Figure 3-4. DTG curves for the data shown in Figure 3-3.

The Friedman plot for Kapton can be found in Figure 3-5. A multi-step reaction is again evident from the curvature of the plot. For each heating rate, there are separate reaction peaks. This indicates the probability of a multiple step reaction. Model-free analysis shows a complex process with three peaks for curves 30 $Kmin^{-1}$ and 20 $Kmin^{-1}$ and only two peaks for 2, 5, and 10 $Kmin^{-1}$. The fluctuation in the number of peaks indicates that the mechanism of the decomposition changes with heating rate. Furthermore, the type of reaction can be determined by comparing the fractional mass loss trend lines discussed previously with Figure 3-2. The fractional mass loss trend lines are the solid linear curves in Figure 3-5, and are found from linear regression at specific values of α ranging from 0.2 to 0.8. In all cases for Kapton, the peak slope is steeper than the fractional mass loss trend line indicating an accelerated reaction, probably autocatalysis. For autocatalysis, the generic governing differential equation, presented in Eqn. 2, defines the reaction model, $f(a_j)$, such that:

$$f(a_j) = (1 - a_j)^n (1 + K_{cat} a_j) \tag{10}$$

where n represents the reaction order and K_{cat} represents the autocatalysis constant.

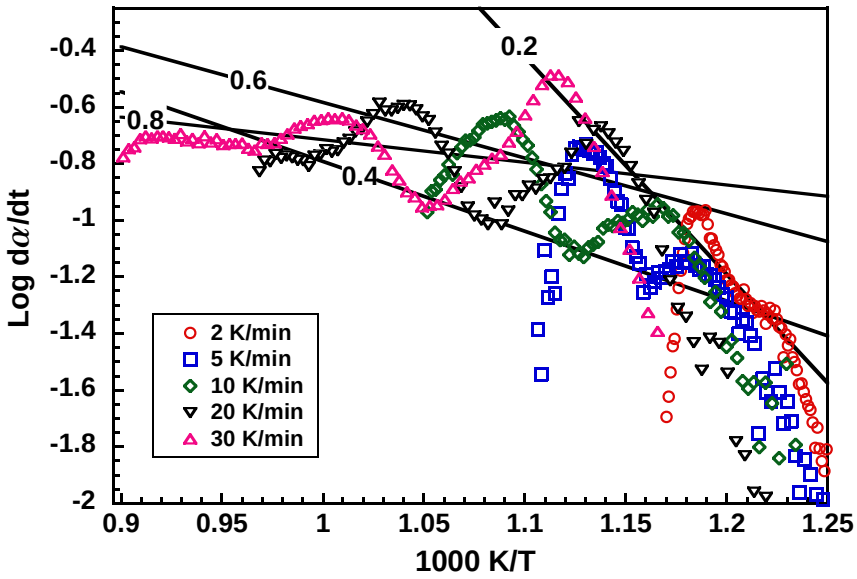

Figure 3-5. Friedman plot from the data shown in Figure 3-3.

The Friedman analysis is used to calculate the activation energy (E_α) and the pre-exponential factor (A_α) from the slope and the *y*-intercept of the fractional mass loss trend lines, respectively [12-14]. The activation energy and pre-exponential factor are shown in Figure 3-6 and presents activation energies from 20 kJ/mol to 190 kJ/mol. The plot of the activation energy with respect to the amount of degradation again confirms the multistep reaction by presenting non-constant activation energy throughout the entire degradation process. The fluctuating activation energy indicates an overlap of multiple reactions. As the reaction begins, the activation energy is about 190 kJ/mol and then shifts to 40 kJ/mol for a fractional mass loss of about 0.35. The activation energy increases to 60 kJ/mol for a fractional mass loss of 0.45, and then decreases to 20 kJ/mol for mass loss 0.8, and finishes by trending upward in the final moments of decomposition. The error bars show that the activation energy for the beginning of the reaction can be well-defined. For the last steps at

the fractional mass loss 0.7 the error bar of activation energy is much higher and the lower value can reach almost zero kJ/mol. The error bars are calculated using standard error from the linear regressions defined by the Friedman Analysis.

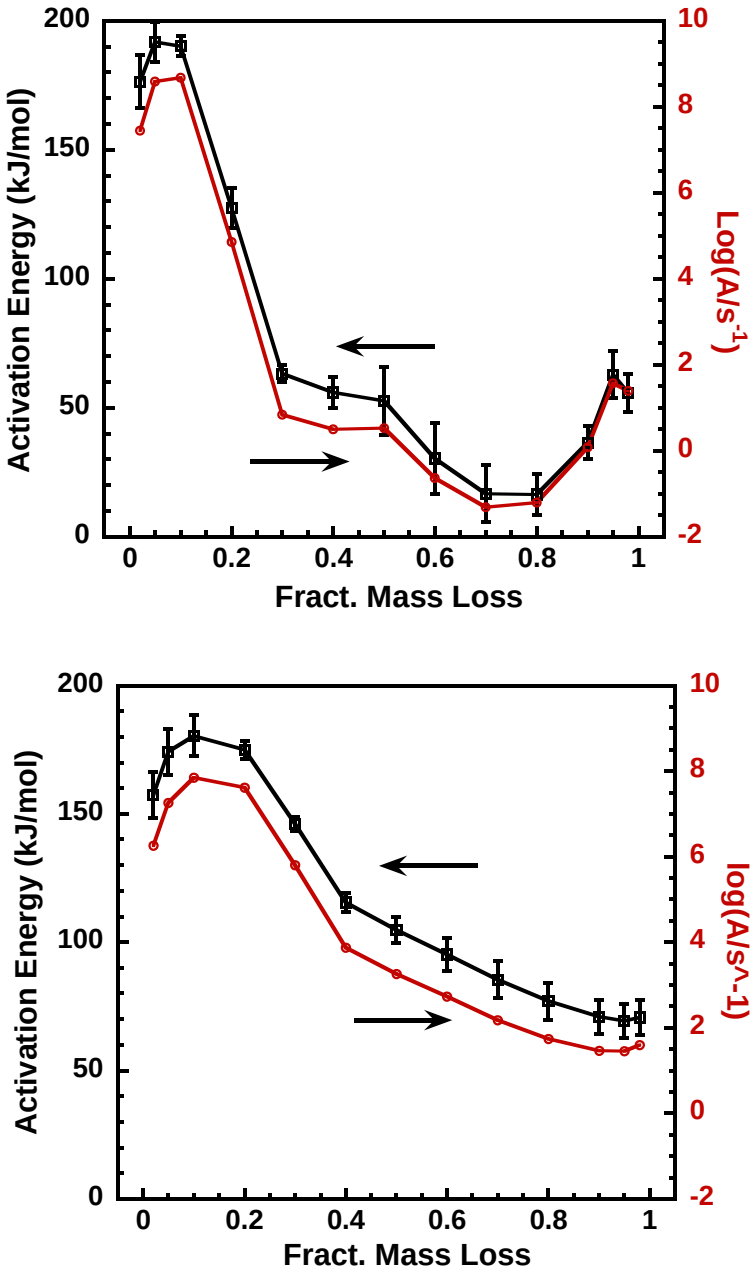

Figure 3-6. Activation energy plot for air atmosphere from (a) Friedman Analysis and (b) Ozawa-Flynn-Wall Analysis

A physical meaning for the mass loss dependent activation energy from the Friedman Analysis is difficult to identify with confidence because of the independence of overlapping degradation mechanisms. Rather, the Friedman Analysis is useful in identifying multistep reactions. Given the complexity of backbone structure in polyimide, the chemical structure can rearrange in tandem with the degradation through aroyl migration or hydrolysis of the imido group. Dine-Hart et al. have proposed possible degradation pathways in their studies of polyimide film [6].

An integral isoconversional method called Ozawa-Flynn-Wall Analysis was also used to calculate the activation energy as a function of fractional mass loss [13,14]. Similar to the differential method used in the Friedman Analysis, the activation energy can be extracted using isoconversional trend lines. The benefit of comparing these two methods for activation energy provides insight into the type of reaction step to best model the degradation. Since the integral method for calculating activation energy cannot utilize separation of variables, degradation kinetics involving competitive reactions show variations between the activation energies between the Friedman and Ozawa-Flynn-Wall Analysis. In conjunction with DTG peaks, the experimental data suggests a minimum of three steps with a combination of competitive and consecutive steps.

For the simulation, a model of three parts was used. The schematic representation of the mechanisms can be seen in Figure 3-7. The first part is the process from reactant A to reactant B, which proceeds along two different paths 1 and 2. The second part is the one elementary reaction from reactant B to reactant C, and the third part is the process from C to D, which also follows two parallel paths. Two different paths for the third part of the model

are necessary because the experimental data, Figure 3-2 and Figure 3-3, show that the decomposition mechanism for the last 60% mass loss depends on the heating rate. A multivariate version of the Borchardt and Daniels method was used to determine to optimal fit of the kinetic parameters by multiple linear regression [15]. The results of the model fit can be seen in Figure 3-8, with parameters given in Table 3-1.

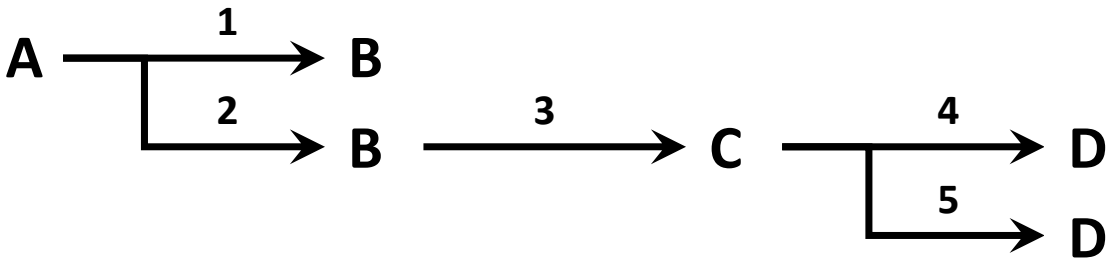

Figure 3-7. Schematic representation of the multistep reaction

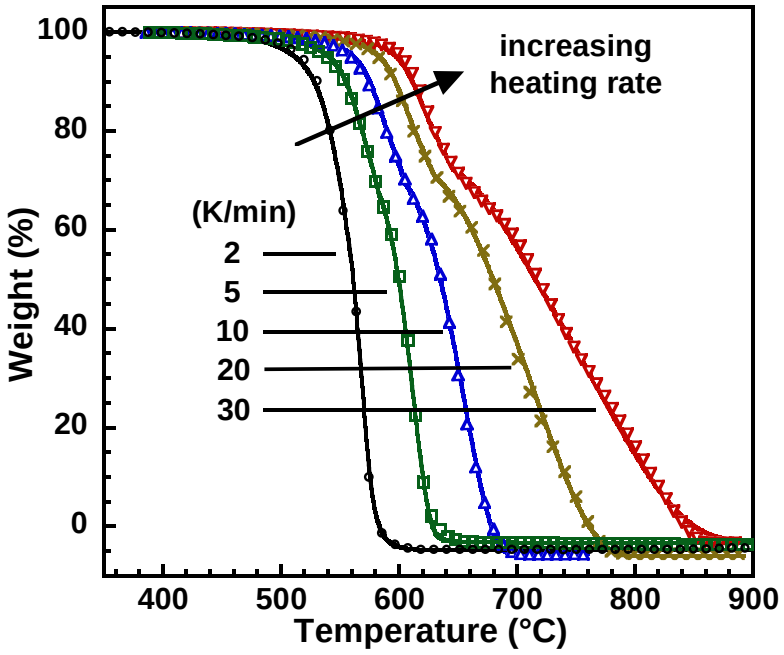

Figure 3-8. Best fit model of the TG data for the four-step reaction models in Figure 3-7, with parameters given in Table 3-1. The curves represent the model and the symbols represent the experimental data.

Table 3-1. Parameters used in the kinetic model.

	Activation Energy (kJ/mol)	Log (A_1/s^{-1})	Reaction Order	Log (K_{cat})
Step 1	189.62	8.40	0.77	0.94
Step 2	189.48	8.38	0.75	0.93
Step 3	168.73	7.73	0.89	0.09
Step 4	0.10	-3.43	3.17	1.65
Step 5	9.79	-3.17	0.40	1.38

These parameters come from the combination of Eqn. 2 with the autocatalytic reaction model found in Eqn. 10 for each step of the reaction diagramed in Figure 3-7. The Arrhenius parameters, E and A, are related to the temperature sensitivity of the reaction [16]. The reaction order and autocatalytic constant provide additional description of the chemical and physical reactions. The autocatalytic constant describes the extent in which the degradation reaction itself acts as a catalyst for that reaction. In thermodynamics of gases and liquids, the reaction order is an integer of stoichiometric equivalence. However, if the reaction takes place in the solid-solid, solid-liquid, and solid-gaseous phases, physical processes influence the reaction rate such as diffusion, phase-boundary reactions, or nucleation. Therefore, the direct evaluation of experimental data with unknown reaction order gives non-integer values. With respect to the first 3 steps, the effects are minimal and an approximate reaction order of $n = 1$ can be used without effecting the model drastically. Yet, in the final two steps, there are significant variations to the reaction order that cannot be approximated away. Therefore, the physical processes influencing the degradation of the final competitive reaction steps differ from the stoichiometric coefficients and play a significant role in the degradation.

From a statistical perspective, the model follows the data with an r^2 value of 0.99991. The large activation energies of the initial steps and very small values of activation energies for the last steps are in agreement with results of Friedman analysis, if the error bars are taken into account.

The kinetic parameters obtained for the multi-step model were then used to develop an isothermal model that would represent degradation across a 4-hour isothermal exposure for an air atmosphere, also obtained by TG analysis. We modeled a temperature spread of 425 to 475°C in 25°C increments. Figure 3-9 shows a comparison of the isothermal experimental data and the mathematical models. Isothermal tests intrinsically have significant uncertainty because of the variability to achieve the set temperature. While the isothermal data and the model prediction differ by up to ~16%, the model captures the general trend and magnitude of weight loss shown in the experimental data. This error is within the bounds of a typical isothermal test, but could be brought down with improvements to isothermal experimental environment such as tighter temperature control and gradients. However, the isothermal model was able to accurately capture the general trend of the mass loss.

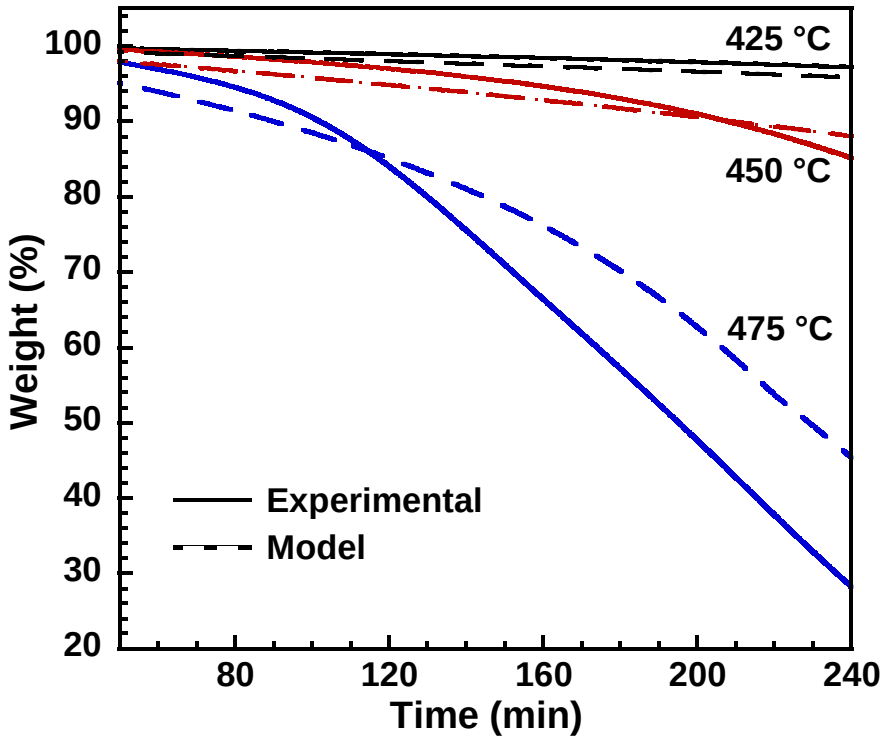

Figure 3-9. TG isothermal curves of experimental data and model prediction.

To further explore the degradation process, evolved gas analysis was conducted during the TG experiments. This coupled FTIR and MS analysis involved monitoring the exit gases as a function of time during the TG experiments at different heating ramp rates. The 3-dimensional FTIR data can be seen in Figure 3-10 and the 2-dimensional FTIR data constructed for analysis is shown in Figure 3-11. The MS data is shown in Figure 3-12.

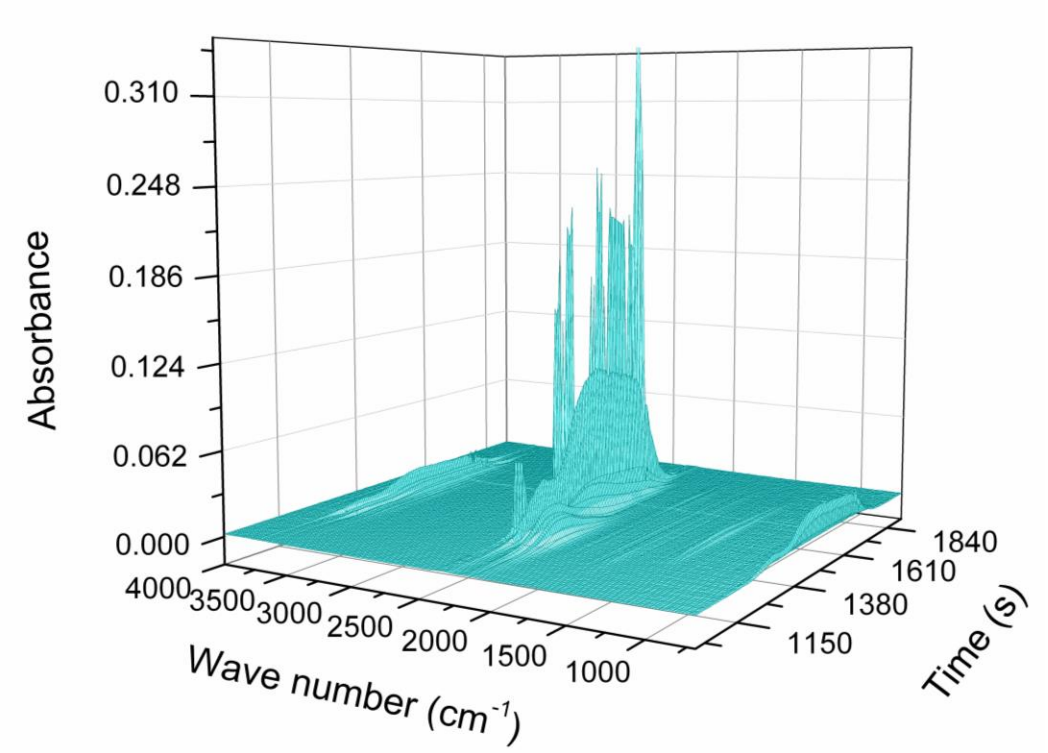

Figure 3-10. 3-dimensional FTIR data for exit gases of a 30 K·min^{-1} ramp rate TG on degradation onset.

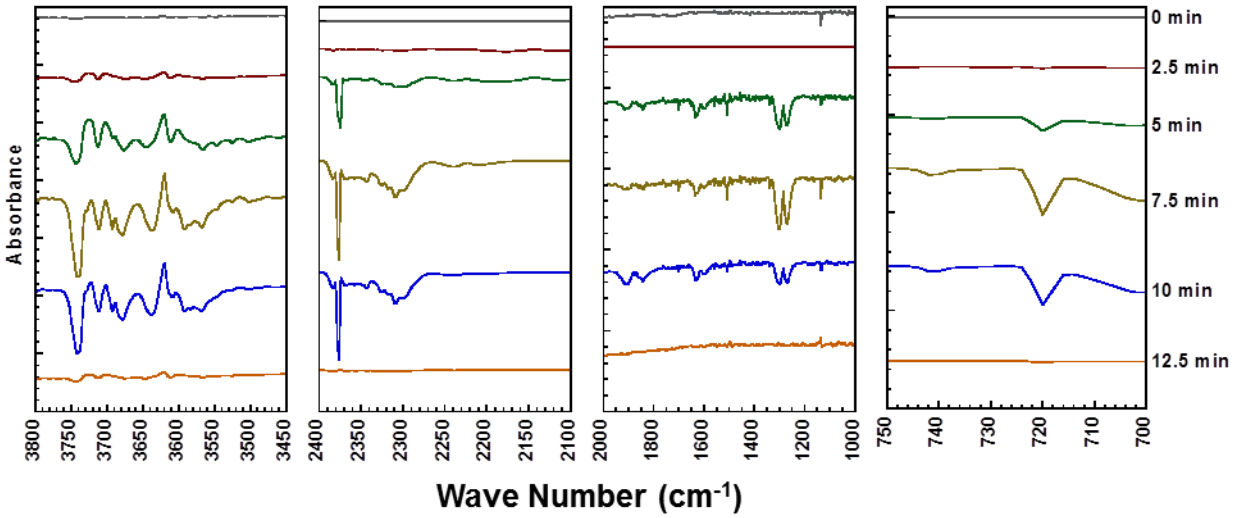

Figure 3-11. FTIR data for exit gases of a 30 Kmin^{-1} ramp rate TG on degradation onset for four different spectral ranges. Peak intensities are only proportional within each range and should not be compared from range to range.

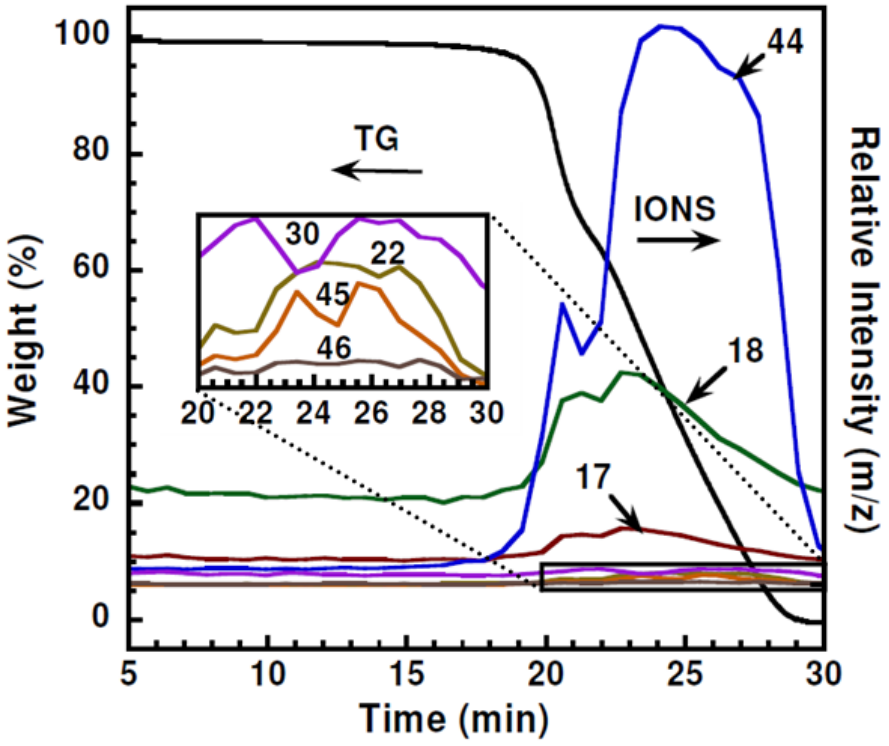

Figure 3-12. MS data for exit gases of a 30 Kmin^{-1} ramp rate TG.

There are four peak groups of interest as seen in the four sections in the FTIR figure. The first major group of peaks revolves around the 3500 to 3800 cm^{-1} wavenumber range. These peaks indicate the bond stretching of functional groups with removable hydrogen (bonds such as NH_2, NH, COOH, and OH) [17]. The second major group of peaks occurs in the wavenumber range 2100 to 2400 cm^{-1}. These peaks carry the largest intensity and indicate bonds such as CO and CO_2 [17]. This is to be expected since carbon dioxide and carbon monoxide are dominant products of degradation. The third set of peaks appears at

wavenumbers around 1000 to 2000 cm^{-1}. Since these fall close to the "fingerprint region" it is difficult to claim specifically what these peaks indicate. However, this peak area signifies bonds such as N=O, N=C, NO_2, and fragmented aromatic rings [17]. The final set of peaks are found at around 720 cm^{-1} and indicates nitro and nitroso compounds (NO bonds) [17]. These conclusions correspond well to typical breakdown mechanisms proposed for Kapton. Dine-Hart showed that under oxidative degradation, Kapton initially evolves CO_2 through hydrolysis of the imido group followed by the decarboxylation of the resulting acid group, evolves CO_2 through an aroyl migration, and CO through extrusion of the imido group [6]. Blumenfeld also shows the evolution of CO_2, CO, and H_2O through the initial oxidative degradation of the aryl ether groups while leaving behind the diimide group [18]. Further degradation at elevated temperatures cleaves the diimide residual into its nitrogen compounds [18].

The mass spectroscopy data corresponds closely to the FTIR data as well. The first major peak identified is mass number 44. This peak, which spreads across the whole TG degradation curve, corresponds to carbon dioxide, which was shown in the FTIR data to be a major exit gas contributor [17]. Peaks 17 and 18 correspond to water and more generally to the removable hydrogen of the functional groups also found in the FTIR data above [17]. Peak 22 is the double ionized peak for carbon dioxide and therefore is overshadowed by the first carbon dioxide peak [17]. Peaks 30, 45, and 46 are indicative of the nitro and nitroso compounds correlating to the FTIR peak in the 720 range [17]. One peak not shown, mass number 28, is the mass number for carbon monoxide [17]. While the FTIR data indicates evolution of carbon monoxide, the mass number also corresponds to nitrogen in its diatomic

form and consequently the nitrogen in the air environment overshadows the carbon dioxide emission.

Both the MS and 3-dimensional FTIR data validate the multistep reaction by presenting multiple peaks in the exit gas analysis. The 3-dimensional FTIR data, shown in Figure 3-10, clearly shows three peaks along the time axis, at around 2400 cm^{-1} wavenumber. In addition, the MS data indicates overlapping peaks, shown in Figure 3-12, as the reaction progresses providing support for the multistep reaction chosen in Figure 3-7.

3.6 Conclusions

This work uses kinetic reaction models to analyze the degradation of Kapton in an air environment. Through the use of DTG, Friedman Analysis, and activation energy plots, a multistep reaction model with acceleration was chosen. Using different acceleration reaction mechanisms to represent the data, the n^{th} order with autocatalysis model does a good job of fitting the data for all reaction steps. The model for Kapton was then verified qualitatively through isothermal experiments at elevated temperatures. Finally, FTIR and MS exit gas analysis from TG experiments at 30 $K \cdot min^{-1}$ were conducted to verify the degradation components for Kapton. The variations in FTIR and MS data peak intensities again authenticate the multistep degradation process of Kapton. Developing mathematical models of the kinetic degradation from TG experiments is important for understanding high temperature degradation of high performance polymers.

3.7 Acknowledgements

This work was funded by NASA under cooperative agreement NNX07AU54A.

3.8 References

[1] Don Farrelly. DuPont employee, personal communications. March 2010.

[2] S. Heltzel, C.O.A. Semprimoschnig, M.R.J. Van Eesbeek. Investigation of the Degradation of Thermal Control Materials by Thermal Analysis. High Perform Polym 2008; 20:492-511.

[3] S. Heltzel, C.O.A. Semprimoschnig. A Detailed Study on the Thermal Endurance of Kapton HN®i and Upilex S®, High Perform Polym 2004, 16:235-248.

[4] T. Ozawa, T. Arii, A. Kishi. Thermogravimetry and evolved gas analysis of polyimide. Thermochim Acta 2000; 352-353:177-180.

[5] T. Ozawa. CONTROLLED RATE THERMOGRAVIMETRY: New usefulness of controlled rate thermogravimetry revealed by decomposition of polyimide, J Therm Anal Calorim 2000; 59:375-384.

[6] R. A. Dine-Hart, D.B.V. Parker, W.W. Wright. Oxidative Degradation of a Polyimide Film, British Polymer Journal 1971; 3(5):222-236.

[7] A. Chong Lua, J. Su. Isothermal and non-isothermal pyrolysis kinetics of Kapton® polyimide Polym. Degrad. Stab. 2006; 91(1):144-153.

[8] D. W. Levi, L. Reich, H.T. Lee. Degradation of Polymers By Thermal Gravimetric Techniques, Polymer Engineering and Science 1965, 5(3):135-141.

[9] M.E. Brown, D. Dollimore, A.K. Galewey. Reactions in the Solid State, Comprehensive Chemical Kinetics, Vol. 22, Elsevier, Amsterdam.

[10] S. Vyazovkin. Kinetic concepts of thermally stimulated reactions in solids: a view from a historical perspective, International Review in Physical Chemistry 2000; 19(1):45-60.

[11] H. Friedman. Kinetics of Thermal Degradation of Char-forming Plastics from Thermo-gravimetry. Applications to a Phenol Plastic. J Polym Sci 1963; 6C:183-195.

[12] T. Ozawa. A New Method of Analyzing Thermogravimetric Data, Bull Chem Soc Jpn 1965; 38(11):1881-1886.

[13] J.H. Flynn, L.A. Wall. General Treatment of the Thermogravimetry of Polymers J Res Natl Bur Stand 1966; 70a(6):487-523.

[14] J. Opfermann. Kinetic Analysis Using Multivariate Non-linear Regression. I. Basic concepts, J Therm Anal Calorim 2000; 60(2):641-658.

[15] Borchardt, H. J.; Daniels, F. The Application of Differential Thermal Analysis to the Study of Reaction Kinetics. J Am Chem Soc 1957, 79, 41–46.

[16] S. Vyazovkin, C.A. Wight. Isothermal and Non-Isothermal Kinetics of Thermally Stimulated Reactions of Solids. International Reviews in Physical Chemistry. 1998; 17(3):407-433.

[17] E. Pretsch, P. Buhlmann, C. Affolter. Structure Determination of Organic Compounds 4th ed., Minneapolis: Springer Berlin Heidelberg, 2000.

[18] A. B. Blumenfeld, A. L. Wdovina. Thermal Behavior and Heat Stabilization of Polyimides and Related Polymers, Polyimides and other High-Temperature Polymers 1991, 183-188.

CHAPTER 4: ELECTROTHERMAL LIFETIME PREDICTION OF POLYIMIDE WIRE INSULATION WITH APPLICATION TO AIRCRAFT

A paper published in *Journal of Applied Polymer Science*

Peter R. Hondred[1], Nicola Bowler[1], and Michael R. Kessler[1]

4.1 Abstract

This work investigates the electrothermal lifetime of a commonly used polyimide wire insulation material, Kapton® through the use of thermogravimetry (TGA) and breakdown voltage testing. From TGA, an isoconversional model-free kinetic evaluation was used to obtain a relationship between the activation energy of degradation for Kapton as a function of weight loss. By relating the electrical life theory and the TGA theory through the model defined by Toop [D. Toop. IEEE Trans. Dielectr. Electr. Insul., Vol. 6, pp. 2-14, 1971], the electrothermal lifetime of Kapton has been calculated for conditions of 12 and 14.7 kV over a temperature range of 250 to 400°C. The resulting model can be used to make lifetime predictions for wire insulation degradation in aging aircraft for improved safety and risk assessment.

4.2 Introduction

Kapton® (poly[(5,7-dihydro-1,3,5,7-tetraoxobenzo[1,2-c:4,5-c']dipyrrole-2,6(1H,3H)-diyl)-1,4-phenyleneoxy-1,4-phenylene]) has been and continues to be a common insulation material for wiring applications in air- and spacecraft. It was developed by DuPont

as a high performance polymer, which has stable material properties between -250 °C and 400 °C. Kapton, a polyimide, is produced through a condensation reaction of pyromellitic dianhydride and oxydianiline in dimethylacetamide.1 It mimics thermoset behavior in that it cannot be melt-processed once formed. Consequently, the process for synthesizing Kapton film involves casting a heavily solvent-laden solution in a drum and curing the film in a low temperature oven to remove the solvent, followed by pulling through a high temperature oven to convert the precursor film, polyamic acid, into the inert polyimide film [1]. The chemical structure of Kapton is shown in Figure 4-1.

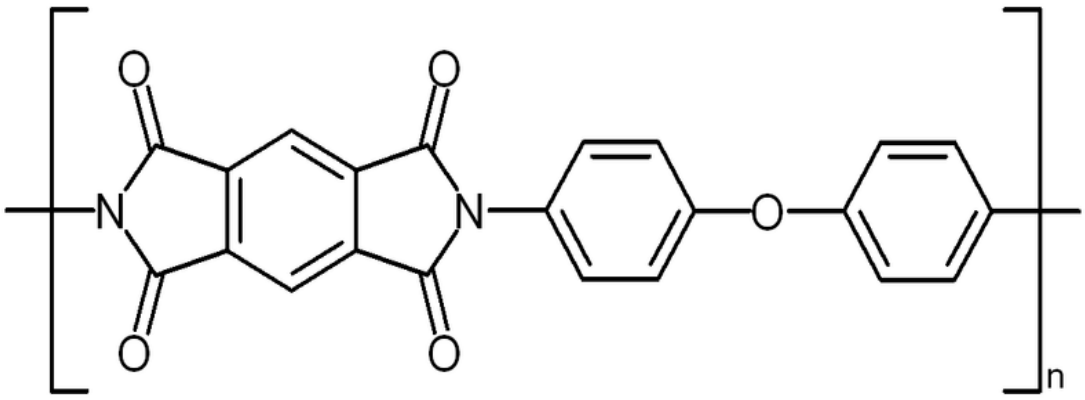

Figure 4-1. Chemical Structure of Kapton

Since Kapton has been used extensively in the aerospace industry for many years, it has been studied at length. Thermal decomposition kinetics investigated by thermogravimetry (TGA), differential scanning calorimetry (DSC), and dynamic mechanical analysis (DMA) have all been documented [2-5].

In addition, Dine-Hart et al discussed the possible crosslinking of Kapton from oxidative degradation [6]. Lua et al. investigated isothermal and non-isothermal pyrolysis of

Kapton in nitrogen gas [7]. Guo et al. explored the use of Fe-FeO nanoparticles to reinforce Kapton fiber [8]. Furthermore, Bruck investigated the decomposition mechanisms of Kapton under oxidative and non-oxidative atmospheres [9]. Degradation of wire insulation materials such as Kapton continues to be an issue of concern, related to safety in the aerospace industry. Consequently, accurate and predictive models that describe the degradation of insulation polymers, that may take into account thermal and electrical history, are important.

The concept of using thermogravimetric analysis in conjunction with electrical stress testing to predict lifetime of insulation material was first proposed in 1971 by Toop [10]. The lifetime model relates electrical life theory to kinetic decomposition theory through TGA analysis. Toop's model is not applicable for all wire insulation materials, in particular those with extremely complex decomposition mechanisms. Toop showed, however, that the lifetime of a material such as Formvar, a wire insulation enamel with a simple thermogram, can be described as accurately from his proposed electrothermal model as it can be by following the failure criteria and test procedures given in ASTM Standard D2307 - 07a "Standard Test Method for Thermal Endurance of Film-Insulated Round Magnet Wire." This ASTM standard is developed for testing thermal endurance of film-insulated round magnet wire.

Toop's theory is built on a chemical rate theory devised by Dakin, which provides a relationship between the material's degree of degradation and physical properties [11]. More recently, Montanari and others have further developed the modeling of aging and degradation of electrical insulation by improving the understanding of physical phenomena that occur during the aging [12-15]. Their work with partial discharge measurements to monitor electrical tree growth in degrading samples continues to advance aging investigation [12].

Building on Toop's model, they also present the theoretical background to relate lifelines for the aging compensation effect theory [13]. Consequently the method is valid not just for parallel linear life lines but also for non-parallel linear life lines [13]. Furthermore, they have described how the presence of space charge accumulation at the interface of the electrode and insulation results in local damage due to dielectric heating and Maxwell stress [14]. Additionally, Montanari and Simoni have published a review of aging phenomenology and modeling [15].

In this work, TGA analysis of Kapton thin film is used to calculate an electrothermal lifetime for the polymer. By correlating TGA theory with lifetime theory, a fitting parameter can relate thermal degradation data to breakdown voltage data. A predicted lifetime, for a given voltage and temperature, is defined using this method.

4.3 Materials & Preparation

Kapton HN thin film sheets, with a thickness of 125 μm, were supplied by DuPont. This specific Kapton polymer is a general purpose film designed to sustain an excellent balance of insulating properties while enduring a wide range of temperatures. The imido groups of the Kapton backbone (see Figure 4-1) are sensitive to ambient humidity. Consequently, the samples were stored in a desiccant dry box to reduce the effects of moisture absorption. Samples for TGA analysis were cut from the thin film sheets by a circular punch of diameter 3.0 ± 0.1 mm, ensuring repeatable sample mass and shape. The sample masses were 3.6 ± 0.5 mg. Samples for breakdown voltage testing were cut into rectangular sheets, 60×90 mm2.

4.4 Methods

A thermogravimetric analyzer, model Q50 from TA Instruments (New Castle, DE), was used for the TGA experiments. The TGA experiments were conducted in an oxidative environment with a nitrogen balance purge gas flow rate of 40 mL/min and an air sample purge gas flow rate of 60 mL/min. The tests were performed over a temperature range of 35 to 900 °C at five different heating ramp rates: 2, 5, 10, 20, and 30 $Kmin^{-1}$. Kinetic analysis was performed with the Netzsch Thermokinetics 2 program (version 2004.05).

Samples for electrical breakdown testing were isothermally heated at 425, 450, 460, 465, 470, 475, and 480 °C for up to 5 hr in an isothermal muffle furnace. These temperatures were chosen to provide uniform sample degradation because Kapton is thermally stable below 400 °C. Prior to degradation, the samples were all dried in a standard convection oven for 1 hour at 150 °C. A simple isothermal TGA analysis of Kapton HN at 150 °C for 1 hour shows 2-3% weight loss and then stabilizes with no additional weight loss; indicating the removal of water from the sample. The samples were then placed in a sealed, pre-weighed, plastic bag. The dried Kapton was weighed to obtain initial weight and then placed in the muffle furnace for degradation. On completion of isothermal heating the samples were again placed in the pre-weighed bag and weighed again to obtain their weight loss. After that, the breakdown voltage of the samples was measured.

A 60 kV dielectric rigidity device (Ceast part number 6135.053 /6135.054) was used for breakdown voltage testing. The experiments were conducted at room temperature in a

flame-resistant bio-oil liquid (Envirotemp® FR3TM Fluid) insulation bath. The tests were conducted in accordance with ASTM Standard D149–09 "Standard Test Method for Dielectric Breakdown Voltage and Dielectric Strength of Solid Electrical Insulating Materials at Commercial Power Frequencies." Breakdown voltage was measured at twenty separate locations, evenly distributed across each 60 x 90 mm^2 specimen, and the values were averaged for each specimen.

4.5 Thermogravimetric Theory

A material property changing through a chemical reaction, a physical reaction, or a combination of the two may be represented, in general, by a differential equation of two functions— $K(T)$ and $f(r)$:

$$\frac{dr}{dt} = K(T)f(r) \tag{1}$$

where dr/dt is the rate of change of the material property, $K(T)$ is the temperature-dependent rate constant, and $f(r)$ is the unknown continuous function representing the chemical and/or physical changes [10]. The function $f(r)$ is not constrained in order that no restrictive assumptions concerning the nature of the chemical and/or physical changes are made.

Applying equation (1) to the kinetics of thermal degradation, replace r by the degree of degradation, α, defined as:

$$\alpha = f(t,T) = 1 - \frac{wt\%}{100} \tag{2}$$

where wt% is the residual weight obtained directly from the TGA experiment. The reaction model, $f(\alpha)$, is dependent on the degradation mechanism of the material.

TGA analysis is a common polymer degradation tool that measures the degree of degradation, i.e. weight loss, with respect to time, t, and temperature, T [16]. It has long been recognized as a means by which life testing can be conducted quickly and accurately, without the need for expensive, long-term aging studies [10]. The degree of degradation, α, varies from 0 (no weight loss) to 1 (complete weight loss). The temperature-dependent rate constant is commonly described by the Arrhenius equation:

$$K(T) = Ae^{-E/RT} \tag{3}$$

where R is the universal gas constant, E is the overall activation energy of the thermal degradation, and A is a pre-exponential factor [17].

To account for the dynamic heating scans at a constant heating rate, the time-dependence can be eliminated from equation (1) by dividing by the heating rate $\beta = dT/dt$ such that:

$$\frac{d\alpha}{dT} = \frac{A}{\beta} e^{-E/RT} f(\alpha) \tag{4}$$

Once the time-dependency has been removed, the kinetic parameters A and E can be obtained through linear transformation of the differential equation (4), leading to the following time independent rate equation:

$$ln\left(\frac{d\alpha/_{dT}}{f(\alpha)}\right) = ln\left(\frac{A}{\beta}\right) - \frac{E}{RT} \tag{5}$$

Equation (5) follows the linear form $y = a_0 + a_1 x$ (with $x = 1/T$) and optimal fit of the kinetic parameters, A and E , is determined using linear regression. The variation in A and E as a function of weight loss is determined by calculating these parameters at several different values of weight loss.

In one approach for kinetic degradation modeling, constant activation energy, E, and pre-exponential factor, A, are assumed in equation (5) [17]. On the other hand, the model-free isoconversional method allows the kinetic parameters to vary by assuming that both A and E are functions of the degree of degradation, A [18]. Friedman's isoconversional method obtains the activation energy by plotting the logarithmic form of the rate equation for each heating rate:

$$ln\left[\beta_i\left(\frac{d\alpha}{dT}\right)_{\alpha,i}\right] = ln[A_\alpha f(\alpha)] - \frac{E_\alpha}{RT_{\alpha,i}} \quad (6)$$

where the subscripts α and i denote a particular degree of degradation and the particular heating rate of the experiment, respectively [18]. The activation energy at each degree of degradation is calculated by linear regression, plotting $ln\left[\beta_i\left(\frac{d\alpha}{dT}\right)_{\alpha,i}\right]$ versus $1/T_{\alpha,i}$ for all of the heating rates tested.

4.6 Lifetime Theory

As previously stated, the electrothermal lifetime theory developed in and followed here is built on the chemical rate theory devised by Dakin, which provides a relationship between the material's degree of degradation and its material properties [12-14]. In the calculation of electrothermal lifetime, the degree of degradation is linked to electrical breakdown voltage. By an empirical correlation, mathematical modeling of the kinetics of degradation can be combined with knowledge of the electrical breakdown voltage to predict lifetime at a particular temperature and applied voltage. The kinetic model, developed by scanning experiments, provides kinetic parameters valid for isothermal lifetime prediction.

Now replacing r in equation (1) by electrical breakdown voltage V means that $f(V)$ is the reaction model dependent on the breakdown voltage mechanism of the material. The function $f(V)$ embodies the chemical and physical effects of applied voltage V on the test piece.

Rearranging and integrating the governing equation with r replaced by V gives:

$$\int_{V_0}^{V_f} \frac{dV}{f(V)} = K(T) \int_0^{t_f} dt \tag{7}$$

where limits V_0 and V_f are the breakdown voltages corresponding to the pristine and the failed samples respectively, and t_f is the time for the breakdown voltage to reach the failure criterion. Taking equation (7) and applying these limits, another function of the breakdown voltage can be realized:

$$\left[\int \frac{dV}{f(V)}\right]_{V_0}^{V_f} = [g(V)]_{V_0}^{V_f} = K(T)t_f \tag{8}$$

and substituting the Arrhenius function for K(T) gives:

$$g(V_f) - g(V_0) = At_f e^{-E/RT}\,, \tag{9}$$

from which:

$$t_f = \frac{e^{-E/RT}}{A}\left[g(V_f) - g(V_0)\right]. \tag{10}$$

Similar to the development given in equations (7) through (10) for electrical breakdown voltage, the generalized differential equation, equation (1), is also a starting point from which to develop g(α), a function of degradation analogous to g(V). By taking the rearrangement in (4), and defining the parameter $x = E/RT$, the separation of variables procedure isolates the temperature and weight loss in the function to give:

$$\frac{\beta}{A} g(\alpha) = -\frac{E}{A} \int e^{-x} x^{-2} dx + C. \tag{11}$$

The initial and final conditions are T_0, x_0, and α_0 and T', x', and α' respectively. Ultimately, at failure, $T' = T_f$. Therefore, equation (11) can be written as:

$$\frac{\beta}{A}[g(\alpha') - g(\alpha_0)] = \frac{E}{R}[p(x') - p(x_0)] \tag{12}$$

where:

$$p(x) = \frac{e^{-x}}{x'} - \int_{x'}^{\infty} \frac{e^{-x}}{x'} dx. \tag{13}$$

As seen in [10], when taking the logarithm of (10) the y-intercept is equivalent to the y-intercept of the logarithm of (12). Consequently, these equations can be assimilated as follows:

$$log(t_f) = \frac{E}{2.303RT} + \frac{Ep(x)}{\beta R}. \tag{14}$$

With the correlation found through p(x), the temperature, T, in equation (14) is defined as the failure temperature of the thermogram, T_f [10]. Since $p(x)$ correlates back to the weight loss in equation (4), the failure temperature is defined as the temperature at which a corresponding weight loss intersects the slowest heating thermogram. This model is limited in application because $K(T)$ in equation 1 focuses on the variation due to temperature, T. However, if the model were to be further investigated, a in situ testing of applied voltage and temperature could be investigated, where equation 1 contains $K(V, T)$. This would involve the capabilities to run in situ testing of voltage and high temperature.

4.7 Thermogravimetric Analysis

Figure 4-2 shows TGA scans of Kapton film at five different heating rates between 2 and 30 $Kmin^{-1}$ in an oxidative environment [19]. These tests began at room temperature and

ended at complete degradation which occurred below 900°C for all of the heating rates studied. Before the onset of degradation, Kapton is extremely stable, as are most polyimides at temperatures below the onset temperature of rapid degradation [1]. The TGA curves show rapid and complete degradation with an increasing spread and shallower slope in the curves as heating rate increases.

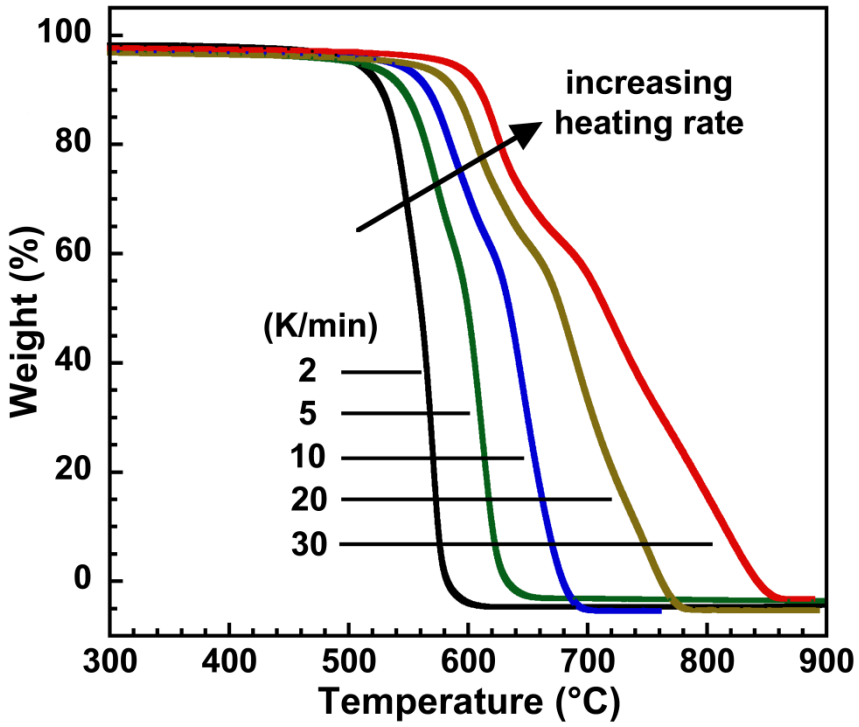

Figure 4-2. TGA Curves for Kapton in an Oxidative Environment

By plotting the TGA data according to Friedman analysis, equation (6), the Friedman plot is developed in Figure 4-3 [18]. This plot is used to calculate the activation energy, E and pre-exponential factor, A. As seen in equation (6), the activation energy is proportional to

the slope of the isoconversional trend lines; a few of these trend lines are highlighted in Figure 4-3.

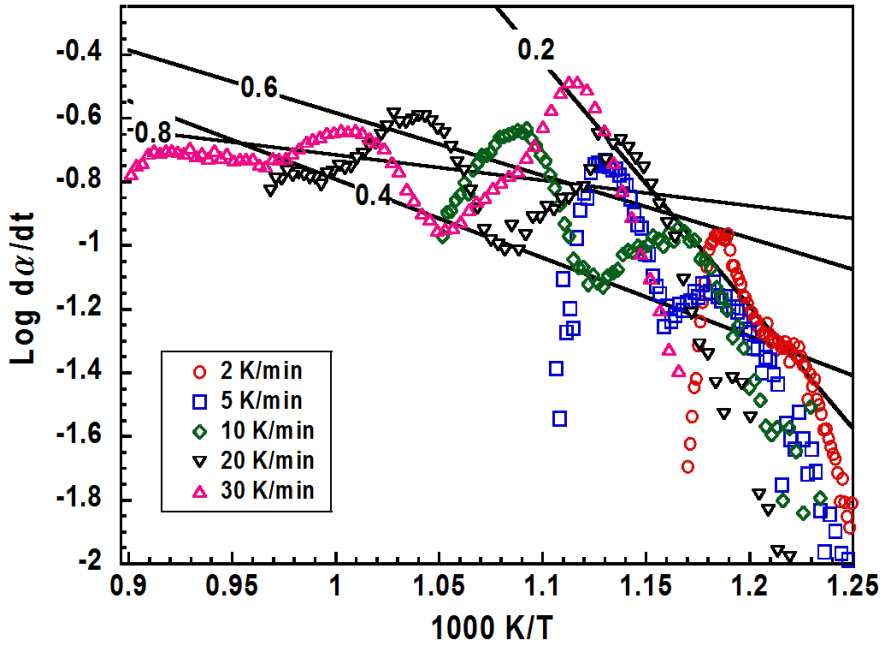

Figure 4-3. Friedman plot from the data shown in Figure 4-2. Four isoconversional fractional weight loss trend lines are represented for 0.2, 0.4, 0.6, and 0.8 fractional weight loss.

From the Friedman analysis, activation energy as a function of fractional weight loss can be obtained as shown in Figure 4-4 [18]. The error bars represent the statistical error between the linear isoconversional trend line adopted in the Freidman analysis and measured data values. The activation energy, E, and the pre-exponential factor, A, follow the same trend in Figure 4-4 because these kinetic parameters are correlated in such a way that the natural log of A is linearly proportional to E.

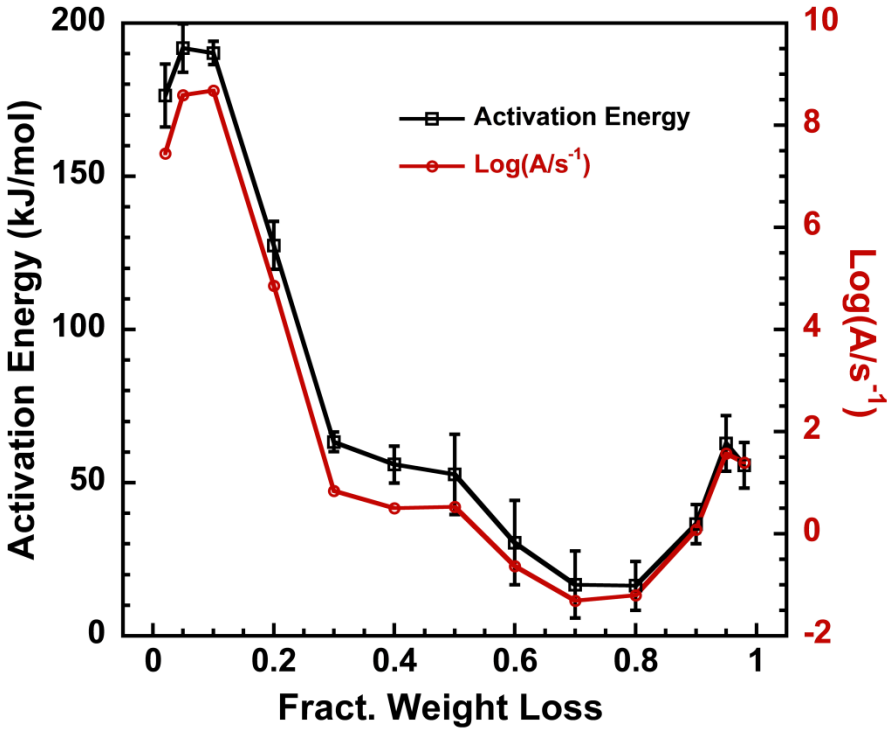

Figure 4-4. Kinetic parameters obtained by Friedman analysis of TGA data on Kapton.

The kinetic pathway for the thermal degradation of Kapton was shown in our earlier work to fit a five step model with both competitive and consecutive reaction steps [19]. The activation energy plotted in Figure 4-4 is the overall activation energy for the complete degradation of Kapton. When the activation energies for the individual steps are separated, five different constant activation energies are obtained. The initial reaction steps, a competitive model, contain an activation energy of 189 kJ/mol [19]. Since the degradation for the electrical breakdown analysis is from the initial degradation steps, this activation energy is used for calculating the lifetime prediction for Kapton.

4.8 Electrical Breakdown Analysis

Measured breakdown voltage of degraded Kapton is plotted in Figure 4-5. A linear fit of the breakdown voltage as a function of degradation is used to represent the trend of the data. This trend line is useful in calculating the lifetime to electrical failure. Each data point in the figure represents the average of twenty test measurements on a degraded sample sheet. The error bars represent the standard error with a 95% confidence interval between the twenty test values.

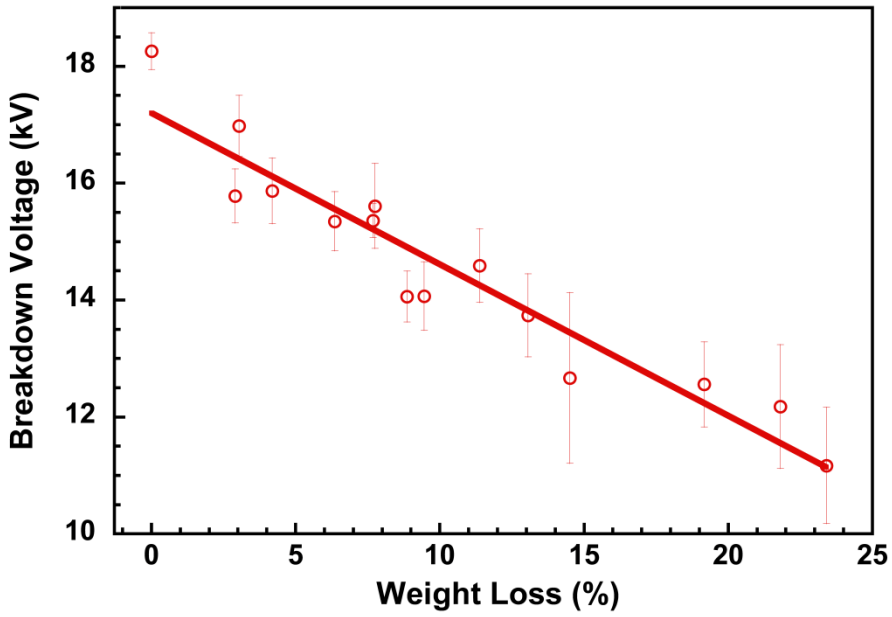

Figure 4-5. Measured breakdown voltage of degraded Kapton film (symbols) with best linear fit (solid line).

4.9 Lifetime Prediction

In the electrothermal lifetime prediction model of (14), time to failure, t_f, is calculated from test temperature and voltage, TGA analysis parameters E and T_f, and the breakdown voltage value. First, a breakdown voltage value is selected (e.g. 12 kV) and the relevant fractional weight loss is read from Figure 4-5 (20%).

During the first 25% weight loss, there are direct correlations between the electrical breakdown characteristics and physical changes in polymeric materials, specifically free volume and free radicals. Free volume, the space between molecules in the amorphous phase, is inversely proportional to electrical breakdown strength [20]. As the polymer degrades, free volume increases as a function of temperature and time because of the increase in molecular size variation. Additionally, free radicals form as the polymer chain ruptures. These radicals relieve electron transport tension, which in turn decreases the electrical breakdown strength [21]. Consequently, the breakdown voltage decreases as the material degrades, as seen in Figure 4-5.

This fractional weight loss defines failure temperature, T_f, from Figure 4-2, i.e. the temperature of the slowest thermogram corresponding to the relevant fractional weight loss (541 °C or 814 K). The failure temperature along with the activation energy of 189 kJ/mol are then utilized in (13) to calculate the correlation fitting parameter $p(x)$.

Using equation (14), the lifelines shown in Figure 4-6 are calculated based on two particular sets of environmental conditions; voltages of 12 and 14.7 kV (10 and 20% weight loss respectively) and a temperature range from 250 to 400 °C. Lifelines for other sets of conditions can also be obtained but these two are chosen for demonstration here. The values of T_f, α, V_f, and E used to calculate the lifelines shown in Figure 4-6 are listed in Table 4-1.

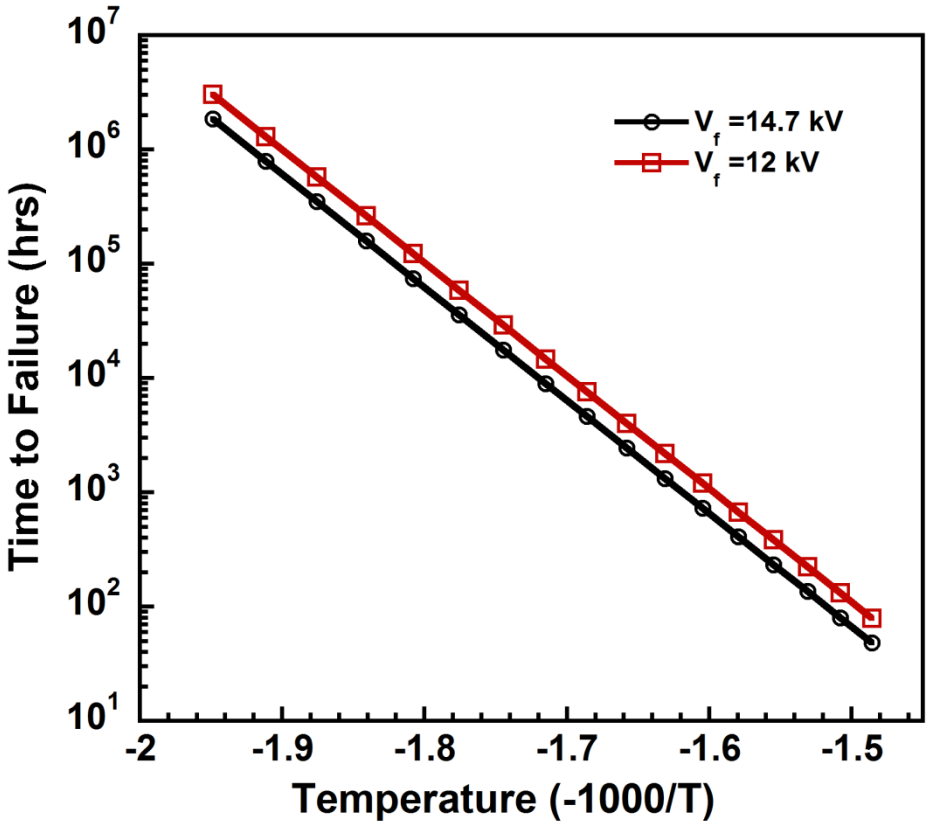

Figure 4-6. Predicted time to failure at 12 and 14.7 kV and for isothermal temperatures ranging from 250 to 400 °C.

Table 4-1. Parameter values used to obtain the calculated lifelines shown in Figure 4-6.

V_f	α	T_f	E	β	t_f at 350°C
12 kV	20%	814 K	189 kJ/mol	120 K/hr	1200 hrs
14.7 kV	10%	801 K	189 kJ/mol	120 K/hr	729 hrs

4.10 Discussion

As stated previously [10], the model presented in this work is not applicable to all materials; specifically those with extremely complex degradation mechanisms. The Kapton

film studied here may, however, be treated in this way by considering only the initial part of the weight loss curves (within the first 25%) where a simple mechanism is responsible for degradation. Further, the thermogram for Kapton is no more complex than the thermogram for Formvar, treated in [10], in which a polyimide film was also treated.

Within the first 25% of weight loss, Kapton remains functional as wire insulation. Beyond 25% weight loss, the thin film failed to maintain the mechanical properties required for standard wire insulation and it was not possible to collect breakdown voltage data. At the elevated temperatures of this degradation study, the the surface of the Kapton film oxidizes. The oxidative layer can be seen on the surface of the material as darkening of the material color and alligator cracking of the surface. The oxidation causes the material to become brittle and deformed as the size of the oxidative layer expands—causing the material to fold over on itself.

Beyond 25% weight loss, the breakdown voltage is expected to drop rapidly, showing a large decrease in breakdown voltage for minor weight losses. This expectation comes from the loss of material properties due to the extensive oxidation of Kapton. In fact, beyond 25% weight loss, there are indications that the Kapton polymer backbone is degraded enough that most of the linear chains are broken. The change in activation energy seen in Figure 4-4 for the first 25% weight loss indicates the rupture of the Kapton backbone—the sharp drop in activation energy is related to the breaking of the stable covalent bonds. When the linear chain is ruptured repeatedly, commonly through aroyl migration or hydrolysis of the imido group, the free radicals, mobile molecules, and oxygen molecules provide pathways for continued degradation at lower activation energies as observed between 30 and 100% weight loss [19]. These types of new pathways have been observed in the mass spectroscopy data

from TGA experiments in which the peak indicating carbon dioxide emission clearly indicates two unique mechanisms. The first mechanism (backbone rupture) endures for the first 25% of degradation and the second unique mechanism (new pathway) appears at around 25% weight loss [19]. Additionally, the nitrogen compounds have distinguishable mechanisms that again indicate a transition at 25% weight loss from the rupture of the major chain to the breaking of subcomponents.

To summarize, Kapton film may be treated by electrothermal analysis based on the criteria used in [10], provided that the lifetime prediction stays within the bounds of Kapton's functional mechanical properties, i.e. within 25% weight loss. In this 25% weight loss, electrical breakdown characteristics and physical changes are related through free volume and free radicals. Beyond the 25% threshold, the mechanical properties are destroyed through the rupturing of the stable covalent bonds in the polymer backbone. This is seen through observing the physical appearance of the degraded Kapton, the reduction in activation energy around 25%, and through the evolved gas analysis reported in [19].

The lifetime model, found if equation 14, could be improved by accounting for the applied voltage in equation 1 by modifying $K(T)$ to $K(V,T)$ where V represents the variation as a result of the voltage. However, in order to utilize this model, testing of both the elevated voltage as well as the elevated temperatures simultaneously would be required. These in situ tests would provide the data required for further mathematical model development.

4.11 Conclusion

In an era in which hundreds of miles of aging wiring are running through commercial aircraft, an accurate and rapid method for monitoring wiring insulation is needed for safety. This lifetime prediction model provides a mechanism for effective calculation of lifetime of electrically and/or thermally degraded Kapton, due to elevated voltage and/or temperature. Through chemical rate theory and kinetic theory for material properties, the TGA rate experiments and breakdown voltage data, activation energy, and failure voltage are used to correlate the weight loss and electrical breakdown to obtain a single lifetime prediction.

This dynamic model is effective for two reasons. First, the model rapidly provides meaningful data—involving days rather than months of testing. This accelerated production of lifetime prediction allows for response times that may assist in avoiding potential failures in systems currently in-service, to prevent catastrophes such as those of the TWA 800 and Swissair 111 flights (July 17, 1996 and September 2, 1998 respectively). Second, this method eliminates the need for understanding the exact degradation and breakdown voltage mechanisms. By operating mathematically with the governing differential equations, the specific mechanism of degradation or breakdown can be bypassed while still maintaining an effective model that can be applied for a wide range of materials—an important requirement for analyzing insulation polymers in a systematic way.

4.12 Acknowledgments

This work was funded by NASA under cooperative agreement NNX07AU54A.

4.13 References

[1] D. Farrelly. DuPont employee, personal communications. March 2010.

[2] S. Heltzel, C.O.A. Semprimoschnig, and M.R.J. Van Eesbeek, "Investigation of the Degradation of Thermal Control Materials by Thermal Analysis", High Perform. Polym., Vol. 20, pp. 492-511, 2008.

[3] S. Heltzel, and C.O.A. Semprimoschnig. "A Detailed Study on the Thermal Endurance of Kapton HN®i and Upilex S®", High Perform. Polym., Vol. 16, pp. 235-248, 2004.

[4] T. Ozawa, T. Arii, and A. Kishi, "Thermogravimetry and evolved gas analysis of polyimide" Thermochim. Acta, 2000; 352-353:177-180.

[5] T. Ozawa, "CONTROLLED RATE THERMOGRAVIMETRY: New usefulness of controlled rate thermogravimetry revealed by decomposition of polyimide", J. Therm. Anal. Calorim., Vol. 59, pp. 375-384, 2000.

[6] R. A. Dine-Hart, D.B.V. Parker, and W.W. Wright, "Oxidative Degradation of a Polyimide Film", Brit. Polym. J., Vol. 3, pp. 222-236, 1971.

[7] A. C. Lua, and J. Su, "Isothermal and non-isothermal pyrolysis kinetics of Kapton® polyimide", Polym. Degrad. Stab., Vol. 91, pp. 144-153, 2006.

[8] Z. Guo, et al., "Electrospun Polyimide Nanocomposite Fibers Reinforced With Core-Shell Fe-FeO Nanoparticles", Journal of Physical Chemistry C, 114(19) 8844–8850 (2010).

[9] S. Bruck, "Thermal Degradation of an Aromatic polypyromellitimide in Air and Vacuo", Polymer, Vol. 6, pp. 49-61, 1965.

[10] D. Toop, “Theory of Life Testing and Use of Thermogravimetric Analysis to Predict the Thermal Life of Wire Enamels”, IEEE Trans. Dielectr. Electr. Insul., Vol. 6, pp. 2-14, 1971.

[11] T. W. Dakin, “Electrical Insulation Deterioration Treated as a Chemical Rate Phenomenon”, AIEE Transactions, Vol. 67, pp. 113-118, 1948.

[12] G. Montanari, “A Comparative Investigation of Electrothermal Endurance Models for Insulating Materials and Systems Characterization”, IEEE Trans. Dielectr. Electr. Insul., Vol. 13, pp. 13-25, 1997.

[13] G. Montanari, “Thermal Degradation of Electrical Insulating Materials and the Thermokinetic Background: Theoretical Basis”, IEEE Trans. Dielectr. Electr. Insul., Vol. 25, pp. 1029-1036, 1990.

[14] G. Montanari, G. Mazzanti, and L. Simoni, “Progress in Electrothermal Life Modeling of Electrical Insulation during the Last Decades”, IEEE Trans. Dielectr. Electr. Insul., Vol. 9, pp. 730-745 2002.

[15] G. Montanari, and L. Simoni, “Aging Phenomenology and Modeling”, IEEE Trans. Dielectr. Electr. Insul., Vol. 28, pp. 755-776 1993.

[16] D. W. Levi, L. Reich, and H.T. Lee, “Degradation of Polymers By Thermal Gravimetric Techniques”, Polym. Eng. and Sci., Vol. 5, pp. 135-141, 1965.

[17] S. Vyazovkin, “Kinetic concepts of thermally stimulated reactions in solids: a view from a historical perspective”, Int. Rev. in Phys. Chem., Vol. 19, pp. 45-60, 2000.

[18] H. Friedman, “Kinetics of Thermal Degradation of Char-forming Plastics from Thermo-gravimetry: Applications to a Phenol Plastic.” J. Polym. Sci., Vol. 6C, pp. 183-195, 1963.

[19] P. Hondred, S. Yoon, N. Bowler, E. Moukhina, and M. Kessler, “Degradation Kinetics of Polyimide Film”, High Perform. Polym., Vol. 23, pp. 335-342, 2011.

[20] J. Artbauer, “Electric strength of polymers”, J. Phys. D: Appl. Phys., Vol. 29, pp. 446-456, 1996.

[21] L. Reich, and S.A. Stivala, “Elements of polymer degradation”, New York: McGraw-Hill, 1971.

CHAPTER 5: TUNG OIL-BASED THERMOSETTING POLYMERS FOR SELF-HEALING APPLICATION

A paper submitted to *Biomacromolecules*

Peter R. Hondred[1], Leo Salat[1], Josh Mangler[2], and Michael R. Kessler[1]

5.1 Abstract

Several bio-renewable thermosetting polymers were successfully prepared from tung oil through cationic polymerization for the use as the healing agent in self-healing microencapsulated applications. The tung oil triglyceride was blended with its methyl ester, which was produced by saponification followed by esterification. The changes in storage modulus, loss modulus, and glass transition temperature as functions of the methyl ester content were measured using dynamic mechanical analysis. In addition, the fraction of cross-linked material in the polymer was calculated by Soxhlet extraction, while proton nuclear magnetic resonance, Fourier transform infrared spectroscopy and TEM were used to investigate the structure of the copolymer networks. The thermal stability of the thermosets as a function of their methyl ester blend contents was determined by thermogravimetric analysis. Finally, the adhesive properties of the thermosets were studied using compressive lap shear tests and the fracture surfaces were analyzed using SEM.

5.2 Introduction

Since the late 1950s, the field of polymers and composites has seen unparalleled growth in this country and world-wide [1]. With this development came the realization that the fossil feedstocks used in the manufacture of traditional polymers are being depleted at a rapid pace [2]. Consequently, petroleum shortages, increasing prices, and environmental concerns are a threat to sustained growth and economic viability of traditional plastics in the industry. Thermosetting polymeric materials must overcome additional environmental concerns, because a majority of petroleum-based materials are non-biodegradable [3,4]. In order to allow further expansion of polymers and composites in a variety of applications, new polymers derived from renewable feedstocks must be developed for the benefit of economy and environment.

Limited research has been performed on the development of high molecular weight polymers from fats and oils [5,6]. One such renewable feedstock avenue under investigation is vegetable oils such as corn, soybean, peanut, canola, tung, and castor oil. R. Larock et al. showed that the unsaturation in the fatty acid chains can be utilized to produce crosslinking thermosetting polymers [7-11]. These polymers exhibit good thermomechanical properties as well as excellent dampening properties [10,12]. In addition, these renewable feedstocks provide varying degrees of unsaturation depending on the oil chosen, so customization for individual polymer applications is readily available.

Targeted variations in fatty acid chain composition allows for the creation of a wide range of material properties. In this work, the thermo-mechanical properties of bulk polymers derived from vegetable oil are investigated as potential healing agents for self-healing applications — specifically crack filling healing [13]. Although there are multiple methods to

approach crack filling healing, all methods rely on the fact that the healing agent polymerizes in the apparent crack and solidifies, creating an adhesive bond to arrest further crack development and maintain the plastic's mechanical integrity [13]. Figure 5-1 illustrates the microencapsulation strategy for crack filling healing.

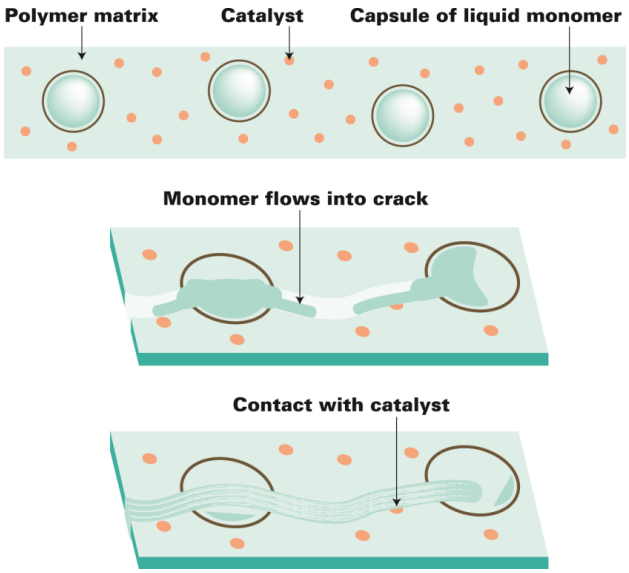

Figure 5-1. Microencapsulation technique with liquid encapsulated monomer and an imbedded solid catalyst

The initial work by Larock et al. indicated that these vegetable oil thermosets present potential for self-healing applications. An effective healing agent must meet the following requirements:

1. Materials must exhibit low viscosity, volatility, and good wettability properties.
2. Minimal diffusion through matrix and fast reaction kinetics.
3. Good adhesive strength and mechanical properties of resulting polymer.

This work utilized a cationic polymerization process for tung oil (a reactive vegetable oil), and blended comonomers to modify viscosity, wettability, reaction kinetics, adhesive strength, and mechanical properties. Previous work showed that comonomers such as styrene and divinylbenzene reduced the non-uniformity of the crosslinking structure and improved the mechanical integrity of the resulting polymers [14]. In addition, methyl ester derivatives of tung oil were blended with tung oil triglyceride in order to modify the crosslink density of the thermosetting network. The primary focus of this paper is on the effect of methyl ester on both the properties of the monomers as well as the properties of the thermosetting polymer. It is anticipated to utilize varying compositions to accommodate the composite material into which these healing agents will be imbedded.

While recent developments in high modulus bioplastics produced materials whose properties resembled those of unsaturated polyesters, current work on self-healing materials utilizes almost exclusively petroleum-based materials. Polymers produced utilizing the unsaturation in vegetable oils are the first step in providing viable material alternatives in the self-healing field.

5.3 Materials

In this work, tung oil, also known as China wood oil, was used. While the common China wood oil for wood finishing, available from any hardware or carpentry store, is suitable for the polymerization process, here we used tung oil purchased from Sigma-Aldrich for ease of supply stability and material consistency. Varying amounts of tung oil methyl ester produced by saponification and esterification of the tung oil itself were blended with the

tung oil. Styrene and divinylbenzene were also purchased from Sigma-Aldrich. Synthesis grade boron trifluoride diethyl etherate ($BF_3 \cdot OEt_2$) purchased from Sigma-Aldrich was used as initiator for the cationic polymerization process. The initiator was mixed with SG1100 (a soybean oil methyl ester purchased from SoyGold, Omaha, NE) to enhance solubility. Figure 5-2 and Figure 5-3 show the structures of tung oil and its corresponding methyl ester, respectively. Tung oil triglycerides are composed of several different fatty acids. The figures show triglycerides and methyl esters based on the dominant fatty acid, α-eleostearic acid, which comprises 82% of the fatty acid chains. This fatty acid is identified by three conjugated double bonds. The remaining 18% fatty acids exhibit less reactive levels of unsaturation.

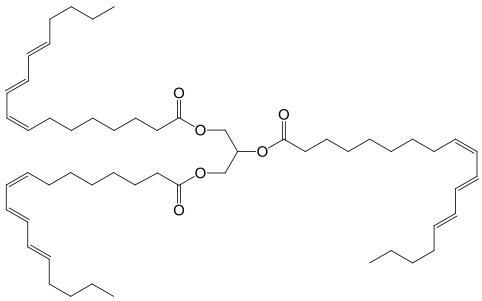

Figure 5-2. Tung oil triglyceride

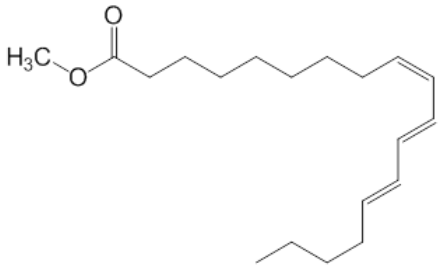

Figure 5-3. Tung oil methyl ester

5.4 Synthesis

The following polymerization process was employed unless explicitly stated otherwise: First, the monomers were hand-mixed at room temperature in predetermined ratios according to Table 5-1. The initiator, boron trifluoride diethyl etherate, and its solubility enhancer were hand-mixed at room temperature separately because boron trifluoride diethyl etherate is moisture sensitive. Therefore, initiator and enhancer were mixed in an inert environment, i.e., in a glove box, sealed in a vial, and removed by syringe as required for the reaction.

The monomer mixture was placed on a stir plate inside an ice bath. Once the monomers had cooled down to 0 °C in the ice bath, a stir bar was placed in the mixture, and the initiator was added via syringe while constantly mixing. The sample was allowed to mix for 10 seconds and then was removed from the ice bath to solidify. Within a matter of seconds, the sample solidified in the vial. Samples were post-cured in the oven for 1 hour at 120 °C to complete the polymerization process. The reaction was a cationic process (shown in Figure 5-4), in which the initiator, boron trifluoride diethyl etherate, reacted with the unsaturation sites in the monomers. Different compositions for these thermosetting polymers are listed in Table 5-1.

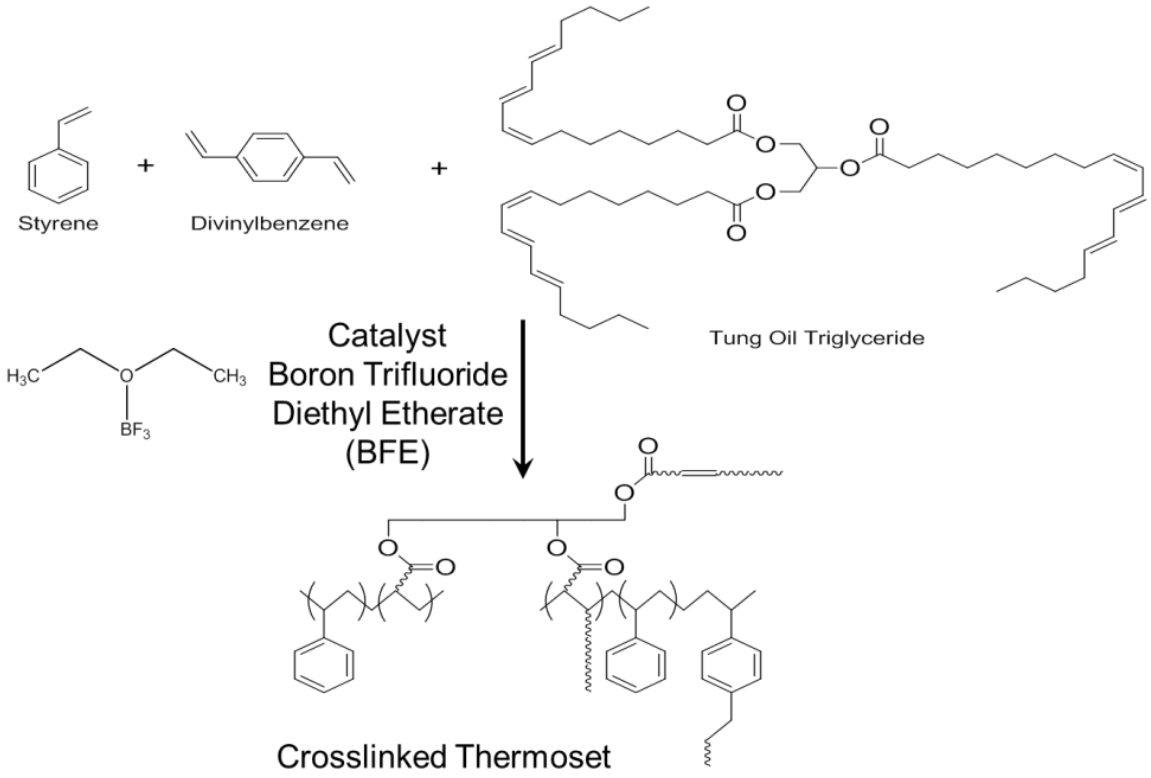

Figure 5-4. Cationic polymerization of tung oil, styrene, and divinylbenzene

Table 5-1. Variation in composition of thermosetting biopolymers in wt.%

	Tung oil triglyceride	Tung oil methyl ester	Styrene	Divinylbenzene	Initiator
47.0% Tung oil	47.0%	0%	30%	15%	8%
42.3% Tung oil	42.3%	4.7%	30%	15%	8%
37.6% Tung oil	37.6%	9.4%	30%	15%	8%
32.9% Tung oil	32.9%	14.1%	30%	15%	8%
28.2% Tung oil	28.2%	18.8%	30%	15%	8%

*The initiator was comprised of 5% SoyGold and 3% $BF_3{\cdot}OEt_2$

The changes in material properties as a function of methyl ester blend were investigated. Tung oil was removed and replaced with its respective methyl ester derivative to change the composition of the polymer. Tung oil methyl ester monomer for synthesis was created by saponification and esterification. For saponification (the cleaving of the fatty acid

chains) 100 g of tung oil and 200 cc of NaOH (10%) solution were mixed, heated for 2 h, and stirred until emulsified. Once emulsified, 300 cc of water was added and the mixture was heated for an additional 30 min. Once the solution became translucent, indicating complete saponification, it was poured into 650 cc of hot water with 100 cc of 20% hydrochloric acid and was heated for an additional 20 minutes until it was transparent. Cooling in an ice bath under constant stirring, the solution solidified into small agglomerations. These agglomerations of fatty acid were washed with water to remove excess salts. Finally, the fatty acid agglomerations required further drying to remove any residual water trapped during the solidification in the cooling-down period, which was accomplished by heating above melt temperature and extracting the phase-separated water. Once the fatty acid was obtained, it was converted into methyl ester by esterification.

For esterification, 50 g tung oil fatty acid was dissolved in 500 ml of methanol and placed on a hot plate to facilitate dissolution. Once dissolved, a catalytic amount of sulfuric acid was added under constant mixing. The solution was distilled for 2 hours and the reaction was monitored for completion using thin-layer chromatography. Once the fatty acid was converted into methyl ester, the solvent was removed utilizing a rotary evaporator. Subsequently, an aqueous workup was used to wash out the acid with water and ethyl ether anhydrous. Mixing with magnesium sulfate for 15 min removed any residual water. Finally, the magnesium sulfate was removed by filtering and washing with ethyl ether anhydrous and tung oil methyl ester was isolated by rotary evaporation. The purity of the sample was verified through NMR. The process of saponification and esterification is shown in Figure 5-5.

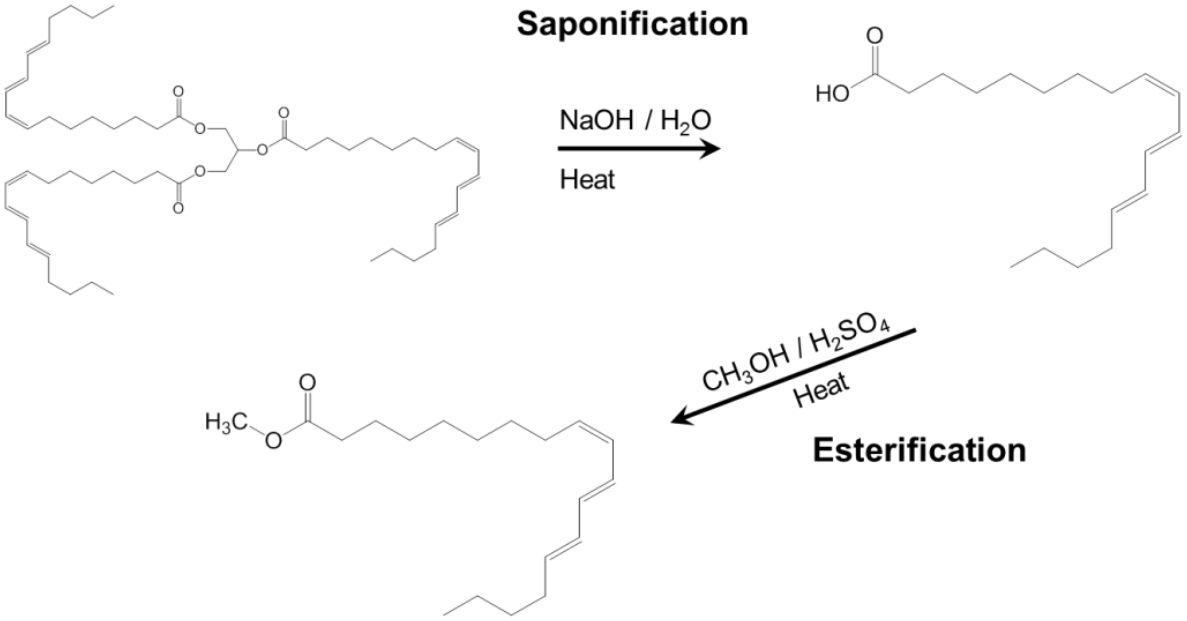

Figure 5-5. Saponification and esterification of tung oil to obtain the methyl ester derivative

5.5 Results and Discussion

Dynamic mechanical analysis was performed on samples with the five different compositions described in Table 5-1. The DMA results are shown in Figure 5-6, Figure 5-7, and Figure 5-8. All tests were run at a fixed heating rate of 10 °Cmin^{-1}. Figure 5-6 shows the change in storage modulus as a result of change in monomer ratios. As tung oil methyl ester was substituted for tung oil triglyceride, the storage modulus in both the glassy and rubbery regions decreased. These data were used to calculate the crosslink density of the thermoset. Crosslink density was determined by calculating the polymer's molecular weight between the crosslinking points. This molecular weight value is calculated from the rubbery plateau (secondary (lower) region in the temperature values of 100 – 150 °C) of the storage modulus found in Figure 5-6.

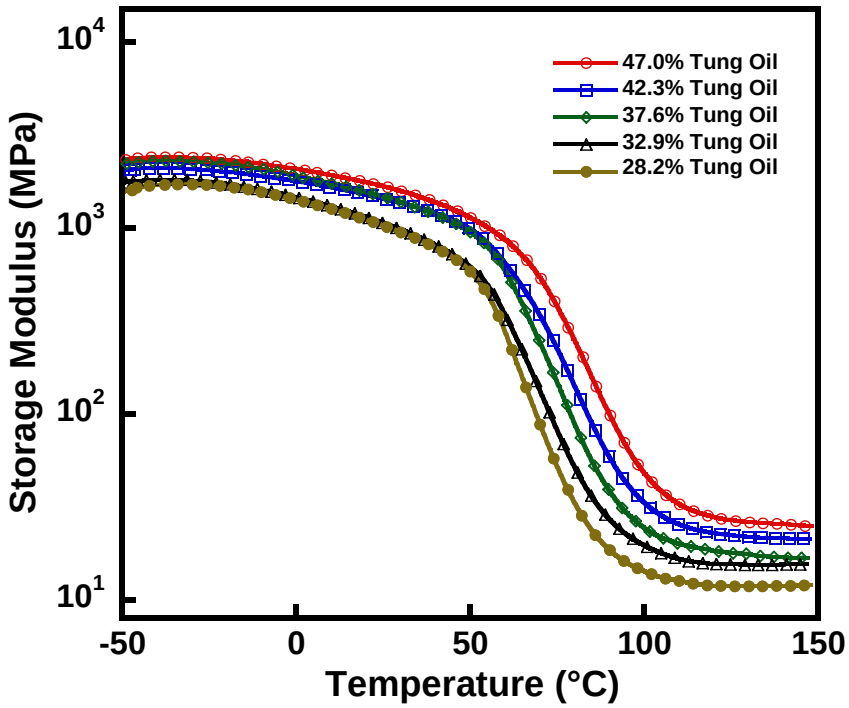

Figure 5-6. Storage modulus of bio-renewable thermosets with varying amounts of methyl ester.

The molecular weight of the chain between crosslink sites, M_c, was utilized to compare the crosslink density of the different polymer compositions, because as the molecular weight between the crosslinks increased, the crosslink density decreased [15]. The following equation is used to calculate the molecular weight between crosslinks:

$$M_c = \frac{3qdRT}{E'_{T_g+50K}} \quad (1)$$

where E'_{T_g+50K} represents the storage modulus at 50 K above the glass transition temperature determined by the maximum peak value of tan δ in Figure 5-7. The variables q, d, R, and T

are the front factor, density of the material, gas constant, and temperature at 50 K above the glass transition temperature, respectively [15]. Here, q = 1 as is standard for the majority of polymers [16]. Table 5-2 provides the crosslink density for the different compositions of tung oil derived thermosets. As expected, the crosslink density decreased, as indicated by the increasing molecular weight between crosslinks, with increasing methyl ester because of fewer available glycerol bonds in the triglyceride.

Table 5-2. Molecular weight between crosslinks.

	47.0% Tung Oil	**42.3% Tung Oil**	**37.6% Tung Oil**	**32.9% Tung Oil**	**28.2% Tung Oil**
M_C	$0.47\ \frac{kg}{mol}$	$0.55\ \frac{kg}{mol}$	$0.67\ \frac{kg}{mol}$	$0.75\ \frac{kg}{mol}$	$0.97\ \frac{kg}{mol}$

Figure 5-7 provides the phase angle, tan δ, for the different compositions of tung oil derived polymers. For each composition, the maximum value of tan δ represents the glass transition temperature listed in Table 5-3. Similar to the decrease in storage modulus, a systematic decrease in tan δ was expected with increasing loading of tung oil methyl ester, because the methyl ester reduced the crosslink density and subsequently increased the free volume and molecular motion and therefore the glass transition temperature decreased.

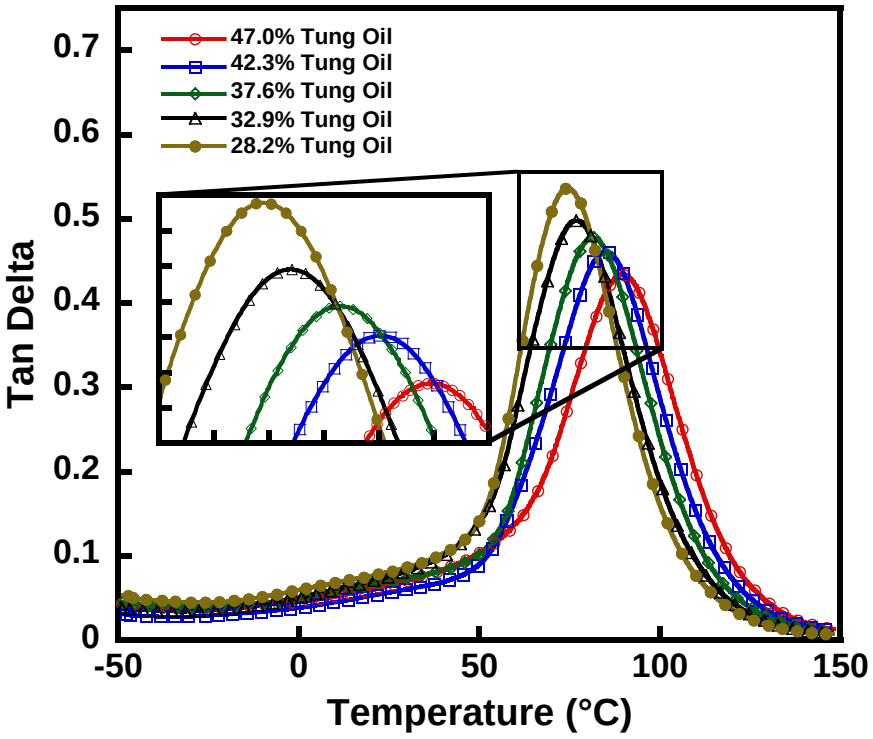

Figure 5-7. Tan δ of bio-renewable thermosets with varying amounts of methyl ester.

Table 5-3. Glass transition temperature based on DMA analysis

	47.0% Tung Oil	42.3% Tung Oil	37.6% Tung Oil	32.9% Tung Oil	28.2% Tung Oil
T_g	89.7 °C	85.1 °C	81.1 °C	76.8 °C	74.5 °C

The loss modulus, shown in Figure 5-8, indicates that phase separation took place. The 47.0% tung oil sample showed one single peak around the 80 °C mark typical for a mostly homogenous polymer. However, as methyl ester was introduced to the formulation, a secondary peak formed, indicating either phase separation or heterogeneous mixing. In addition, the pronouncement of the lower peak increased and shifted to lower temperatures with increasing methyl ester content. The reactivity of methyl ester was higher than that of

tung oil triglyceride, therefore the methyl ester reacted earlier and created a softer phase in the polymer.

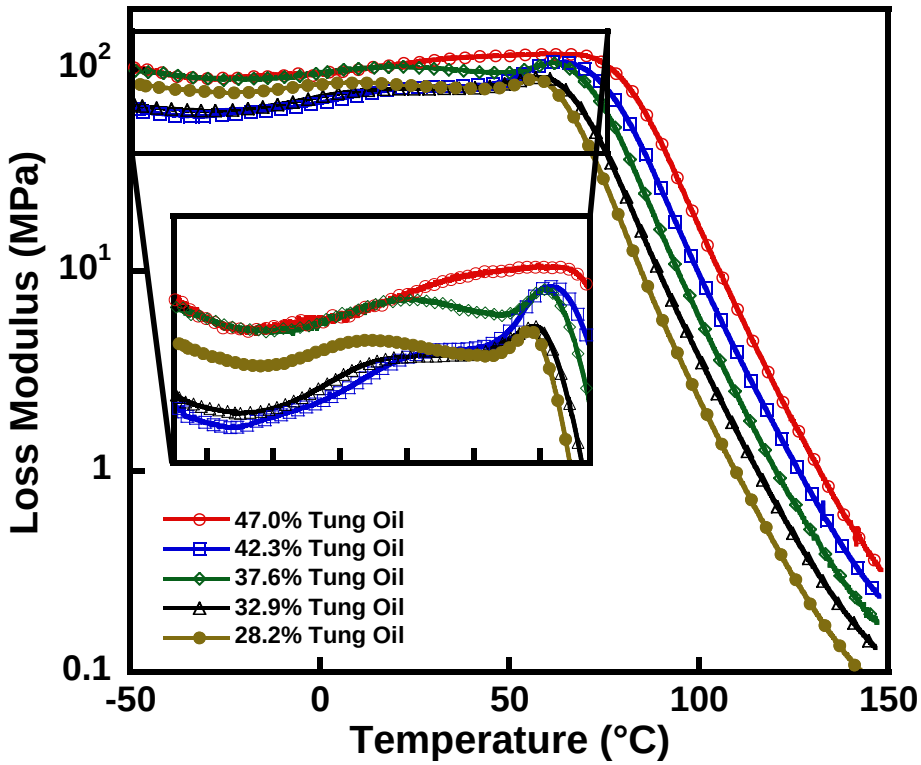

Figure 5-8. Loss modulus of bio-renewable thermosets with varying amounts of methyl ester.

The higher reactivity of the methyl ester was corroborated through differential scanning calorimetry of the curing polymer seen in Figure 5-9. With increasing methyl ester content the heat flow curve formed an additional reaction peak, indicating that tung oil methyl ester reacted faster than the other constituents in the thermoset.

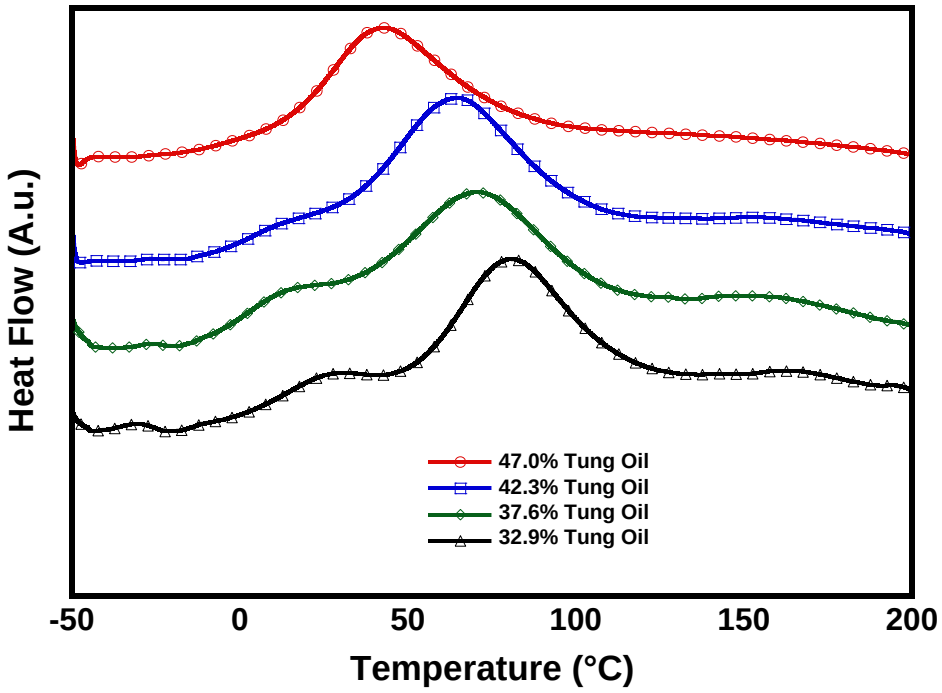

Figure 5-9. Curing of tung oil composites once mixed. Test run at a temperature rate of 3 °C per min

Note: Samples of 28.2% tung oil were not tested because the reaction accelerated too fast to capture it

Because the loss modulus curves indicated phase separation, transmission electron microscopy was used to investigate the microstructure of the thermosetting networks of 32.9% and 47.0% tung oil polymers. The TEM images in Figure 5-10, especially at the 10 nm scale, show phase separation in both samples investigated. The phase separation is shown as light and dark regions in the TEM images. Styrene and divinylbenzene have high electron densities due to their phenolic rings, therefore phases rich in styrene and divinylbenzene are depicted as dark areas in the TEM images. Consequently, the lighter areas represent triglyceride and methyl esters. The TEM images show phase separation on the scale of three

to five nanometers. At this small scale, the phases consist of only a few molecules, possibly bordering on a random co-block structure.

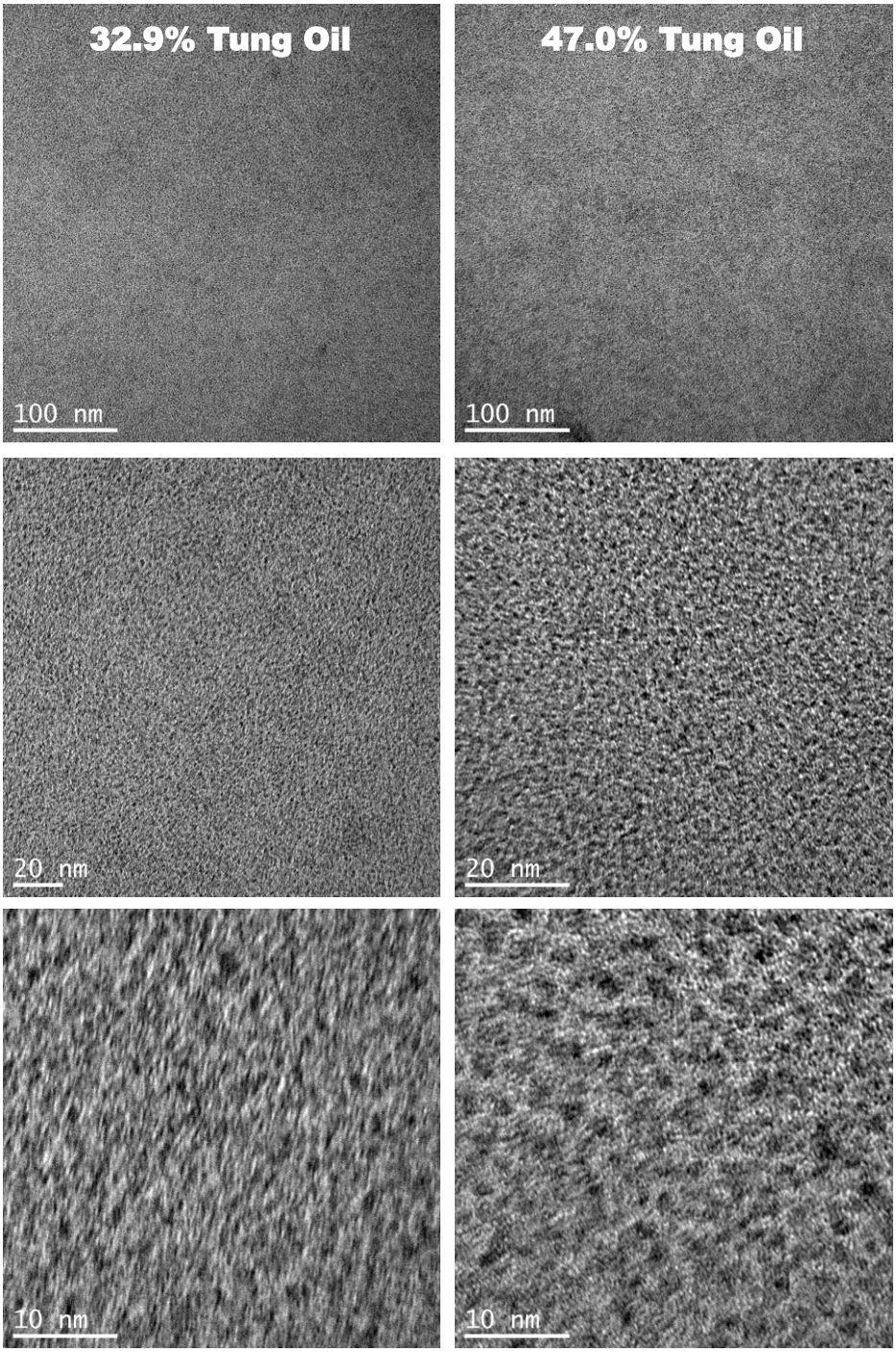

Figure 5-10. TEM of 32.9% and 47.0% tung oil polymers

While using storage modulus to identify the crosslinking regularity, the molecules involved in the crosslinking are not identified. Soxhlet extraction identifies monomers that are incorporated into the thermoset network and the monomers that are not interconnected. The thermosets were washed with a refluxing solvent for 24 h in a Soxhlet extractor to remove the soluble portion of the polymer. The monomer components not incorporated into the network were dissolved in the solvent and then separated and identified by NMR. Figure 5-11 shows the NMR data from the soluble portion of the thermosets. As seen in the figure, the majority of the soluble portion represented various methyl esters. The first obvious methyl ester detected was the SoyGold used to homogenize the BFE during mixing. SoyGold has few double bonds and none are conjugated, therefore the reactivity of SoyGold is low and it was not incorporated into the thermosetting network. In addition, tung oil fatty acids are only 82% α-eleostearic acid, which is the fatty acid with three conjugated double bonds. The remaining mixture is constituted by several other fatty acids—fatty acids with much less reactivity due to fewer double bonds and less conjugation. Because the esterification and saponification process cannot separate these fatty acids from the α-eleostearic acid, the tung oil methyl ester added to the reaction contains all the variations of methyl ester derived from the fatty acids, including those that do not incorporate into the crosslinked network. The NMR shows that these methyl esters are not being incorporated. Peaks forming at 0.5 – 4.0 show key resonance of general methyl esters. This peak range also contains the identifiers for the SoyGold methyl ester used as a solubility enhancer. Peaks above 4.0 show other minor components that were not incorporated, such as remaining glycerin bonds broken from the triglyceride during the saponification and benzene rings from a few styrene and

divinylbenzene monomers that were not tied into the network. Table 5-4 shows the weight percentage of extractable components in the fully cured thermoset. While the soluble content increased with increasing methyl ester content, the majority of the tung oil methyl ester was incorporated into the network.

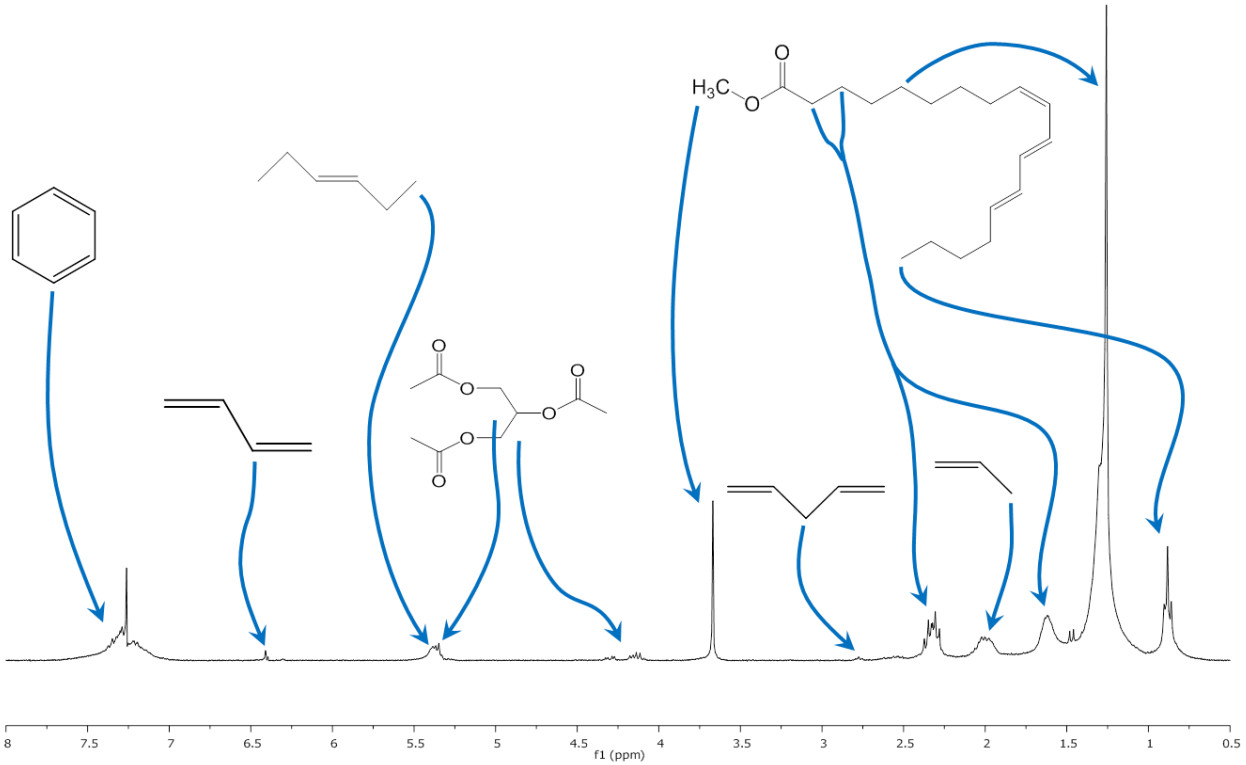

Figure 5-11. NMR of Soxhlet extraction of bio-renewable thermosets with varying amounts of methyl ester.

Table 5-4. Weight percentage of soluble thermoset content

	47.0% Tung oil	**42.3% Tung oil**	**37.6% Tung oil**	**32.9% Tung oil**	**28.2% Tung oil**
wt%	3.3%	4.2%	5.2%	7.4%	9.5%

Figure 5-12 shows the thermal stability of the thermosets. Thermogravimetric analysis showed that tung oil triglyceride underwent significant mass loss at approx. 275 °C, while neat tung oil methyl ester exhibited significant mass loss at 175 °C. Despite the large difference between thermal stability of methyl ester and triglyceride, the thermal stability of the thermosets did not show a significant reduction.

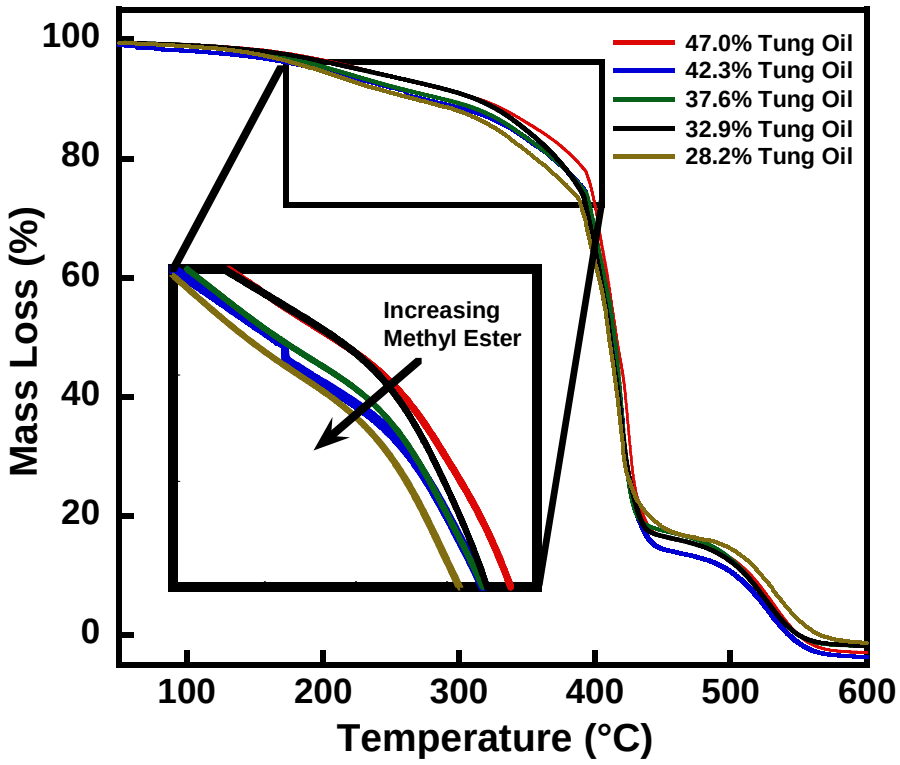

Figure 5-12. Thermogravimetric analysis of bio-renewable thermosets with varying amounts of methyl ester.

The thermosets underwent compressive lap shear testing according to ASTM D3846-08 to investigate their adhesive properties. Because the thermosets were to be used as self-healing adhesives for bio-composites, the lap shear specimens were made from glass fiber

bio-composites similar in composition to the bio-composites proposed for self-healing applications. The bio-composites were used solely as a substrate to which the tung oil based thermosetting polymer was applied. Figure 5-13 shows the lap shear strength values for tung oil-based thermoset samples.

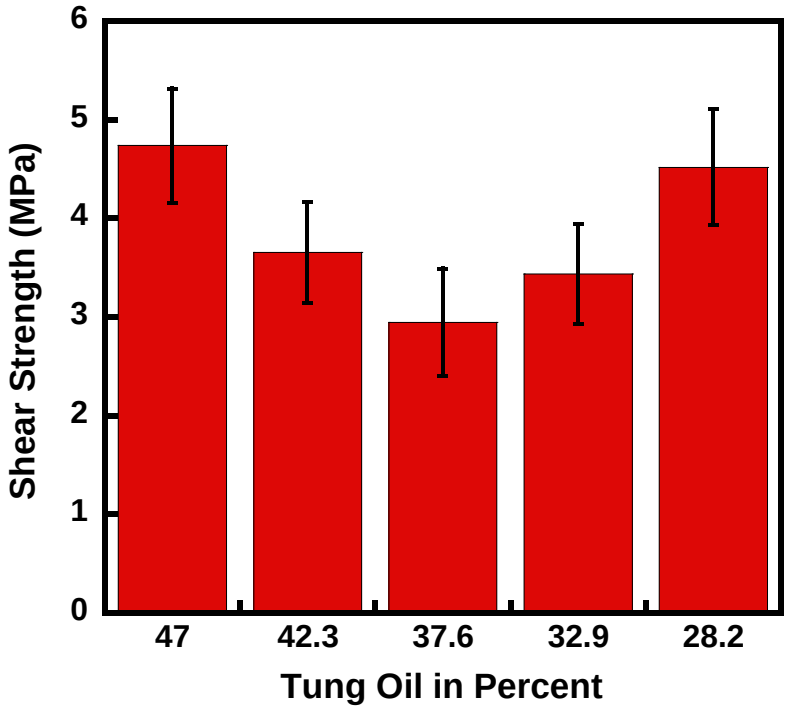

Figure 5-13. Compressive lap shear strength of bio-renewable thermosets with varying amounts of methyl ester.

Scanning electron microscopy of the sheared surfaces showed how the polymer fractured under compressive shear stress, see Figure 5-14 and Figure 5-15. The SEM images revealed adhesive failure when the thermoset did not contain methyl ester. As the loading of methyl ester increased, the failure mode shifted to a cohesive failure as seen in the SEM images for 28.2% and 32.9% tung oil thermosets. In both cases, fiber pullout was clearly

detected. In addition, SEM analysis showed that the thermosets transitioned from a brittle to a ductile failure mode. In thermosets without methyl ester components, the fracture surfaces showed brittle shearing, while increasing methyl ester content led to ductile failure of the thermosets. The fracture surfaces for the 42.3%, 37.6%, and 32.9% tung oil based thermosets showed signs of microcracks on the fracture surface. These microcracks formed in samples transitioning from brittle to ductile failures. The low shear stress value for 37.6% tung oil thermosets is likely caused by a combination of several factors—brittle to ductile transition, adhesive to cohesive failure transition, and microcracks. Figure 5-15 shows a higher magnification of the fracture surfaces to highlight the microcracks, fiber pullout, and ductile verse brittle failures.

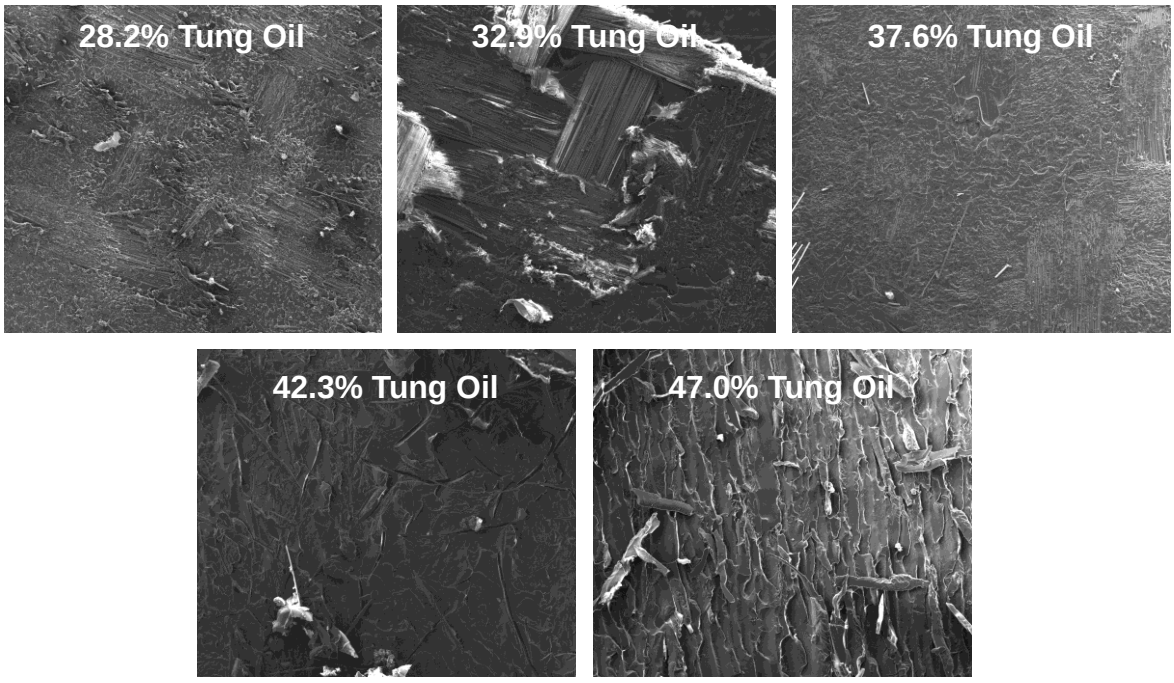

Figure 5-14. Lower magnification (75×) SEM images of crack surfaces

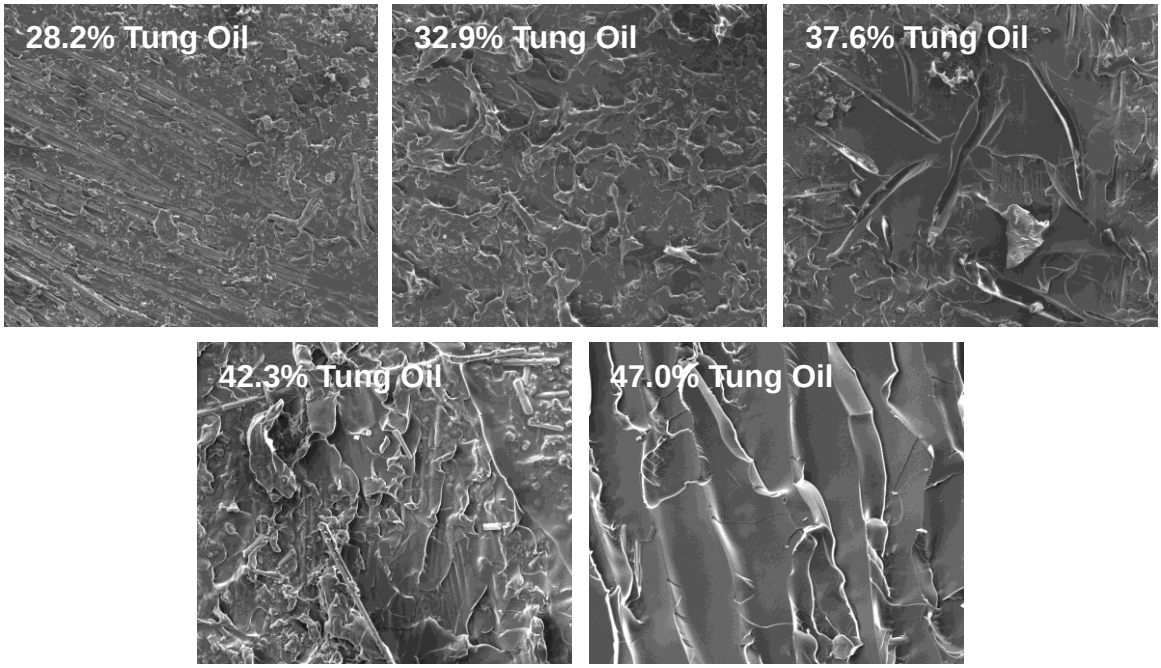

Figure 5-15. Higher magnification (300×) SEM images of crack surfaces

5.6 Conclusion

Tung oil methyl ester can be utilized to modify the properties of tung oil based thermosetting polymers. This modification provides a uniform change in storage modulus and glass transition temperature, useful when tailoring to a specific application. In addition, methyl ester content increased the reactivity of the thermosets, which provided an added benefit because self-healing applications require rapid kinetic reactions. The thermal stability of the thermosets was not compromised by the addition of methyl ester.

While the addition of methyl ester caused a mixed shear stress response, all thermosets investigated provided more than adequate adhesive strength to cure microcracks. However, with an increase in methyl ester content, the thermosets exhibited cohesive failure, caused by the failure to maintain the bonds between fiber and matrix. Possible fiber

treatments may improve the cohesive bonding of the polymer and consequently improve the shear strength properties.

For self-healing applications, thermosetting materials made from tung oil triglycerides, tung oil methyl esters, styrene, and divinylbenzene provided excellent material properties. Their mechanical properties and thermal stability identified them as structurally sound and stable candidates for crack healing. In addition, the low viscosity and fast kinetics provided for the required properties for flowing into a microcracks and solidifying in the crack plane. Once cured, these thermosets offered good adhesive properties, sustaining shear stresses exceeding 1 MPa. While in the past encapsulated self-healing work has been dominated by petroleum-based monomers, biorenewable materials, such as tung oil, can provide the low viscosity, fast kinetics, mechanically sound, and thermally stable thermosets that is able to arrest microcracking.

5.7 References

[1] Osswald, T. A.; Menges, G. Materials Science of Polymers for Engineers. Hanser Gardner: Cincinnati, 2003, p 16.

[2] Chiellini, E.; Cinelli, P.; Corti, A. Developments and Future Trends for Environmentally Degradable Plastics. In Renewable Resources and Renewable Energy: A Global Challenge. Graziani, M.; Fornasiero, P., Eds. CRC Press: Boca Raton, FL, 2007, p 63.

[3] Bisio, A. L.; Xanthos, M. How to Manage Plastics Waste: Technology and Market Opportunities; Hanser Publishers: Munich, New York, 1995.

[4] Mustafa, M. Plastics Waste Management: Disposal, Recycling, Reuse; Marcel Dekker: New York, 1993.

[5] John, L. A.; Myers, D. J. New soybean oil–styrene–divinylbenzene thermosetting copolymers. II. Dynamic mechanical properties. In Practical Handbook of Soybean Processing and Utilization; Erichson, D. R., Ed.; American Soybean Association, St. Louis, MO; The American Oil Chemist's Society: Champaign, IL, 1995.

[6] Formo, M. W. In Bailey's Industrial Oil, Fat Products, Vol. 2, 4th ed.; Swern, D., Ed.; Wiley: New York, 1982, p 343.

[7] Larock, R. C.; Li, F. Thermosetting Polymers from Cationic Copolymerization of Tung Oil: Synthesis and Characterization, J. Appl. Polym. Sci. 2000, 78, 1044.

[8] Li, F.; Hanson, M. V.; Larock, R. C. Soybean Oil-Divinylbenzene Thermosetting Polymers: Synthesis, Structure, Properties and Their Relationships, Polymer 2001, 42, 1567.

[9] Li, F.; Larock, R. C. Novel Polymeric Materials from Biological Oils, J. Polymers and the Environment 2002, 10, 59.

[10] Li, F.; Hasjim, J.; Larock, R. C. Synthesis, Structure, Thermophysical and Mechanical Properties of New Polymers Prepared by the Cationic Copolymerization of Corn Oil, Styrene and Divinylbenzene, J. Appl. Polymer Sci. 2003, 90, 1830-1838.

[11] Li, F.; Larock, R. C. Synthesis, Structure and Properties of New Tung Oil-Styrene-Divinylbenzene Copolymers Prepared by Thermal Polymerization, Biomacromolecules 2003, 4, 1018-1025.

[12] Andjelkovic, D. D.; Lu, Y.; Kessler, M. R.; Larock, R. C. Novel Rubbers from the Cationic Copolymerication of Soybean Oils and Dicyclopentadiene, 2-Mechanical and Damping Properties, Macromol. Mater. Eng. 2009, 294, 472-483.

[13] T. C. Mauldin, M. R. Kessler : Self-healing Polymers and Composites, International Materials Reviews. 2010, 55(6), 317-346

[14] Li, F.; Larock, R. C. J. Polym. Sci. Part B: Polym. Phys. 2000, 38, 2721; 2001, 39, 60.

[15] X. Sheng, J. K. Lee, M. R. Kessler. The Influence of Cross-link Density on the Properties of ROMP Thermosets, Polymer. 2009; 50, 1264-1269

[16] G. Levita, S. DePetris, A. Marchetti, A. Lazzeri. Crosslink density and fracture toughness of epoxy resins J Mater Sci, 26 (1991), pp. 2348–2352

CHAPTER 6: RARE EARTH TRIFLATE INITIATORS IN THE CATIONIC POLYMERIZATION OF TUNG OIL-BASED THERMOSETTING POLYMERS FOR SELF-HEALING APPLICATIONS

A paper ready for submission

Peter R. Hondred, Carole Autori, and Michael R. Kessler

6.1 Abstract

Rare earth triflates were successfully used to initiate the cationic polymerization of tung oil based thermosetting polymers. These bio-renewable thermosets are developed and evaluated for use as an encapsulated healing agent in self-healing materials. The tung oil based polymer is comprised of predominantly tung oil with styrene and divinylbenzene used as a reactive diluent and to improve the initiator solubility and homogeneity of the resulting thermoset. While traditional cationic polymerization utilizes moisture sensitive Lewis acids as initiators, rare earth triflates offer a new approach to polymerization where moisture sensitivity is not a significant concern. Nine different rare earth triflates were investigated—ytterbium, scandium, samarium, cerium, gadolinium, erbium, terbium, holmium, and neodymium. The thermosets were tested for their thermomechanical properties and the analysis included effects of initiator type on the storage modulus, loss modulus, tan delta, glass transition temperature and thermal stability. Finally, the adhesive properties of the thermosets were

studied using compressive lap shear tests and the fracture surfaces were analyzed using scanning electron microscope and energy-dispersive X-ray spectroscopy.

6.2 Introduction

Recent projections speculate that the fossil feedstock reserves required for traditional polymer development will be depleted in the next 80 years at the current trends for petroleum usage [1]. The petroleum reserves have been used since the 1950s and their use for plastic has only expanded exponentially both in this country and world-wide as the field of polymers and composites grows in size and scope [2]. Without finding additional feedstocks, petroleum prices will necessarily increase and supply decrease resulting in great concerns to the viability of the traditional plastics industry. However, alternative feedstocks from renewable resources are gaining traction in the polymer and composites industry. In order to supply the feedstock required to replace even a portion of the petroleum used in plastic, continued work on thermoplastic and thermosetting materials is required.

Renewable feedstocks such as carbohydrates, starches, and proteins have all offered promise to replace petroleum and have consequently been studied extensively. However, few renewable feedstocks offer high molecular weight polymers capable of replacing petroleum products requiring enhanced material properties. One such option as shown by R. Larock and M. Kessler is the polymerization of agricultural oils such as soybean, corn, caster, tung, and linseed [3,4]. Limited research has been performed on the development of high molecular weight polymers from fats and oils [5,6]. However, these oils, which are one of the most

abundant and inexpensive renewable materials, have been shown to provide excellent mechanical properties once polymerized [7,8].

These oils, or triglycerides, are comprised of three fatty acids connected with a glycerin bond. The unsaturation in the fatty acid chains provides reactive sites for the thermosetting network as seen by R. Larock et al. [9-13]. These polymers exhibit good thermo-mechanical properties as well as excellent dampening properties [4,10]. To produce these polymers, a process known as cationic polymerization uses an intiator, typically a Lewis acid, to begin the polymerization process in the fatty acid chain of the triglyceride. Cationic polymerization is a chain growth process where the cationic initiator transfers its charge to a monomer which becomes reactive. Since each oil offers a different reactivity do to the number and location of the unsaturation in the fatty acids, the mechanical properties of the resulting polymers can be customized for the resulting bio-renewable polymer by carefully choosing the oils for the starting monomer blend.

In this work, rare earth triflates are used as the initiator to transfer the charge to the unsaturated areas of the fatty acid chains. One major drawback in cationic polymerization is the moisture and air sensitivity of the cationic initiator. Most Lewis acids, especially the chiral molecules, are sensitive to moisture and air resulting in decomposition or deactivation of the acid [14]. However, Kobayashi et al have shown that lanthanide triflates are effective catalysts while maintaining stability in water [15-17]. Additionally, these triflates have been proven effective in the ring opening polymerization of DGEBA and cycloaliphatic epoxy resins [18,19]. Additionally, rare earth triflates have been used to cationically cure epoxy resin/polyimide systems [20]. This work specifically investigates the effectiveness of utilizing rare earth triflates as a cationic initiator in agricultural oil systems and compares

how the thermo-mechanical properties change as a result of changing the rare earth triflate chosen to begin the polymerization process.

Self-healing polymers, which traditionally are not bio-based, but bio-inspired, are designed to elicit a healing response at the site of damage. Typically, these polymers incorporate an encapsulated liquid healing agent, which is released into a crack plane upon damage. The released healing agent encounters an embedded initiator and polymerizes to bond the crack surfaces closed [13]. As was the case with previous work on vegetable oils, the thermo-mechanical and adhesive properties of the resulting thermosets are investigated for potential healing agents in self-healing applications [21]. The proposed strategy for self-healing through microencapsulated healing agents is seen in Figure 6-1.

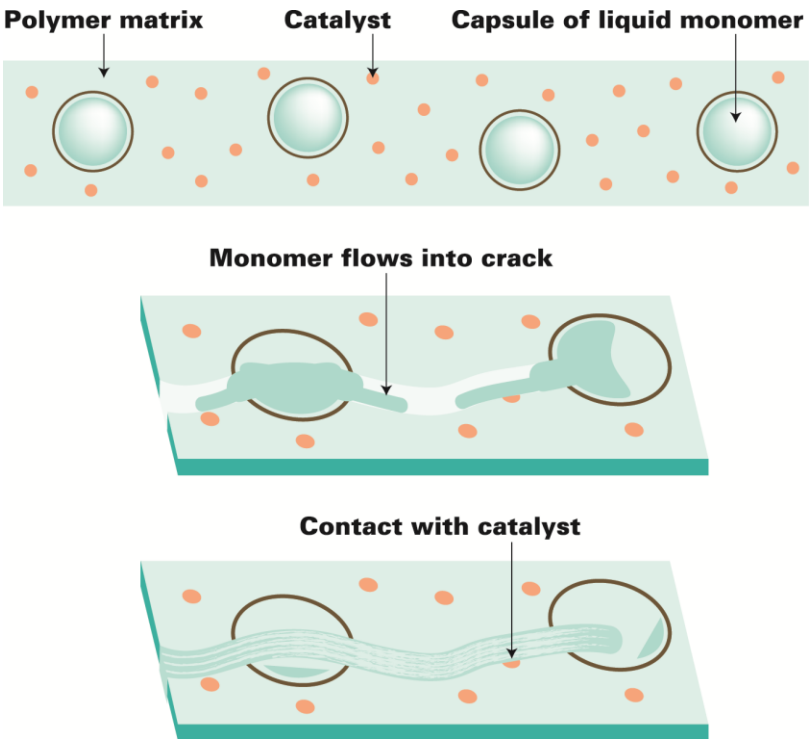

Figure 6-1. Microencapsulation technique with liquid encapsulated monomer and an imbedded solid catalyst

The agricultural oils would be encapsulated into the capsules holding the liquid monomer and the rare earth triflates would be imbedded directly into the matrix so that upon crack propogation, the triflate is exposed on the surface for the polymerization process. Previous research has shown that tung oil based thermosetting composites offer an excellent thermo-mechanical properties while also offering good adhesive properties [22]. In that work, a Lewis acid, boron trifluoride diethyl etherate, was used as the cationic initiator [22]. However, for self-healing applications, this initiator is not ideal since it is a liquid and consequently also needs encapsulated and the initiator is also deactivated by moisture. Overcoming the sensitivity to moisture and air as well as eliminating the need for a second encapsulation of the initiator is where rare earth triflates offer major benefit.

To investigate how different rare earth triflates change the mechanical properties of the resulting polymer, nine rare earth triflates are investigates as cationic initiators—ytterbium, scandium, samarium, cerium, gadolinium, erbium, terbium, neodymium, and holmium. These triflates polymerized monomers composed of tung oil, styrene, and divinylbenzene. The resulting polymers were tested for their mechanical properties through dynamic mechanical analysis (DMA). The thermal stability was tested using thermogravimetric analysis (TGA) and differential scanning calorimetry (DSC) was conducted to verify fully cured samples with their respective glass transition temperatures. The samples were also subjected to compressive lapshear testing in order to determine the adhesive properties. Additionally, the fracture surface was studies using SEM to investigate the failure mode of the adhesive.

6.3 Materials

The agricultural oil chosen in this work, tung oil, is commonly referred to as China wood oil and is used for wood finishing in carpentry work. While it is accessible at any hardwood store, the tung oil for this work was purchased from Sigma-Aldrich to maintain material consisitency from sample to sample. Styrene and Divinylbenzene were also purchased from Sigma-Aldrich. The triflates—ytterbium, scandium, samarium, cerium, gadolinium, erbium, terbium, holmium, and neodymium—were all purchased from Sigma-Aldrich to reduce variability from one company to another. Figure 6-2 and Figure 6-3 show the generic structure of rare earth triflates and of tung oil, respectively.

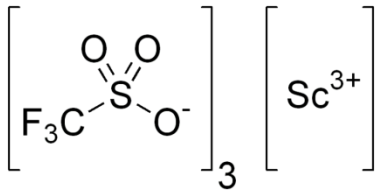

Figure 6-2. Structure of a rare earth triflate (example: scandium)

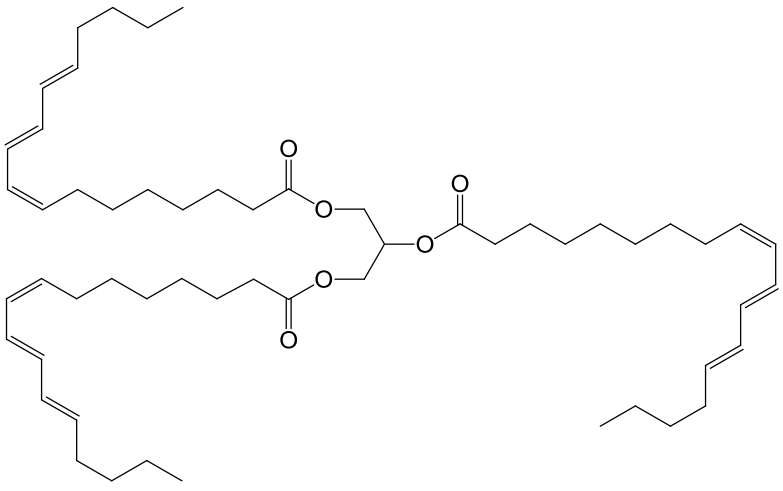

Figure 6-3. Tung oil triglyceride

6.4 Synthesis

The following polymerization process was utilized to make all samples unless explicitly stated. First, the tung oil is blended with its comonomers styrene and divinylbenzene at room temperature and mixed by hand to dissolve the monomers together. Once dissolved, the predetermined amount of rare earth triflate was added to the monomer blend. The samples were mixed with direct horn sonication for 1 minute in an ice bath. Once the rare earth triflate particles were mixed/dissolved in the monomer blend, the sample was placed in a heated sonication bath at 50 °C until solidification. This kept the remaining small triflate particles evenly suspended in the material whereas without the sonication bath, the particles would settle out to the bottom of the mixture. Once solidified, the polymer was placed in an oven for 5 hrs and cured at 120 °C to complete the polymerization process. It should be noted that Samarium and Ytterbium required an additional 4 hrs at 120 °C to fully cure the samples. Figure 6-4 shows the polymerization process for the tung oil biopolymer with rare earth triflates and Table 6-1 provides the composition of the thermoset. The focus of this work is on the changes in mechanical properties of biorenewable thermosetting polymers from tung oil as the cationic initiator is varied. So the monomer composition is consistent for all samples as seen in Table 6-1.

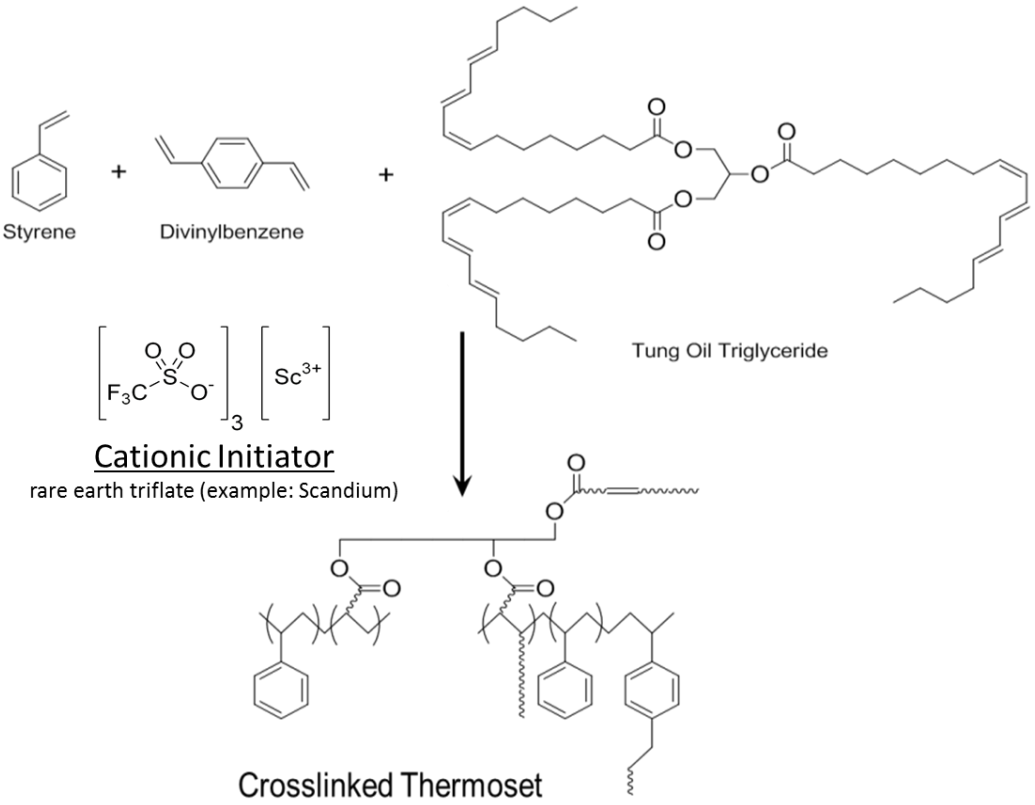

Figure 6-4. Cationic polymerization of tung oil, styrene, and divinylbenzene

Table 6-1. Composition of thermosetting biopolymers in wt.%

	Tung oil triglyceride	Styrene	Divinylbenzene	Initiator
Tung oil	48.5%	31.0%	15.5%	5%

6.5 Results and Discussion

Throughout the synthesis of the polymers, the list of nine rare earth triflates was reduced down to six polymers with good mechanical properties. Three rare earth triflates—neodymium, holmium, and terbium—did not produce consistent polymers for characterization. In fact, both neodymium and holmium did not polymerize in the sonication

bath unlike the rest of the rare earth triflates did even after 24 hrs. Additionally, terbium failed to produce a uniform polymer but instead produced three distinct phases easily distinguishable by color and material hardness.

After the polymers had finished curing in the oven, DSC was conducted to verify full cure. The scans, seen in Figure 6-5, show that each polymer had fully cured. All heat flow scans show broad glass transitions temperatures as well as multiple glass transitions. R. Larock et al has shown that the variation in fatty acids in the triglyceride brings about a broad glass transition temperature making the polymer an excellent dampening material [23].

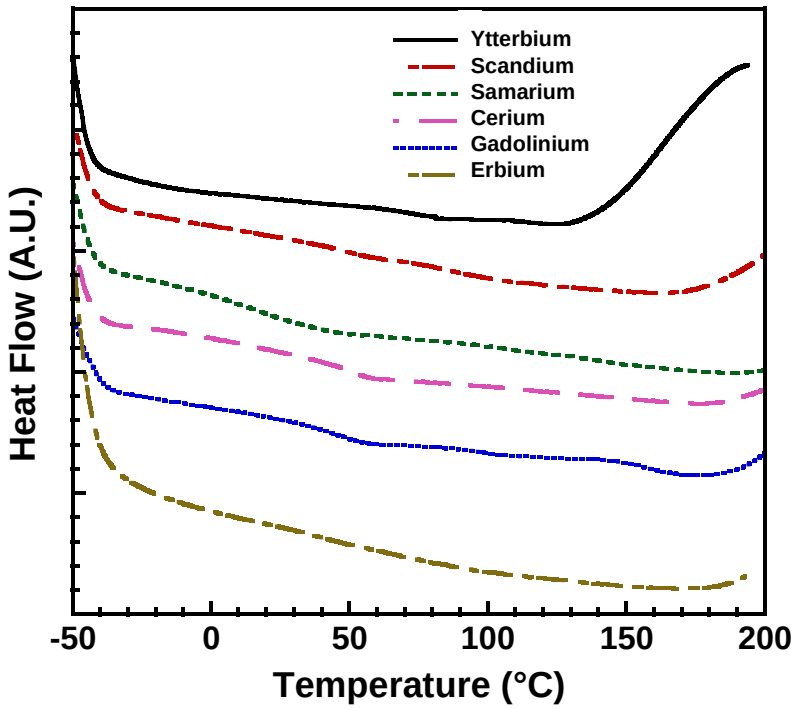

Figure 6-5. DSC of fully cured triflate polymers

DMA of their various polymers was conducted on these six rare earth triflates polymers. Figure 6-6 shows the storage modulus, representing the elastic portion, for the samples. The

storage modulus, especially the rubbery plateau is extremely dependent on the initiator used. Additionally, the trends in the glassy region are not the same as the rubbery plateau. For example, scandium holds a lower storage modulus relative to the other polymers at room temperatures but holds the highest modulus in the rubbery region.

By looking at the storage modulus in the rubbery plateau 50 K above the glass transition temperature, the molecular weight between the crosslinks is calculated using the following equation [24]:

$$M_c = \frac{3qdRT}{E'_{T_g+50K}} \quad (1)$$

where E'_{T_g+50K} represents the storage modulus at 50 K above the glass transition temperature determined by the maximum peak value of tan δ in Figure 6-8. The variables q, d, R, and T are the front factor, density of the material, gas constant, and temperature at 50 K above the glass transition temperature, respectively [15]. Here, q = 1 as is standard for the majority of polymers [25]. The molecular weight between the crosslink of each polymer is shown in Table 6-2.

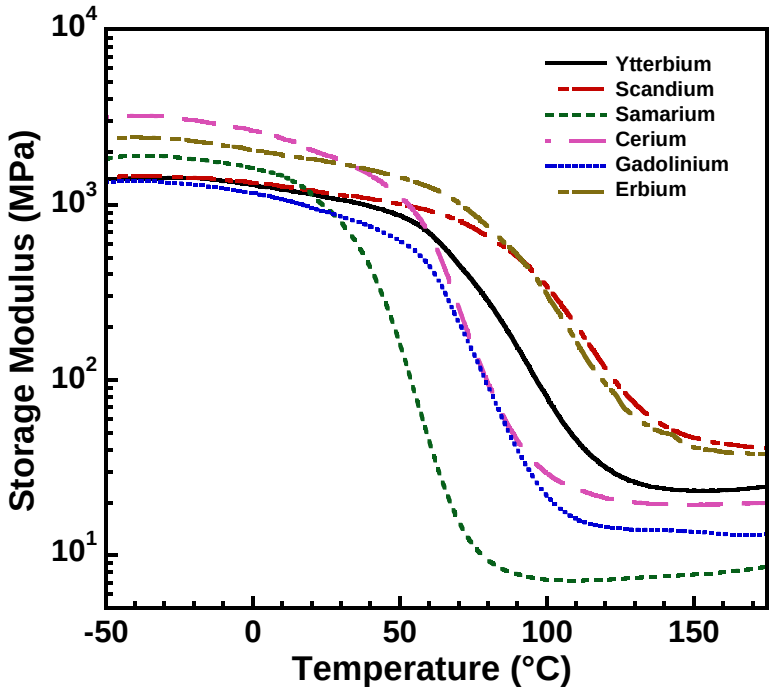

Figure 6-6. Storage modulus from the polymers initiated by various rare earth triflates

Table 6-2. Molecular weight between crosslinks

	Ytterbium	Scandium	Samarium	Cerium	Gadolinium	Erbium
M_C	$1.59\frac{kg}{mol}$	$0.94\frac{kg}{mol}$	$4.73\frac{kg}{mol}$	$1.77\frac{kg}{mol}$	$2.60\frac{kg}{mol}$	$0.99\frac{kg}{mol}$

Figure 6-7 provides the loss modulus, or energy dissipated from heat representing the viscous portion of the polymer, from the DMA. In the glassy region of the loss modulus, several of the thermosets show phase separation indicated by multiple peaks in the data curve, i.e. the three peaks in ytterbium. As with the storage modulus, the trend in the glassy region is not the same in the rubbery region for the loss modulus.

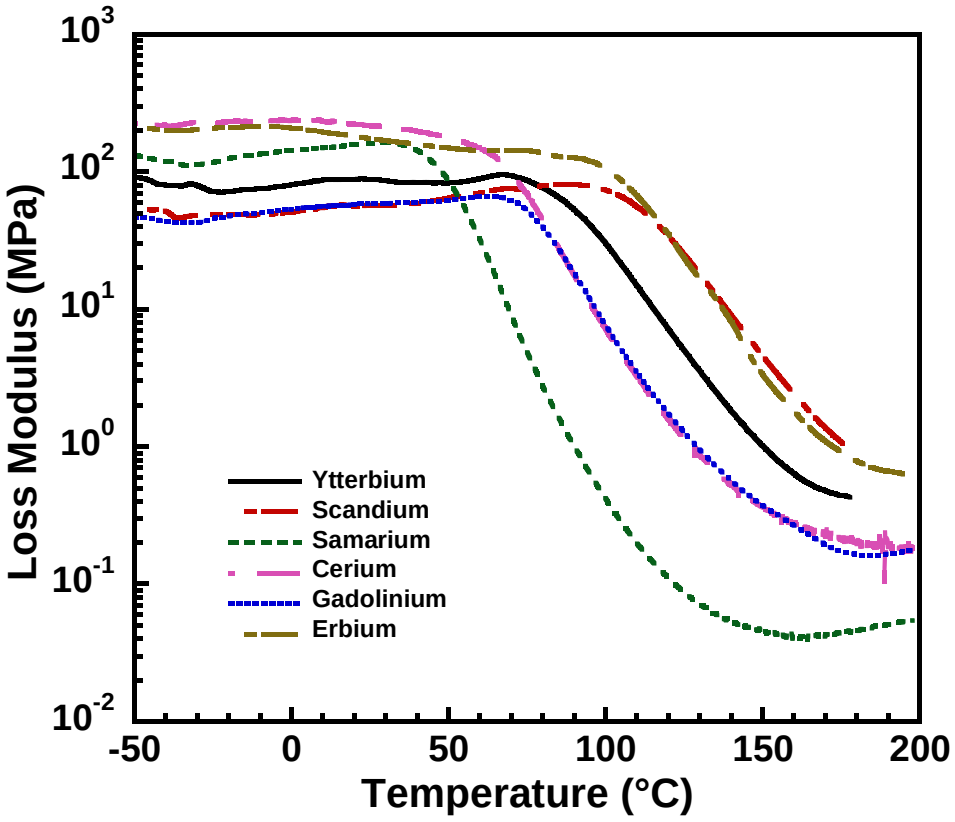

Figure 6-7. Loss modulus from the polymers initiated by various rare earth triflates

The phase angle, tan δ, is determined by the loss modulus over the storage modulus and the dominant peak is a method of measuring the glass transition of a specific polymer. Figure 6-8 shows the phase angle data from the DMA. The resulting glass transition temperatures are seen in Table 6-3. The phase angle data shows that the glass transition of the samples were highly dependent on the initiator used. The lowest glass transition was 61.1 °C for the samarium triflate polymer and the highest glass transition temperature was 118.5 °C for the scandium triflate polymer which gives a large spread in the glass transition of 57.4 °C.

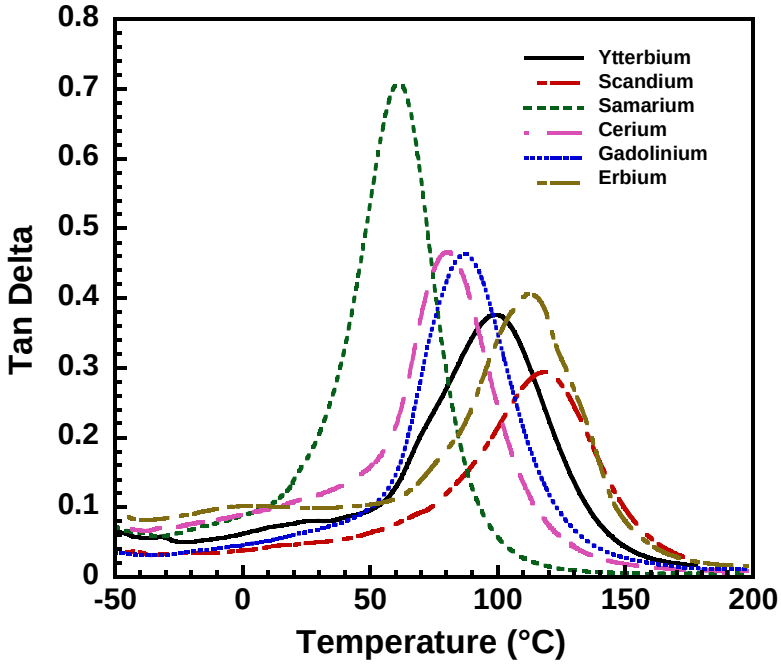

Figure 6-8. Tan δ for the polymers initiated by various rare earth triflates

Table 6-3. Glass transition temperature based on DMA analysis

	Ytterbium	Scandium	Samarium	Cerium	Gadolinium	Erbium
T_g	99.7 °C	118.5 °C	61.1 °C	80.1 °C	86.9 °C	112.3 °C

With the various glass transition temperatures and the large change in molecular weight between the crosslinks, the thermal stability of the polymers was a concern. Figure 6-9 provides the thermal degradation curves for the different thermosets. The scans were run at 20 $Kmin^{-1}$ and in and air environment. The polymers with the lower glass transitions and lower crosslink densities were less stable in air. Samarium, having the lowest glass transition temperature and crosslink density is the least stable of the polymers showing initial signs of degradation earlier than the other polymers.

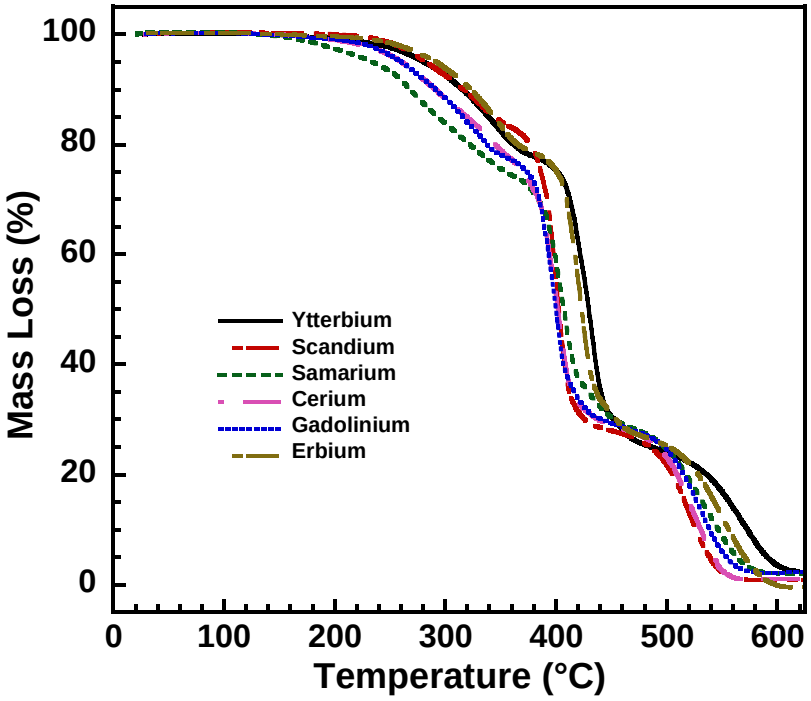

Figure 6-9. Thermal degradation of thermosetting polymers initiated by rare earth triflates

Once the thermo-mechanical properties of the bulk material were determined, the adhesive properties of the polymer were assessed for self-healing applications. The thermosetting biopolymer was used as an adhesive to bond bio-composites similar in composition to those proposed for self-healing applications. Compressive lap shear testing according to ASTM D3846-08 examined the adhesive properties of the thermoset. The maximum shear strength can be seen in Figure 6-10. All samples provided excellent adhesive properties more than adequate for self-healing applications.

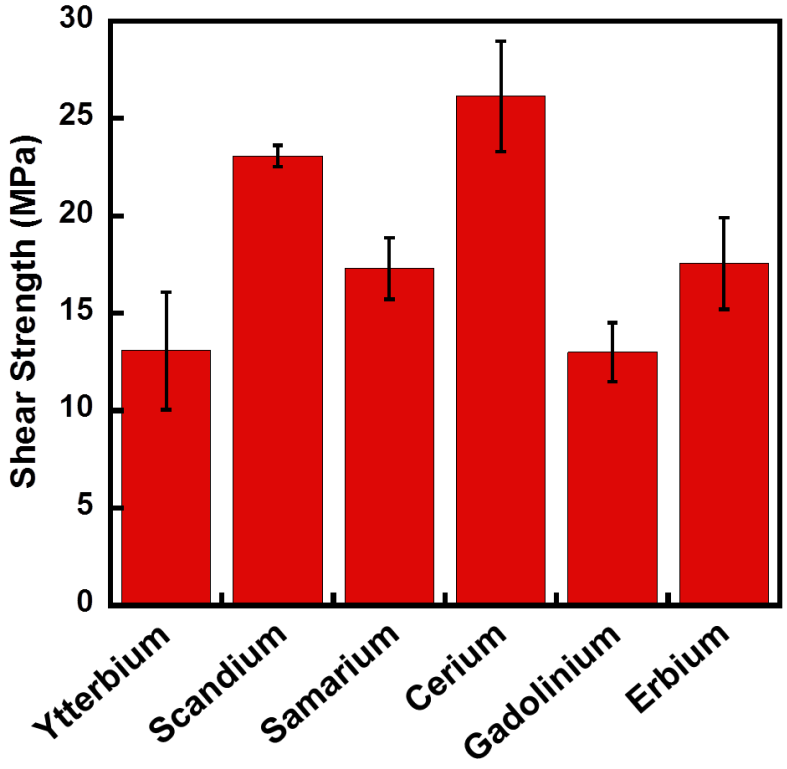

Figure 6-10. Maximum shear strength for thermosetting polymers from rare earth triflates

Once the compressive lap shear samples were fractured, the shear surface was analyzed with scanning electron microscope (SEM) to verify mode of failure. Figure 6-11 shows the imaging of the fracture surfaces. The SEM images reveal the mechanism for failure is a brittle adhesive failure evident in the smooth fracture surfaces. However, the scandium triflate thermoset reveals some fiber pullout in the bottom left corner of the image indicative of a cohesive failure.

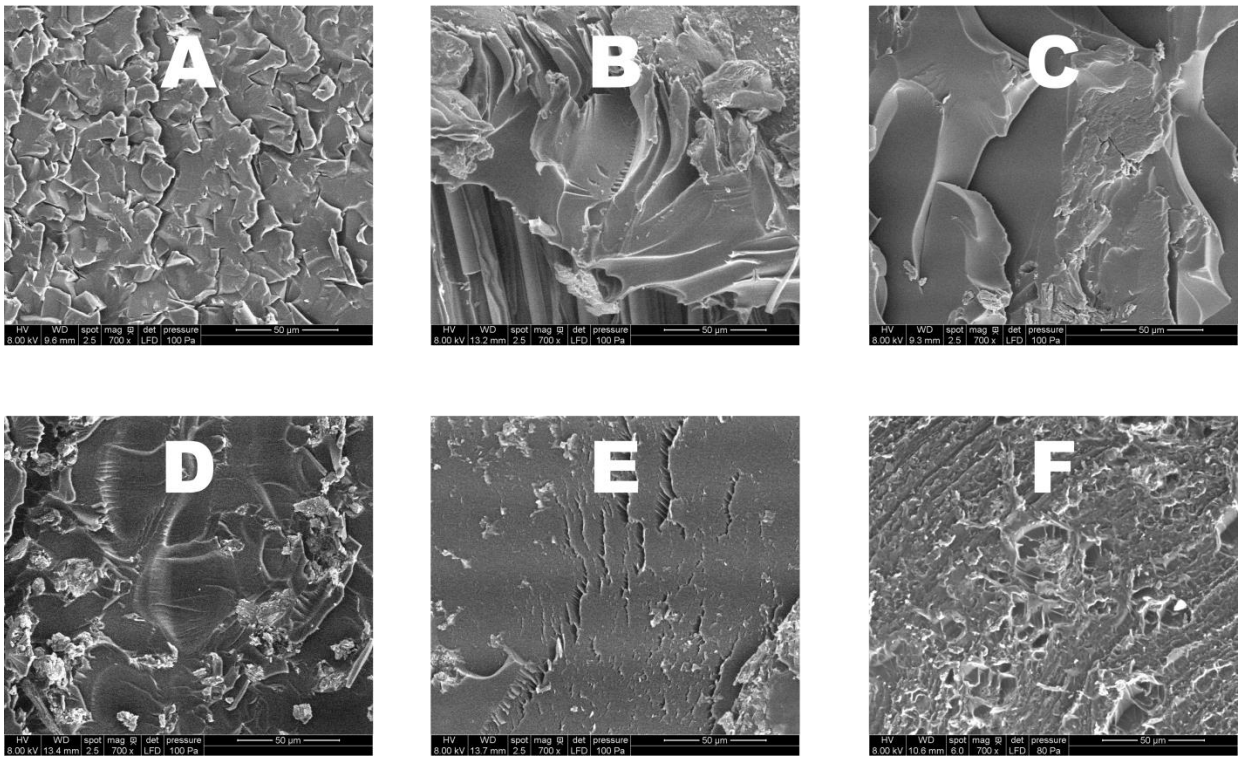

Figure 6-11. SEM (700×) of fractured surfaces for A) ytterbium, B) scandium, C) samarium, D) cerium, E) gadolinium, and F) erbium

Further imaging also shows that the rare earth did not fully dissolve. Small particulates were seen in the shear surface and can be seen in Figure 6-12. When making samples, the monomers were mixed with the sonication horn but were not cured in the heated sonication bath. Instead, the samples were used to make the lapshear samples and then fully cured in the oven. Since the sonication bath was not used to make samples, the triflates did not receive as much of an opportunity to dissolve. Energy-dispersive X-ray spectroscopy (EDS) identified the elements found in these particulate areas. The analysis can be seen in Figure 6-13. The particulate area contained elevated levels of rare earth triflate (erbium) and oxygen indicating the initiator whereas the other areas contained elevated levels of carbon

which is indicative of polymer rich areas. The EDS images show mirror images for the carbon vs. oxygen and erbium mapping.

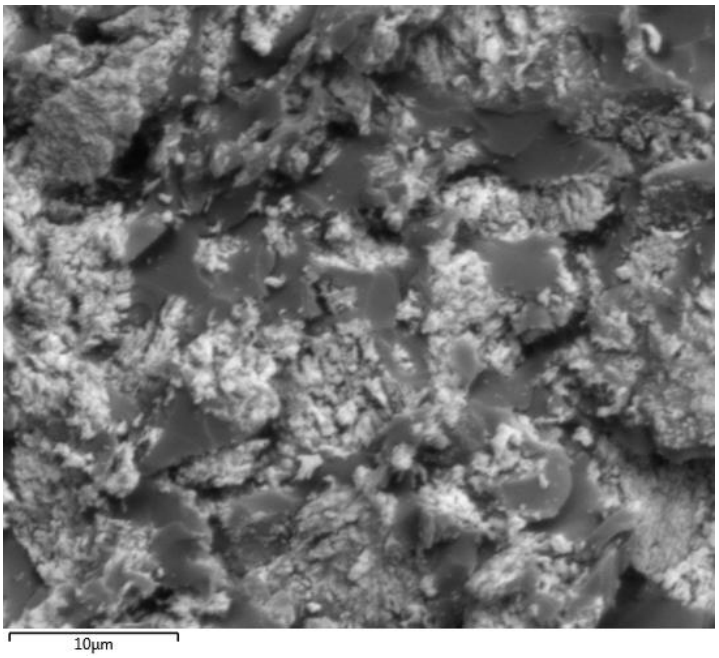

Figure 6-12. SEM used for EDS of triflate particles (example: erbium)

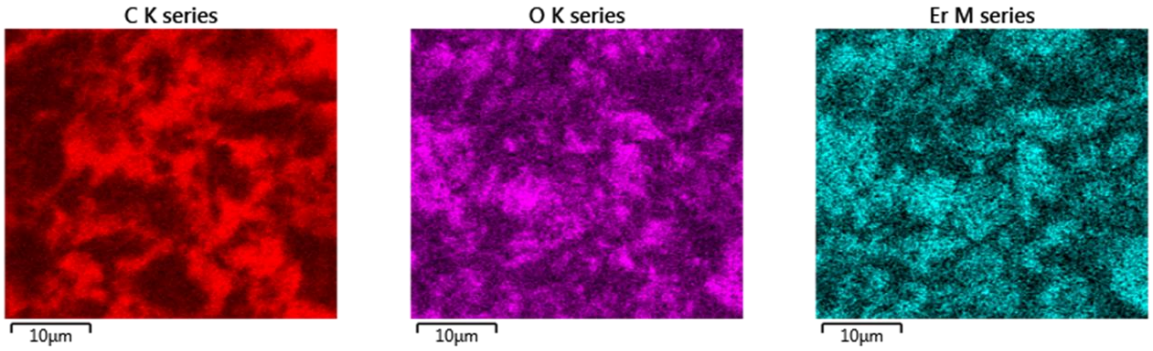

Figure 6-13. EDS of the particulates found on the fracture surface

6.6 Conclusion

Rare earth triflates were successfully used to polymerize tung oil based biorenewable thermosetting polymers. Of the 9 rare earth triflates tested, 6 were capable of cationically polymerizing the tung oil based materials into hard glassy thermosets. By varying the rare earth triflates the thermomechanical properties of the resulting polymers can be tailored for specific applications ranging in glass transition temperature requirements—a more than 50 °C variation. The trend in glass transition temperature paralleled the crosslink density of the samples. In general, as the crosslinking of the polymer increased, so did the glass transition temperature.

The adhesive testing verified the resulting polymers were more than adequate to arrest the microcracks and bond them together in self-healing applications. The SEM shows the failure mode is primarily a brittle failure and the fracture surface exposed undissolved rare earth triflate particles. In a self-healing application, the triflate would be imbedded in the composite and the crack surface would expose the particles. As the monomers interact with the exposed particles, the polymerization process begins and heals the crack. With these rare earth triflate particles still not completely dissolved and yet the resin polymerizing into a strong polymer, the imbedded rare earth triflates should offer enough dissolution in a self-healing application to arrest the crack. The lack of sensitivity to moisture and air also improves the ease of production by replacing the moisture sensitive Lewis acids with rare earth triflates all while offering excellent thermomechanical properties and hopefully reducing the use of petroleum based monomers.

6.7 References

[1] Chiellini, E.; Cinelli, P.; Corti, A. Developments and Future Trends for Environmentally Degradable Plastics. In Renewable Resources and Renewable Energy: A Global Challenge. Graziani, M.; Fornasiero, P., Eds. CRC Press: Boca Raton, FL, 2007, p 63.

[2] Osswald, T. A.; Menges, G. Materials Science of Polymers for Engineers. Hanser Gardner: Cincinnati, 2003, p 16.

[3] Larock, R. C.; Li, F. Thermosetting Polymers from Cationic Copolymerization of Tung Oil: Synthesis and Characterization, J. Appl. Polym. Sci. 2000, 78, 1044.

[4] D. D. Andjelkovic, Y. Lu, M. R. Kessler, R. C. Larock: Novel Rubbers from Cationic Copolymerization of Soybean Oils and Dicyclopentadiene. II. Mechanical and Damping Properties, Macromolecular Materials and Engineering. 2009; 294, 472-483

[5] John, L. A.; Myers, D. J. New soybean oil–styrene–divinylbenzene thermosetting copolymers. II. Dynamic mechanical properties. In Practical Handbook of Soybean Processing and Utilization; Erichson, D. R., Ed.; American Soybean Association, St. Louis, MO; The American Oil Chemist's Society: Champaign, IL, 1995.

[6] Formo, M. W. In Bailey's Industrial Oil, Fat Products, Vol. 2, 4th ed.; Swern, D., Ed.; Wiley: New York, 1982, p 343.

[7] M. A. R. Meier, J. O. Metzger, U. S. Schubert, Chem. Soc. Rev. 2007, 36, 1788.

[8] E. W. Eckey, ''Vegetable Fats and Oils'', ACS Monograph Series, Reinhold Publishing Co., New York 1954

[9] Larock, R. C.; Li, F. Thermosetting Polymers from Cationic Copolymerization of Tung Oil: Synthesis and Characterization, J. Appl. Polym. Sci. 2000, 78, 1044.

[10] Li, F.; Hanson, M. V.; Larock, R. C. Soybean Oil-Divinylbenzene Thermosetting Polymers: Synthesis, Structure, Properties and Their Relationships, Polymer 2001, 42, 1567.

[11] Li, F.; Larock, R. C. Novel Polymeric Materials from Biological Oils, J. Polymers and the Environment 2002, 10, 59.

[12] Li, F.; Hasjim, J.; Larock, R. C. Synthesis, Structure, Thermophysical and Mechanical Properties of New Polymers Prepared by the Cationic Copolymerization of Corn Oil, Styrene and Divinylbenzene, J. Appl. Polymer Sci. 2003, 90, 1830-1838.

[13] Li, F.; Larock, R. C. Synthesis, Structure and Properties of New Tung Oil-Styrene-Divinylbenzene Copolymers Prepared by Thermal Polymerization, Biomacromolecules 2003, 4, 1018-1025.

[14] S. Kobayashi, et al. Air-stable, storable, and highly efficient chiral zirconium catalysts for enantioselective Mannich-type, aza Diels–Alder, aldol, and hetero Diels–Alder reactions. Proceedings of the National Academy of Sciences. Vol. 101. No 15. 5476-5481. (2004)

[15] S. Kobayashi, "Lanthanide Trifluoromethanesulfonates as Stable Lewis Acids in Aqueous Media. Yb(OTf)3 Catalyzed Hydroxymethylation Reaction of Silyl Enol Ethers with Commercial Formaldehyde Solution," Chemistry Letters, 1991, pp. 2187-2190.

[16] S. Kobayashi, Rare-Earth-Metal Trifluoromethanesulfonates As Water-Tolerant Lewis-Acid Catalysts In Organic-Synthesis Synlett., (1994) 689.

[17] S. Kobayashi, M. Sugiura, H. Kitagawa and W. W.-L. Lam, Rare Earth Metal Triflates in Organic Synthesis, Chem. Rev., 102 (2002) 2227.

[18] P. Castell, M. Gali_, A. Serra, J. M. Salla and X. Ramis, Polymer, 41 (2000) 8465.

[19] C. Mas, A. Serra, A. Mantecón, J. M. Salla and X. Ramis, Macromol. Chem. Phys., 202 (2001) 2554.

[20] X. Wang, et al. Effects of Rare Earth Metal Triflates on Cationic Curing of Epoxy Resin/Polyamide Systems. Volume 51, Issue 5, 2012.

[21] T. C. Mauldin, M. R. Kessler : Self-healing Polymers and Composites, International Materials Reviews. 2010, 55(6), 317-346

[22] P. Hondred, L. Salat, J. Mangler, M. Kessler. Tung Oil-Based Thermosetting Polymers for Self-Healing Applications. (In Process)

[23] Li, F.; Larock, R. C. "New Soybean Oil-Styrene-Divinylbenzene Thermosetting Polymers. IV. Good Damping Properties," Polym. Adv. Tech. 2002, 13, 436.

[24] X. Sheng, J. K. Lee, M. R. Kessler. *The Influence of Cross-link Density on the Properties of ROMP Thermosets*, Polymer. 2009; 50, 1264-1269

[25] G. Levita, S. DePetris, A. Marchetti, A. Lazzeri. Crosslink density and fracture toughness of epoxy resins J Mater Sci, 26 (1991), pp. 2348–2352

CHAPTER 7: GENERAL CONCLUSIONS

7.1 Thermal Degradation Kinetics and Lifetime Prediction Modeling

7.1.1 General Discussion

Polymers for aerospace wire insulation were evaluated for thermal stability using thermogravimetry analysis and kinetic modeling applied to predict their thermal degradation. Isoconversional and model-based kinetics were used to expand the kinetic model to fully describe the degradation of the polymers. For all three polymers, PTFE, ETFE, and Kapton, the reaction kinetics are governed by an autocatalytic reaction model. For the case of PTFE, the polymer degradation is best described by a single step autocatalytic reaction model. For ETFE, the degradation is best described by a consecutive three step autocatalytic reaction model. Finally, Kapton degradation is described by a five step consecutive and competitive reaction model governed by autocatalysis. In the case of Kapton, electrical breakdown testing was integrated with thermal degradation and, using lifetime theory, an electrothermal lifetime prediction model for aerospace wire was determined.

First, thermogravimetric analysis (TGA) was conducted on the common polymers for wire insulation in aerospace, PTFE, ETFE, and Kapton. These TGA experiments were conducted at multiple heating rates and in an oxygenated environment. The multiple heating rates reveal information on the reaction steps by separating the individual mechanisms. These mechanisms, or reaction steps, are visible when the derivative of the thermograms is calculated. The peaks in the DTGA show the minimum number of step required to adequately describe the degradation. For PTFE, ETFE, and Kapton, the DTGA showed the minimum number of peaks as one, two and three respectively.

Using the DTGA as a starting point for the models, the Friedman analysis was conducted. The Friedman analysis uses isoconversional model-free kinetics to identify fluctuating activation energy. The Friedman analysis also confirms the minimum number of reaction steps from the DTGA—these are identified as peaks in the Friedman analysis as well. The activation energy is calculated from the slope of the isoconversional trend lines in the Friedman analysis. The change in slopes on the Friedman plot offers insight into the reaction type. In all cases an autocatalytic model was inferred from the Friedman plot and proved to be the best represented the degradation.

The activation energy plot, especially in the case of Kapton, provided information of the formation of the reaction steps—either consecutive or competitive. By comparing the activation energy determined from the Friedman analysis to the activation energy determined by the Ozawa-Flynn-Wall analysis the step can be determined. The Friedman analysis is a derivative based calculation of activation energy and the Ozawa-Flynn-Wall analysis is an integral based calculation of activation energy. In the case of an integral analysis, the separation of variables does not allow for competitive reactions and the two calculated activation energies are necessarily different in the case of competitive reactions. Therefore, the competitive portions of the model for Kapton were necessarily determined from the activation energy analysis. To further confirm the competitive and consecutive reaction for Kapton, an examination of the off gas produced during the degradation was conducted. Mass spectroscopy and fourier transform infrared spectroscopy was conducted to validate the theoretical model for the degradation with experimental analysis. The off gas analysis showed competing reactions with a total of 5 mechanisms. This result confirmed the five step competitive and consecutive autocatalytic reaction developed for Kapton.

In the case of Kapton, voltage breakdown testing was conducted on samples degraded at different temperatures and for different lengths of times in order to compare the breakdown strength of the materials under various degrees of degradation. These data were combined with the thermal degradation data to develop lifetime prediction models for Kapton under various temperatures and voltages. The lifetime curve for Kapton follows an exponential function seen by the linear form in the semi-log plot of the lifetime model. These findings would indicate a linear dependence of breakdown voltage on conversion.

7.1.2 Recommendations for Future Research

This work could be strengthened by further investigation into the degradation both the theoretical model and the experimental investigation. First, spectroscopic investigation further along with thermogravimetric and breakdown voltage study would offer better insight into the degradation process. Second, the lifetime prediction model could be further developed to incorporate an explicit voltage dependent term in the Arrhenius equation—in either the activation energy, pre-exponential factor, or both. Third, long term aging testing to verify the model would be recommended.

While some spectroscopic investigation was conducted on the off gases of Kapton during thermal degradation, a more extensive investigation of the degradation pathway would be recommended for Kapton as well as for PTFE and ETFE. The completely mapped degradation mechanism through experimental results would lend extensive credibility to the kinetic models.

The current model uses thermogravimetric aging to degrade the sample. To completely develop the lifetime prediction model, efforts to determine if voltage plays an active role in the degradation process are recommended. To develop this, *in situ* electrical and thermal degradation would be required. The current model for lifetime prediction relates to situations where heat is degrading the insulation from an initial state where the breakdown voltage is V_0 to a final state where the breakdown voltage is V_f and the lifetime model gives the time for the reduction of breakdown voltage to reach the applied voltage value. This is only the case if the lifetime of the insulation under voltage plays no role in generating the degradation. To remove this assumption, aging from electrical degradation as well as thermal degradation is necessary. Using a more complex experimental degradation process, the model could address the electrical degradation through an additional variable.

Additionally, experimental lifetime testing is recommended to validate the model. Simultaneously elevating the thermal environment of the sample while applying a specific voltage until failure would verify the model experimentally. These tests should be run in multiple tests which include holding one variable—temperature or voltage—constant while varying the other and vice versa. Isolating the effects of the temperature or the voltage would give an indication of the more important variable to degradation and the environmental parameter to be most concerned about when operating out in the field.

7.2 Biorenewable Polymers for Self-healing Application

7.2.1 General Discussion

Polymers from bio-based feedstocks were developed through cationic polymerization for self-healing applications. After investigating multiple options for the agricultural oil of choice, tung oil was chosen for its high reactivity due to the dominant fatty acid chains containing three conjugated double bonds. While the bio-based materials contained co-monomers derived from petroleum—styrene and divinylbenzene—the bio content of the resulting thermosetting polymers were just over 50 wt%.

In the first part of the biopolymer work, the tung oil based polymer was modified by replacing the triglyceride with the methyl ester derived from tung oil. The methyl ester offered a lower viscosity and higher reactivity of the monomer composition. These traits are important for self-healing applications. However, the methyl ester did decrease the mechanical properties of the resulting polymer. The methyl ester was introduced at increments of 4.7 wt% of the polymer and directly replaced 4.7 wt% of tung oil triglyceride. The maximum loading of tung oil methyl ester was 28.2 wt% and was not increased further due to the difficulty in maintaining a homogeneous polymer above this loading.

The dynamic mechanical analysis showed a systematic change in the mechanical properties as the methyl ester was substituted. First, the storage modulus in both the glassy region and rubbery region decreased. The rubbery plateau gave an explanation as a crosslink density analysis was conducted from the data which showed a decrease in the number of crosslinks in the polymer. This decrease arises from the glycerin bond found in triglycerides and not in the methyl esters. Consequently, a point of crosslinking is removed when the oil is replaced by methyl esters. Second, the glass transition of the polymer was decreased with

increasing methyl ester loading. At the largest loading of methyl ester, the glass transition temperature was depressed by 17% of its original value. The systematic change in glass transition temperature allows for tuning of the healing agent, the tung oil biopolymer, to the polymer matrix of the specific application. Third, the dynamic mechanical analysis revealed that higher loadings of methyl ester showed signs of phase separation. This separation is apparent in the secondary peak arising in the loss modulus of the polymer. Transmission electron microscope confirmed nano-sized phase separation where the styrene and divinylbenzene were separated from the oil. The phase separation is on the order of a few molecules. Therefore, this nano phase resembles a random coblock polymer with a few repeat units in each block.

The tung oil bio-polymer shows high thermal stability. In an air environment, all the samples maintained their thermal stability into the 200-300 °C range. The thermogravimetric analysis shows that the addition of methyl ester to the bio-polymer does not decrease the thermal stability significantly. All samples so very similar trends in the thermal degradation confirming that the addition of methyl ester will not jeopardize the integrity of the thermosetting polymer.

The tung oil samples also showed that the adhesive properties are acceptable for self-healing applications. Any adhesive with shear strength above 1 MPa is considered an adequate adhesive. Consequently, the tung oil samples with methyl ester would all make good adhesives for self-healing applications. Additionally, scanning electron microscope was used to investigate the surface of the shear failure. The addition of methyl ester changed the failure mode from a brittle failure to a ductile failure. Also the methyl ester cause the failure

mode to shift from cohesive failure to an adhesive failure where at higher loadings of methyl ester, the fibers began to pull out of the adhesive.

In the second part of the biopolymer work, several rare earth triflates were used as initiators for the cationic polymerization of tung oil biopolymers. This work compares the thermomechanical and adhesive properties of the biopolymers polymerized under eight different rare earth triflates—scandium, samarium, cerium, erbium, terbium, neodymium, ytterbium, and holmium. These triflates were used as an initiator for the benefit of processing in an air environment. Most Lewis acids used in cationic polymerization are moisture sensitive, however, rare earth triflates are not as susceptible and therefore hold a potential for easy processing.

The dynamic mechanical analysis shows that the thermosets mechanical properties were comparable with the tung oil based thermosets polymerized with boron trifluoride diethyl etherate. The storage modulus was between 1 – 3 MPa at room temperature which compares to a storage modulus of 2 MPa at room temperature for the tung oil polymer made in the first part of this work. Similarly, the loss modulus is comparable for triflate samples.

The rare earth triflates provided an extremely large range of glass transition temperatures. Through dynamic mechanical analysis, the glass transition temperature chosen from the tangent delta is well above room temperature—anywhere from 60 °C to 110 °C depending on rare earth triflate of choice. However, using differential scanning calorimetry, the samples showed multiple glass transition peaks, some of which are below 0 °C.

The thermal stability of the rare earth triflates was also comparable. The samples were stable into the 200 to 300 °C range depending on the triflate of choice. With the thermal

stability shown, the tung oil samples polymerized from rare earth triflates would be acceptable for self-heal applications.

The compressive lap shear testing showed the rare earth triflate affected the adhesive properties of the polymer. The shear strength of cerium was as high as 20+ MPa while erbium only maintained shear strength of 5 MPa. However, all trifates provided a polymer with adequate adhesive strength for further investigation into self-healing applications. Additionally, scanning electron microscope showed the types of failure mechanisms for all the triflate samples. The common failure mode is a ductile cohesive failure where the adhesive itself loses its integrity. In some instances, the scanning electron microscope identified areas with small particulate. These regions are catalyst rich regions and by using EDS, the elemental concentration shows that the catalyst was not fully dissolved in these areas.

Overall, the tung oil thermosets, both the methyl ester modified and the rare earth triflate initiated, are shown to be viable polymers for self-healing applications. The mechanical properties offer rigid glassy polymers at room temperature with high storage modulus. The glass transition temperatures are well above room temperature as well. Furthermore, the thermal stability and adhesive properties are within the requirements for self-healing applications.

7.2.2 Recommendations for Future Research

This work would benefit from further pursuing the self-healing aspects of the project. In the self-healing model proposed, the healing agent is encapsulated into microcapsules and

imbedded into the bulk polymer matrix. Consequently, the monomers for healing necessarily need to be encapsulated and healing efficiency determined.

Previously, microcapsules have been successfully prepared by Kessler et al [1,2]. The encapsulation technique utilizes micelles during an emulsion. The micelle directs the addition of the monomers for the microcapsule shell to the surface of the droplets and then the polymerization process begins. After the polymer shell cures, the capsules are removed and dried for imbedding into the bulk polymer. Urea-formaldehyde capsules are extensively used in microencapsulation. In addition to the urea-formaldehyde capsule, a new shell material using a ternary system of melamine, urea, and formaldehyde (MUF) offers improved mechanical, adhesive, and storage properties as well as maintaining a glass transition temperature over 120 °C [3-5]. The processing of these capsules is simpler while simultaneously improving the uniformity in the capsules.

Once encapsulated, the shell material properties require optimization. Through monitoring and changing manufacturing parameters of the microcapsule such as pH level, agitation rate, reagent rations, and reaction temperature, the capsule's quality and effectiveness for self-healing changes. Optimum capsules will need to be determined through experimental testing of diameter, wall thickness, rupture strength, elastic stiffness, and environmental stability.

Once microcapsules have been developed, optimized and imbedded into bulk polymer, experimental assessment of self-healing is required. One such technique measures how the healing agent system cures when initiated by catalyst which has been encapsulated in the matrix and then exposed using the parallel plate rheometry system [6]. By combining catalyst dissolution kinetics with polymerization kinetics, the simulated self-healing system

can determine if the healing agent is capable of polymerizing. Based on these test, the promising systems should be subjected to height tapered double cantilever beam testing. Under mode I loading, the healing efficiency, η, is calculated by comparing the fracture toughness of the pristine sample to the repaired sample using the following equation:

$$\eta = \frac{K_{IC}^{Repaired}}{K_{IC}^{Pristine}} \times 100\% \quad (1)$$

Finally, prolonged stability of the healing agent should be investigated to determine effective healing when previously exposed to extreme temperatures and humidity. The use of temperature and humidity cycling offers information on the environmental effects to healing. Furthermore, alternate co-monomers should be investigated to improve healing efficiency, environmental stability, or increase the biorenewable portion of the healing agent monomers. One potential option for improving the amount of biorenewable in the monomer composition is to substitute in molecules with highly reactive unsaturation such as eugenol for the styrene and divinylbenzene.

7.3 References

[1] Brown, E. N.; Kessler, M. R.; Sottos, N. R.; Moore, J. S.; White, S. R. “In Situ Poly(ureaformaldehyde) Microencapsulation of Dicyclopentadiene,” J Microencapsul. 20 (2003) 719.

[2] Yoon, S.; Park, H.; Hong, S.; Lee, J.; Kessler, M. R.; White S. R. "Manufacturing Process of Microcapsules for Autonomic Damage Repair of Polymeric Composites," Journal of the Korean Society for Composite Materials, Accepted for publication (2002).

[3] Liu, X.; Sheng, X.; Kessler, M. R.; Lee, J. K. "Synthesis and Characterization of Melamine-Urea-Formaldehyde Microcapsules Containing ENB-based Self-healing Agents, Macromolecular Materials and Engineering," In Press. (cover issue) (doi: 10.1002/mame.200900015).

[4] Liu, X.; Lee, J. K.; Kessler, M. R. "Norbornene-based Self-healing Agents and Their Microencapsulation" Proceedings of the International Conference on Smart Materials and Nanotechnology in Engineering. July 8-11, 2009, Weihai, China.

[5] Liu, X.; Lee, J. K.; Kessler, M. R. "Microencapsulation of self-healing agents with melamine-urea-formaldehyde by the Shirasu Porous Glass (SPG) Emulsification Technique" Proceedings of the International Conference on Smart Materials and Nanotechnology in Engineering. July 8-11, 2009, Weihai, China.

[6] Liu, X.; Lee, J. K.; Yoon, S. H.; Kessler, M. R. "Characterization of Diene Monomers as Healing Agents for Autonomic Damage Repair," J. Appl. Poly. Sci. 101 (2006) 1266.

APPENDIX A: IOWA STATE UNIVERSITY SYMBI GK12 PROGRAM: A CASE STUDY OF THE RESIDENT ENGINEER'S EFFECTS ON 8TH GRADERS ATTITUDES TOWARD SCIENCE AND ENGINEERING

A paper published in 2012 ASEE Annual Conference Proceedings

Peter R. Hondred[1], Karri Haen[2,3], Adah Leshem[3*], and Michael Kessler[1]

A.1 Abstract

Symbi, Iowa's NSF GK12 program, is a partnership between Iowa State University and the Des Moines public school system in an effort to develop innovative and engaging STEM (Science, Technology, Engineering and Math) activities for middle school students. STEM graduate students are selected to serve as resident scientists or engineers and spend one full day each week throughout the academic school year in a middle school science classroom. These GK12 Fellows engage the students by providing inquiry-based learning experiences and authentic demonstrations, which bring relevance by relating the science curriculum to real world challenges. In addition, the Fellows serve as role models for STEM based occupations and encourage the students to develop the skill-sets they will need to be competitive in the 21st century global economy. Each Fellow's research background provides a unique venue for enhancing the classroom curricula. Here we present a case study showcasing the activities and interactions of Symbi GK12 Fellows in the classroom with implications for other partnerships between graduate students and middle schools. In this

case study, the primary research focus of the author, a GK12 Fellow, is on materials science and engineering, a field completely absent from middle school curricula. By providing hands on demonstrations and reliable scientific expertise, 8th grade students showed a significant increase in not only academic understanding but also in attitudes toward science and engineering related fields. These findings were supported through pre- and post-survey instruments, and student testimonies. These results suggest that middle school students benefit from the involvement of the resident engineer in the classroom.

A.2 Introduction

On the 27th of April 2009 at the National Academy of Sciences, President Obama said, "I want to persuade you to spend time in the classroom, talking and showing young people what it is that your work can mean, and what it means to you […] to thinking about new creative ways to engage young people in science and engineering." These words came in the wake of growing concern for the lack of students pursuing degrees and careers in STEM (Science, Technology, Engineering and Math) related fields. Currently, the pool of engineers in the United States is undersized to meet the needs of our society and economy [1]. If current trends do not change, the demand for engineers will surpass the supply of engineers in the US [2].

A startling number of students in the US are failing to pass science benchmark standards at a proficient level. According to the National Center for Educational Statistics, fewer than 1 out of 3 students perform at or above the proficiency level in 8th grade science [3]. Students from low income and underrepresented minority families scored significantly lower on the national report card [4]. Additionally, the public school students performed well

below private and Catholic schools, especially in the inner city public school setting [4]. These scores demonstrate that the K12 public science education in the United States is substandard.

In an effort to address student STEM literacy and preparation for STEM careers, Iowa State University has partnered with the Des Moines Public Schools to foster students' interest in science and engineering by incorporating STEM Ph.D. candidates as resident scientists/engineers in middle school classrooms. This partnership is funded by the National Science Foundation (NSF) through the Graduate Stem Fellows in K-12 Education Program (GK-12). NSF funds several GK-12 programs at national universities. Each university has specific and unique goals for their program. A goal of Iowa State University's GK-12 program, Symbi, is to increase K12 students' scientific literacy: that is, to increase student understanding of the relevance of STEM to real world challenges and to help them be more aware of STEM careers. The program name Symbi was chosen for the symbiotic relationship between the fellows and the middle school students.

The lead author of this article is a Symbi GK12 fellow and "resident engineer" who is majoring in materials science and engineering and conducting research on polymers. The resident engineer was paired with a middle school science teacher in the Des Moines Public School District, and spent one full day each week, for one academic year, in the science classroom. The resident engineer was able to provide a unique classroom experience by periodically introducing the students to aspects of his own research, including the use of biopolymers in material self-healing applications. Several activities were designed to provide students with the opportunity to learn about the field of polymer science. These activities were related to the science topics covered in the curriculum and provided relevance to real

world issues and challenges. This study focuses on the impact this fellow has had as a resident engineer on the students in his classroom.

A.3 Research Questions

In this case study, researchers were interested in the effects of a resident engineer on eighth grade students' science content knowledge and attitudes toward science and engineering. Specifically, this study asks whether the resident engineer improves the interest of students in science and engineering such that significant improvement in the scientific knowledge of the students can be detected. The current study was guided by two basic research questions:

1. Do the classroom activities, demonstrations, and experiments provided by the resident engineer positively affect the attitudes of students toward science and engineering, specifically in fields relatively unexplored by 8^{th} grade science classrooms such as polymers?
2. Are there significant changes in student knowledge about polymers after exposure to materials science demonstrations?

A.4 Research design

This case study focuses on a defined classroom situation in which a series of demonstrations involving polymers, showcasing polymer engineering concepts, were conducted by the resident engineer. Four different demonstrations were conducted with the objective of enhancing the energy unit of the science curriculum. The demonstrations used in the classroom were as follows:

1. **Thin Film BioPolymer** – This activity involved the polymerization of a thin film biopolymer. The film cast in this polymerization process was made from a mixture of water, gelatin, and glycerol. The demonstration utilized laboratory equipment such as beakers, hot plate, flasks, and scales to show how polymers are made in the laboratory. During the demonstration, a discussion on the nature of polymers, how they are made, where they are found, and how often they are used in daily life was utilized to expand students' knowledge of polymers. The resident engineer connected the thin films to the students' life by discussing applications involving smart phones and electronic thin film display covers.
2. **Nylon 6,10** – A second polymerization process was demonstrated for students to experience a fraction of the many methods for making polymers. In this demonstration a solution of sebacoyl chloride and heptane was added to a solution of hexamethylenediamine and water. At the interface of the two insoluble solutions, a thin film of nylon forms and a fiber is pulled for students to see. A discussion about the origin of nylon, the uses for nylon, and the processing of nylon was done.
3. **Exothermic Reaction** – This activity demonstrates the conversion of potential energy stored in chemical bonds to thermal energy. For this experiment, hydrogen peroxide was added to yeast and mixed for 10-15 seconds. During this time, the temperature of mixture raises and a discussion on the importance of understanding your material reactions, especially in polymerization, is crucial for safety as well as an excellent way to explain the application to the energy unit in the science curriculum.
4. **Endothermic Reaction** – Similar to the exothermic reaction, this activity used a mixture of vinegar and baking soda. As the temperature decreases, the lead author

discussed with the students the effects of endothermic reactions and again references the need for understanding a reaction and applying it to the science curriculum.

In order to evaluate the effect of the resident engineer in the classroom, pre- and post-survey instruments were implemented to assess 8th grade student attitudes to science and engineering as well as student understanding of concepts relating to materials science engineering (described below).

A.5 Classroom demographics

The resident engineer was paired with the eighth grade science class at Meredith middle school, Des Moines, IA. The middle school has a total of 607 students, of which 162 were in the eighth grade science classroom that interacted with the resident engineer. The student population of Meredith middle school is 58% underrepresented minority families and 69.4% of all students qualify for free or reduced lunches. These demographics are comparable to the national average of 56% underrepresented minority families from the 2009-2010 National Center for Education Statistics (NCES) data [5].

A.6 Results

Before the classroom demonstrations listed above, the students were given a pretest survey to gauge their understanding and interests in polymers. After the demonstrations were conducted, the students were given the same survey in order to understand the effects of the polymer demonstrations. Questions 1-3 were answered on a scale of 1 to 5 where 1=No Interest and 5=Very Interested. Questions 4-9 were true or false questions. Table A-1 shows the data for questions 1-3 and Table A-2 shows the results for the true or false questions. These questions were as follows:

1. What is your interest in science?
2. What is your interest in materials?
3. What is your interest in polymers?
4. Are plastics a type of polymer?
5. Are polymers made from petroleum?
6. Are plastics made from vegetable oils?
7. Are all man made polymers bad for the environment?
8. Are some polymers safe to eat?
9. Do I use polymers all the time?

Table A-1. Class demonstration survey – Questions on students' interest

	Pre-Class Survey		**Post-Class Survey**		**Single Tailed Paired *t*-test**
	Mean	Std. Dev.	Mean	Std. Dev.	Significance
Question 1	3.40	0.98	4.06	0.82	3.02 E-17
Question 2	3.02	1.18	3.68	1.00	4.64 E-17
Question 3	1.80	0.95	3.55	0.99	1.73 E-40

Table A-2. Class demonstration survey – True or False Questions

	Pre-Class Survey (% Correct)	**Post-Class Survey (% Correct)**	**Single Tailed Paired *t*-test**
Question 4	70.8	94.9	3.26 E-8
Question 5	50.4	60.6	4.00 E-02
Question 6	34.3	62.8	9.06 E-8
Question 7	72.3	93.4	3.56 E-7
Question 8	36.5	92.0	1.25 E-22
Question 9	65.0	91.2	2.46 E-8

It is worth noting that the resident engineer had been in the 8th grade class for almost a full semester before the classroom demonstrations were performed. Because of this, the students were already familiar with, and comfortable with, the resident engineer in the classroom.

In addition to the survey questions and statistics, a tangible difference in the students and their interest in science was observed by the resident engineer. Upon his arriving, many students are excited to see him. They often wanted to see what demos, labs, or experiments were brought and what the class was going to be doing. Students made comments such as, "Hey science dude, you make science class cool" or "what awesome science stuff are we doing today?" and "I wish you could come every day." In fact, on the day of the polymer demonstrations, few students had any idea that polymers were in many of their foods, let alone that they had eaten a polymer. Once students found out that polymers were in food and that some polymer engineers work with making candies like gummy animals, they were quite interested to learn more about these kinds of jobs.

A.7 Discussion

In middle school the focus of STEM is solely on science and mathematics [6]. However, the study of engineering is an excellent way to incorporate science, mathematical and technological principles into examples of real world phenomena. [7]. Engineering concepts provide an effective way for educators to interweave subjects, especially in the middle grades, and to help their students identify and formulate problems, design solutions, test and improve designs, and communicate results to others. By introducing engineering

concepts at an early age, especially through hands-on activities, students can improve their understanding of the subject matter and its relevance to their lives [7,8].

The absence of engineering concepts in the middle school math and science curricula not only stunts the potential for higher learning of students, but it is also reinforces a stereotype that science and engineering are tedious and uninteresting fields full of difficult concepts and far removed from the average person. Many middle school students are uninterested in science because they do not see the relevance to their life experiences and a perception of their inability in science [9]. In fact, most students' attitudes toward science decreases throughout middle school and high school and these attitudes are strongly linked to their best friends' attitudes toward science [10]. However, the influence of teacher encouragement has shown to have a positive effect on students [11]. Furthermore, introducing engineering concepts in middle school increases student interest especially in students who generally do not become engaged in the science classroom [8,12].

The data from the classroom survey shows these students' opinions align with the national pattern. The data also supports the observation of the resident engineer that many students do not know what polymers are. The true and false questions from the survey show few students know what polymers are. Question 3 points out students are not interested in polymers and this lack of interest is most likely from a lack of knowledge about polymers. When the students were asked to articulate what a polymer was, very few could give a cohesive answer about polymer understanding. Of all the questions on the survey, only one question, number 5, did not indicate a significant change in student understanding. There is no surprise this question showed insignificant change considering the question was designed to gauge the students' initial understanding of polymers and that the demonstration did not

involve discussion of petroleum based polymers. However, all other questions showed a significant increase in understanding of polymers. Students were able to better answer basic questions about polymers as well as expressing an increased interest in polymers.

Despite polymers being vital to our current society, it is not surprising few school curriculums provide an opportunity for the students to explore the nature of polymers. This case study is another example of presenting polymers to students through an interactive environment where they can freely explore, question, and investigate a few aspects of polymers. After the class was finished, several students remained after every demonstration to ask more questions and get more tangible experience with the materials.

Additionally, the classroom profited from a scientist in the classroom who can connect real world application to the classroom curriculum. Primarily, this benefit was seen in the increased understanding students held about science and engineering as solutions to real world problems. When the resident engineer first entered the class, the students would often respond with, “who cares,” after the resident engineer would talk about interesting science phenomenon. However, when the classroom began to learn how the materials they were learning about had real world application such as polymers in food, clothing, and airplane parts, students became engaged. Students were even asking where they will see science they learned in their everyday life before the resident engineer could offer applications for them. For example, throughout the classroom demonstrations, students became more comfortable and interested in asking questions about polymers. In fact, few had any idea that they had ever worn a polymer (nylon, polyester, spandex, or rayon). Furthermore, the resident scientist provided a tangible figure who was working to solve

actual problems involving polymers. By offering concrete examples of careers in science and engineering, students began to see themselves more in a scientific role in their future careers.

These results are supported by the Symbi first-year cohort student attitudes data collected and analyzed by Iowa State University's Research Institute for Studies in Education (RISE) [13], which showed significant change in 241 eighth grade students' perceptions of science after involvement in the Symbi GK-12 program. For instance, students showed an increased interest in both problem-solving and engineering concepts. Increased interest in problem-solving was complimented by decreased interest in obtaining answers from the teacher. These results showed that students were beginning to develop critical thinking skills, and were more interested in solving their own problems by taking ownership of the problem instead of relying on a teacher to fall back on for the quick answer.

A.8 Conclusions

The results of this study show that 1.) Introducing engineering concepts in middle school increases student interest especially in students who generally do not become engaged in the science classroom, 2.) Despite polymers being vital to our current society, few school curriculums provide an opportunity for the students to explore the nature of polymers, and therefore students are not interested in them, 3.) The classroom profited from a scientist in the classroom who can connect real world applications to the classroom curriculum by stepping in as a mentor scientist/engineer.

Introducing middle school students to engineering concepts is beneficial to their cognitive development by requiring them to learn several disciplines simultaneously—thus improving not only their science skills but also their mathematics, reasoning, and

communication skills. Despite the fact that the public school system has placed a focus on STEM curriculum, few classrooms offer a program that actually advances engineering for students. Often this comes from teachers who lack the ability to comfortably introduce engineering topics to class. However, when students are introduced to new topics in which they obtain hands-on experiences in science through an engineering viewpoint, students' interests significantly increase. From the survey alone, simply introducing the students to the hands on demonstration increased their interest in science as a whole from 3.40 to 4.06 on a scale of 1 to 5—a statistically significant change.

Often, students are not interested in a topic for the sheer reason that they don't know anything about it. This is quite evident by the change in interest of polymers before and after the classroom demonstrations. The students' interests in polymers went from 1.80 to 3.55 on a scale of 1 to 5. From the resident engineer's perspective, students asked more questions and showed more interest after an introduction to polymers concepts. Students asked about different polymers in food, why certain polymers respond differently to external stimulus, and how polymers break. By providing students relevancy for why they are learning the information in their curriculum, students can begin to see themselves as potential future engineers. Once the students found out about polymers in food, several students were excited about the idea of a job studying the properties of candy. The resident engineer discussed possible applications for biopolymer thin films such as coatings for smart phones and electronics which immediately piqued the interests of several students. The class was even interested in the applications for nylon. The students were shocked at the wide applications for nylon such as fishing line, clothing, drum sticks, parachutes, and a wide variety more.

Scientific learning is vastly enhanced once a personal interest is taken in a topic because additional investment is made by the individual to better understand the material.

Past research has shown it is not enough to just get students to learn the material to encourage students to pursue science and engineering careers. Students drop out of their respective science and engineering fields despite having the ability to handle the material. Often attrition happens because students don't see themselves aligning with engineering. However, by fostering the interest in science and engineering, and by providing a figure that represents science and engineering, students begin to see themselves aligning with these fields more closely. In fact, students that are influenced and encouraged by a mentor early are three times more likely to pursue STEM careers [14].

By offering eighth grade students the opportunity to work with a resident engineer, the class is exposed to a mentor who provides design based learning from an engineering perspective. Students get a better appreciation for why science is important in everyday life by interacting with a scientist/engineer and that engineer's presence makes the profession of engineering more tangible. They benefit from experiencing materials such as polymers thereby increasing their interest in new topics they had not heard of before. The results of the surveys show that students experience significant benefit from their resident engineer interactions both in attitude toward science and their understanding of new material, thereby hopefully causing them to become more interested in following STEM careers in their future.

A.9 Limitations

This case study was limited to a single classroom interaction. The scalability and sustainability of a program such as this is always in question. However, one goal of the

Symbi program is to assimilate these lessons in a database and disseminate the materials for others to use. The resident engineer is one of several graduate students in the Symbi program. In order to expand the model to an evidentiary basis, the program could look at rotating each resident engineer through different classrooms and collect data on each interaction to observe the effects on multiple classrooms and age groups. Furthermore, the program should look into providing teachers materials to facilitate the demonstrations on their own and evaluate how students respond to material with and without the resident engineer.

It is well-known that teacher knowledge influences student learning. While it might not be feasible to have a resident engineer in every classroom for the long term future, utilizing the materials developed by the resident can provide a foundation for teachers to draw from when looking to introduce engineering concepts in to their classroom. Although the classroom would no longer benefit from the resident scientist as a mentor to the classroom for which students obtain a better appreciation for the profession, it is the authors' feeling that when a teacher is confident in offering the engineering concepts to the classroom, the classroom as a whole can gain substantial academic improvements and individual interest in the classroom. The resident engineer's work provides the support for the teacher to confidently present the material to the classroom in a way that emphasizes engineering concepts.

A.10 References

[1] N. Tran, and M. Nathan. *Pre-College Engineering Studies: An Investigation of the Relationship between Pre-College Engineering Studies and Student Achievement in Science and Mathematics.* Journal of Engineering Education. 2010. 143-157.

[2] Business Roundtable. *Tapping America's Potential: The Education for Innovation Initiative.* Washington DC. Business Roundtable. 2005.

[3] U.S. Department of Education. Institute of Education Sciences, National Center for Education Statistics. Nation's report card 2009.

[4] U.S. Department of Education, Institute of Education Sciences, National Center for Education Statistics, National Assessment of Educational Progress (NAEP), 2009 Science Assessment.

[5] U.S. Department of Education, Institute of Education Sciences, National Center for Education Statistics, State Education Data Profiles, 2009-2010.

[6] R. Bybee. *What is STEM Education?* Science. Vol. 329. 2010. 996.

[7] C. Rogers, M. Portsmore. *Bringing Engineering to Elementary School.* Journal of STEM Education. Vol 5. Iss. 3 and 4. P. 17-28. 2004.

[8] H. Kim. *Inquiry-Based Science and Technology Enrichment Program: Grean Earth Enhanced with Inquiry and Technology.* Journcal of Science Education Technology. 2011. 20:803-814.

[9] Talton, E. L., and Simpson, R. D. (1986). Relationships of attitude towards self, family, and school with attitude toward science among adolescents. Science Education 70: 365–374.

[10] George, R. 2000. Measuring change in students' attitudes toward science over time: An application of latent variable growth modeling. Journal of Science Education and Technology, 9: 213–225.

[11] Keeves, J. P. (1975). The home, the school, and achievement in mathematics and science. Science Education 59: 439–460.

[12] P. Cantrell, G. Pekcan, A. Itani, and N. Velasquez-Bryant. *The Effects of Engineering Modules on Student Learning in Middle School Science Classrooms.* Journal of Engineering Education. 2006. 301-309.

[13] Kemis, M. & Haen, K. (2011). Changes in attitudes toward science and science careers of eighth grade students. Ames, IA: Iowa State University, Research Institute for Studies in Education.

[14] G. Nicholls, H. Wolfe, M. Besterfield-Sacre, and L. Shuman. *Predicting STEM Degree Outcomes Based on Eighth Grade Data and Standard Test Scores.* Journal of Engineering Education. 2010. 209-222.

APPENDIX B: IOWA STATE UNIVERSITY SYMBI GK12 PROGRAM: A CASE STUDY OF THE MATERIALS SCIENCE ENGINEER'S APPROACH TOWARDS ADDRESSING COMPLEX SCIENTIFIC PROBLEMS IN THE 8TH GRADE CLASSROOM

B.1 Abstract

The Des Moines public school system has partnered with Iowa State University to develop innovative and engaging STEM (Science, Technology, Engineering and Math) activities for middle school students through NSF's GK12 program. Iowa State's GK12 program, Symbi, pairs a senior graduate student (i.e., GK12 Fellow) with a middle school science teacher and classroom for the duration of an academic year. These GK12 Fellows engage the students by providing inquiry-based learning experiences and authentic demonstrations, which bring relevance by relating the science curriculum to real world challenges. Each Fellow's research background provides a unique backdrop for enhancing the classroom curricula. Here we present a case study showcasing the activities and interactions of one Symbi GK12 Fellow in the classroom who uses alternative ways to approach the science curriculum by addressing complex problems through the lens of a materials science engineer. In this case study, the primary research focus of the author, a GK12 Fellow, is on materials science and engineering, specifically polymers, a field completely absent from middle school curricula. By providing hands on demonstrations and

reliable scientific expertise, 8th grade students have the opportunity to experience science not as a collection if discreet units unrelated to each other but instead focus on how science and scientific thought is woven into everything around us. As a result, students expressed their enthusiasm and interest in the exciting concepts being brought to the classroom by the GK12 Fellow. These results suggest that middle school students benefit from taking an integrated approach to science using materials science engineering as the scaffolding for its implementation.

B.2 Introduction

"I want to persuade you to spend time in the classroom, talking and showing young people what it is that your work can mean, and what it means to you […] to thinking about new creative ways to engage young people in science and engineering," – words from President Obama at the National Academy of Sciences on the 27th of April 2009 as he urged the scientific community to find ways to cultivate the next generation of scientists and engineers. A task that provides some hurdles considering these words came in the wake of growing concern for the lack of students pursuing degrees and careers in STEM (Science, Technology, Engineering and Math) related fields. According to the National Center for Educational Statistics, students who perform at or above the proficiency level in 8th grade science is fewer than 1 out of 3 students [1]. The national report card identified students from low income and underrepresented minority families as scoring significantly lower than the national average [2]. Furthermore, the public school students performed well below private and Catholic schools, especially in the inner city public school setting [4]. These scores

demonstrate that K12 public science education in the United States is critically in need of new instructional approaches that provide students opportunities to think like scientists and engineers. Additionally, the United States has an undersized pool of engineers to meet the needs of our society and economy [3]. If current trends do not change, the demand for engineers will surpass the supply of engineers in the US [4].

To address the student STEM literacy and preparation for STEM careers, the National Science Foundation (NSF) funds the Graduate Stem Fellows in K-12 Education Program (GK-12). To help address these issues and those raised by the President, Iowa State University has partnered with the Des Moines Public Schools by incorporating STEM Ph.D. candidates as resident scientists/engineers in middle school classrooms with the goal of fostering students' interest in science and engineering. NSF funds several GK-12 programs at national universities. At each university specific and unique goals are developed and Iowa State University's GK-12 program, Symbi, is to increase K12 students' scientific literacy: that is, to increase student understanding of the relevance of STEM to real world challenges and to help them be more aware of STEM careers. The program's name Symbi was chosen for the symbiotic relationship between the fellows and the middle school students.

The lead author of this article is a Symbi GK12 Fellow and "resident engineer" who is majoring in materials science and engineering and conducting research on polymers. The resident engineer was paired with a middle school science teacher in the Des Moines Public School District, and spent one full day each week, for one academic year, in the science classroom. The resident engineer was able to provide a unique classroom experience by periodically introducing the students to aspects of his own research, including the use of biopolymers in material self-healing applications. Several activities were designed to provide

students with the opportunity to learn about the field of polymer science. These activities were related to and ultimately aligned with the science topics covered in the curriculum and provided relevance to real world issues and challenges. This study focused on the impact this fellow has had as a resident engineer on the students in his classroom.

B.3 Research questions

In this case study, researchers were interested in the effects of a resident engineer on eighth grade students' enthusiasm and interest in science topics both in and out of the classroom. Specifically, this study asks whether the resident engineer improved the interest of students in science and engineering such that students recognized scientific ideas outside of the classroom and became more inquisitive in science class. The current study was guided by two basic research questions:

1. Do the classroom activities, demonstrations, and experiments provided by the resident engineer positively affect the attitudes of students toward science and engineering, both in and outside the classroom?
2. Do students find the concepts of science to be more integrated and applicable to real life?

B.4 Research design

This case study focused on the demonstrations brought to the eighth grade classroom by the resident engineer during the first semester of the 2012-2013 school year. These

experiments, demonstrations, and discussions were designed with the effort to engage science in a way that broadens students' understanding of science not only in that specific field but also in other related fields — showing how scientific concepts flow through all facets of life. A sample of the classroom demonstrations were as follows:

1. **Introduction to Materials** — The resident engineer introduced himself to the students with a sampling of scientific demonstrations revolving around Materials Science and specifically polymers, his field of study. These demonstrations involved, shape memory alloys, electromagnetism with magnet and copper pipe, and glass transition in polymers. Each demonstration was related back to real life applications such as dental braces, electric generators, and polymers such as tires, toys, and packaging respectively. The shape memory alloy was bent into a unique shape and a discussion about why metals bend followed. Then, the metal was placed in a pot of boiling water only to have the metal revert back to its original shape. Discussion about the reason and the benefits of its use in daily life took place.

   For electromagnetism, neodymium magnets were simultaneously dropped down PVC and copper piping. Students were then asked to "discover" the reason why the magnet falls slower down the copper pipe by working through the differences between the metal and the plastic piping. Further discussion lead to how free moving electrons and magnets can be utilized with the information gleaned from the demonstration to develop the idea of an electric generator. Finally two rubber balls with different glass transition temperatures were presented to the class. At room temperature one bounces and one does not. Then each rubber ball is cooled and

heated and then change in bounce (both height and sound) was observed. The data collected were discussed in how a polymer transitions from glass to rubbery through the glass transition temperature. The glass transition in polymers was the primary focus, as it presented an important part of the resident engineer's research.

2. **Friction of Fluids** — In the forces and motion unit, a majority of science classes teach friction as a resistive force between two objects usually two solids. In class, the resident engineer worked to expand the students' understanding of friction in fluids by experimenting with the viscosity of corn syrup, water, and combinations. Students dropped marbles down graduated cylinders filled with a given fluid. They then measured the amount of time it took the marble to reach the bottom of the cylinder. Additionally, another demonstration of viscosity with corn syrup and food coloring was used to show that mixing in extremely viscous materials can be difficult. The demonstration used the understanding of laminar flow to "spread" corn syrup and in one direction "mixing" it. Then reversing the direction, the corn syrup and food coloring is "unmixed" back to its original state [5]. Discussion was then developed around making plastic materials and how important viscosity can be for filling molds and other challenges viscosity might bring.
3. **Minute to Win It** — To demonstrate that forces and motion are all around us, the use of simple games from the television show "Minute to Win It" were utilized to provide students a fun hands-on demonstration of forces and motion. Students worked in small groups and rotated through stations where a single minute to win it game was sitting. In order to play the game, the students needed to identify three forces and motion vocabulary words and definitions that directly related to the solution before

completing the game challenge. Students were then allowed to participate in the game for a minute in an attempt to complete the challenge as a reward for utilizing their vocabulary words. In the remaining moments, a brief discussion ensued about how forces and motion concepts are so commonplace that people often do not even think about their use in everyday life.

4. **Car Accident Detective** — At the culmination of the forces and motion unit, student were asked to assume the role of private investigator in a simulated car accident. Students were given a packet of documents that provided the information they would need to solve the "who-done-it" aspect of the accident. Students were asked to use critical thinking skills in conjunction with their understanding of forces and motion to determine who was at fault and write a one-page paper outlining the evidence and rational for who was at fault in the accident. The documents students were given provided them with eyewitness accounts, accident reports, accident schematics, tire tracks, weather reports, vehicle information, and stopping distances for cars with certain tires.
5. **Exploring Energy Consumption** — During the energy unit, students were introduced to many types of energy as well as the transfer of energy from one type to another. To further explain the concepts of conservation of energy through energy transfer, students were given a giant box full of packing peanuts (their energy). Students were then given the task to quickly pass the packing peanuts from one person to another down a chain. Any peanuts that fell to the floor were required to stay on the floor — those represented energy lost to the environment. Later, students counted up the packing peanuts that made it down the chain — those represented

successful energy transfer. Students associated the notion of the conservation of energy by seeing that all the packing peanuts could be accounted for. Additionally, kilowatt meters were brought into the classroom and several appliances were measured to see how much energy was consumed by different objects such as hair dryers, microwaves, lights, power drills, and pencil sharpeners. A discussion was then led on energy use and utilization.

In order to evaluate the effect of the resident engineer in the classroom, focus group interviews were conducted with small groups of 8th grade students. The purpose of these focus groups was to assess the students' attitudes towards science and engineering, both inside and outside the classroom. Two separate focus groups were conducted with students and each lasted approximately 45 minutes. The focus groups consisted of a total of seven students, one female and 6 male. A third party moderator facilitated the focus groups in order to remove as much partiality and bias as possible. Students were made aware the focus group was voluntary and no repercussions would happen for any type of answer or for choosing not to participate in the focus group. The moderator followed a structured interview process by asking a series of questions and allowed the participants to respond at will with their thoughts and comments pertaining to the questions.

B.5 Classroom demographics and context

The resident engineer was paired with the eighth grade science class at a middle school in Des Moines, IA. The middle school has a total of 594 students, of which 190 were

in the eighth grade science classroom that interacted with the resident engineer. The resident engineer joins the science classroom once a week on Fridays and brings in demonstrations, experiments, or other interesting science concepts for the students. The material presented and concept brought by the resident engineer is often associated to the curriculum and yet unique from the course itself. There are six class periods of science all lasting 42 minutes long.

The student population of the middle school is 38% underrepresented minority families and 68.2% of all students qualify for the free or reduced lunch program. According to the Iowa Department of Education, those eligible for free or reduced lunch at the chosen middle school mirror the district in eligibility at 69.6% in the 2011-2012 school year [6]. However, these numbers are higher than the state and national average of 39% and 45% respectively [6,7]. These demographics are somewhat lower than the national average of 56% underrepresented minority families from the 2009-2010 National Center for Education Statistics (NCES) data [7].

B.6 Results

For each demonstration listed above, the students were extremely engaged and interested in the experiments and demonstrations. In fact, once the class was introduced to the notion of a resident scientist to the classroom, they are quite eager for what is happening Friday, constantly asking, “What are we doing Friday,” or “I wish it was Friday for cool science.” Over the semester, the resident engineer saw a tangible difference in the students and their interest in science. As the semester progressed, students began bringing questions

into the classroom that they encountered about science at home. Even recently, students are starting to question things they hear in the news about science. In fact, after the energy transfer unit and talking about mechanical power, a student asked about coming up with a way of developing energy through the use of water in rivers while trying to think outside of the box. Often students make comments such as, “I wish you were here every day,” or “I use to think science was boring but you really show how cool it is.”

During the focus groups, students were asked several questions about their thoughts and experiences in science class. In the analysis of the interview transcripts several themes and findings clearly emerged related to the research questions. Students’ responses and comments focused on:

1. How much fun science class is when the resident engineer comes into the classroom.
2. How the resident engineer gives them a way to grasp the topics by not only providing definitions but also demonstrating the concepts in a tangible understanding way.
3. How they repeatedly highlight and remark about the demonstrations used in the classroom by the resident engineer.
4. How they are expressing an increased awareness of science outside of the classroom.

First, the students were asked about their thoughts and interest in the science classroom. Students were asked to expound on the similarities and differences in science, especially when the resident engineer comes to the classroom.

MODERATOR: *What makes learning science different than learning in other subjects?*

STUDENT 1: More things about science like it goes more in-depth about everything.
STUDENT 2: You can have more fun in science than any other subject.
STUDENT 3: Yeah, time flies by really fast.

MODERATOR: *Tell me, what makes science more fun than any of the other subjects?*
STUDENT 1: You are not just sitting there the whole time like in math or reading, we actually get up and do things.
STUDENT 2: You don't just sit there and not do anything. Science on Fridays you can get up to do cool things.

MODERATOR: *Do you get up and do science on Monday through Thursday?*
All STUDENTS: Sometimes.
STUDENT 4: But not necessarily and not like Friday.

MODERATOR: *But in general, you guys enjoy learning about science?*
All STUDENTS: Yeah.
STUDENT 5: I think that it is my favorite subject … because we learn a lot more cool stuff in that class than any other.

In connection with these questions about "why do you like science" and "how is science different when the resident scientist comes", many students focused on the way information was presented to them. Often, they felt the average class day they were given many definitions and had difficulty grasping the information whereas the resident engineer was able to present the information in a way that provided a demonstration or diagram that allowed the students to visualize and better understand the material. This can be seen in the following focus group responses:

MODERATOR: *If you were going to walk into a science classroom, what are the things you would expect the teacher to be doing?*

STUDENT 7: Explaining to us a lot of things we don't understand.

MODERATOR: *So, what kind of things do you do when [the resident engineer] comes that help you understand?*

STUDENT 7: Well, [the resident engineer] has a lot of hands-on projects that we do. Experiments. And lately we have been doing a lot of labs too.

MODERATOR: *What makes science interesting to you?*

STUDENT 4: Well [the resident engineer], well sometime he makes it interesting with experiments. It was fun … and he helps put you into groups so you learn what you don't learn.

STUDENT 1: [the resident engineer] makes it easier to learn.

STUDENT 3: [the resident engineer] makes it fun and like you get to experiment with all these different things.

STUDENT 5: I learn a lot!

MODERATOR: *[Student 1] talk to me a little more about what you said.*

STUDENT 1: Well, like he makes it easier for us to understand. Like last year, and the year before I did not understand science and now it is way easier and I get straight As.

MODERATOR: *When you think about [the resident engineer] and [the teacher] working together, what stands out?*

STUDENT 5: But sometimes [the teacher] explains it in a way I don't understand and [the resident engineer] speaks it in a way that I understand.

STUDENT 6: It is like English!

MODERATOR: *What does [the resident engineer] say and does he do?*

STUDENT 1: [the resident engineer] would draw a picture for us on the board and like explain it more.

STUDENT 3: [the resident engineer] will demonstrate it.

STUDENT 2: Yeah [the resident engineer] demonstrates it.

STUDENT 4: [the teacher] would give like the definition and everything but it's a little harder to understand. But [the resident engineer] would come in on Fridays and draw pictures and show us [examples].

STUDENT 3: For motion, [the teacher] was like momentum is …… and I did not even understand her. Then [the resident engineer] come in and okay momentum is …… And then he demonstrated it.

STUDENT 1: And it was easier to understand.

While being asked about how science class is unique on the days the resident engineer comes to the classroom, many students began excitedly sharing specific examples of what they really enjoyed learning and experimenting with in the classroom. This is readily evident in the focus groups seen here:

MODERATOR: *Tell me what makes science more fun than others?*

STUDENT 5: Like on Fridays, [the resident engineer] sets up crock pots and stuff around testing like we did to see how many watts each thing had like a curling iron, drill, fan, …

STUDENT 3: Yeah, and remember the experiment where we had to figure out the tire tracks?

STUDENT 1: Yeah, the car wreck that you had to figure out. That was fun.

MODERATOR: *Are there any other examples that you really remember?*

STUDENT 7: We just did a paper about finding the facts about a car crash. … And I remember the minute to win it games. I had a lot of fun with that.

MODERATOR: *And [the resident engineer] specific expertise like as an engineer and those kinds of things. Do you think you would get that otherwise if [the resident engineer] wasn't in the middle school classroom? Do you think topics like that would come up?*

STUDENT 7: Not really. A lot of times I talk to him about my questions. He comes around and asks us questions.

Finally, the focus group highlighted the way in which students are becoming more aware of the science around them, not only in the classroom but at home as well. Specifically, students were taking concepts they were learning about in school when the resident engineer was there and finding ways to apply it at home. This can be seen in the students' responses below:

MODERATOR: *Can you think of how do you use what you learn in school outside of school?*

STUDENT 7: Yeah, like um, my science fair project the energies [the resident engineer] talked to us about I could figure out voltage and everything I needed to make a light, light up.

MODERATOR: *So, science fair was done outside of school. Good. What about at home or anything?*

STUDENT 7: Yeah, we were talking about electrical and everything and thought about the electrical when the power went out.

MODERATOR: *Do you think having [the resident engineer] in the classroom makes you think about science more?*

STUDENT 7: Yeah, cause it give me more. [The teacher] knows a lot but having someone who really knows about stuff helps a lot.

MODERATOR: *How have you used the concepts you learned in science outside of school?*

STUDENT 3: Well, I was actually in the car and like saw a car crash and they said one of them was drunk and I probably could have told that by how the car had skid.

STUDENT 6: Since we have learned like the 7 types of energy, I have been going around and looking at how much different type of energy at home.

MODERATOR: *So, having [the resident engineer] in the classroom, would you say has helped you think about science?*

All STUDENTS: Yes. A lot.

B.7 Discussion

The focus of STEM in middle school classrooms is often limited to only science and mathematics [8]. However, the study of engineering is an excellent way to incorporate science, mathematical and technological principles into examples of real world phenomena [9]. Engineering provides the link between scientific understanding and application. Students are always interested in why they need to know the information and teachers are always struggling to present valid reasons for the applications. Hands-on activities provide problem solving, designing, testing, and enhancement which helps students in the middle school classroom integrate multiple subjects into one activity. For all demonstrations or experiments

presented in the classroom, time was given to apply the concepts to everyday life. Whether it was dental shape memory wire, making electrical generators, melting plastics, using electrical appliances, or "playing" detective in a crime scene accident, applying scientific topics to concrete technology and activities solidifies the concepts in students' minds. Students can strengthen their knowledge of the scientific concepts and the relevance to their lives by being introduced to engineering concepts at an early age, especially through hands-on activities [7,10].

Several students have expressed in class that they would be more interested in pursuing a career in science after their 8th grade experience because they can see how applicable science class can be on a daily basis. Most were not aware of how prevalent scientific technology is around them and the opportunities for careers in science. Often times middle school students find science uninteresting simply because they do not see a relevance to their live experiences [11]. By having an influential and encouraging teacher presenting the significance of science in their lives, a positive effect has been shown in students [12]. By providing engineering concepts student show an increased interest in science especially in the students generally disengaged in science and therefore focusing on a group of students often forgotten [8,13].

Despite materials and engineering being vital to our current society, few school curriculum plans provide students a chance to explore concepts about materials and engineering. This case study outlines an interactive way where students learn broader concepts and at times are directed specifically to materials science engineering where they can freely explore, question, and investigate. In fact, students were so interested in the

classroom activities that after almost every day the resident engineer was in the classroom, students remain behind to ask questions and share ideas.

The classroom specifically profited from a resident engineer by providing a fun and interactive environment where students learned through multiple learning styles. Furthermore, students were presented with activities that were engaging and at the end of the semester they were able to identify those activities. As a result, several students shared in the focus groups that they are thinking about science class. One student specifically shared a story of when he witnessed a car accident and one of his first thoughts was born out of the car accident detective activity—thinking he could determine how the accident happened.

Science becomes more fun when you can not only experiment and demonstrate concepts but when you can also correlate it to everyday life. By connecting to real world application, students became more engaged and felt science class was fun. These connections come through the demonstrations the students were recalling as well as the discussion during and after each class. When the resident engineer first came to the class, several students readily interjected "who cares" after tackling a scientific topic. Yet after a few weeks, students were more willing to listen because they could see how often these topics are used. For instance, a few students were quite interested in how a generator works when the temperature drops well below room temperature. Additionally, the resident scientist exhibits the tangible career opportunity in science. Students seem more interested in science careers after he was in the classroom. In fact, one student admitted in a focus group that 6th and 7th grade science had not made sense and he was failing. Now that the resident scientist has been in the classroom 8th grade science seems simpler and now this students is excelling in the class.

These types of responses are not unique for this classroom. Data collected from the first year of Symbi Fellows and collected by the university's Research Institute for Studies in Education shows a significant increase in 241 eighth grade students' perception of science after being introduced to a resident engineer or scientist. Eighth graders showed an increase in problem-solving and engineering concepts once they were introduced to them. Furthermore, the data showed a decrease in wanting the answer given to them by teachers. Coupling this with the increase in problem-solving, the data shows independence in seeking out the truth in science class. This can easily be seen in the car accident detective project when the students wanted to figure out and think through who was actually at fault in the accident.

B.8 Conclusions

The results of this study show that 1.) science can be fun and students will engage the topics, 2.) a resident engineer can provide additional explanation through demonstrations and illustrations that helps students learn better, and 3.) the resident engineer's effective classroom activities stay with students and effect their thoughts about science outside of the classroom — specifically thinking about science and questioning in general.

In middle school when the mind is developing, introducing engineering concepts and critical thinking benefits cognitive development by forcing the utilization of several disciplines simultaneously. As a result, not only science becomes a stronger topic for them but so do math, reasoning, and communication skills. In the acronym STEM, the E stands for engineering and yet few classrooms focus their curriculum on engineering aspects,

specifically by applying the classroom content to real world application. So, it is not surprising when students are presented with hands-on experiences, their interest significantly improves. From the focus groups alone, all the students confessed that when the resident engineer brought in activities, those activities caused the students to think more critically about science and the world around them not only in the classroom but also away from school. The disinterest from most students is not from animosity but simply out of a place of indifference when they see no relevance to the curriculum being taught to their own life. Once students were offered explanations for why science is so relevant, many students were eager to learn. By fostering this interest in students through showing how applicable science is to everyday life, students are three times more likely to pursue STEM careers if engaged in science early [14].

Having a resident engineer in the classroom provides eighth grade students a mentor who can design learning activities from an engineering perspective — offering not only the content but also an application for the students to connect. This results in a better appreciation for why their science class is so important for them and simultaneously, having an engineer offers a tangible figure to associate with the scientific career. The focus groups show that students are benefitting greatly from the resident engineer in the classroom. One of the most exciting results of this case study is the extracurricular scientific thought being developed in students. If scientific thought can be cultivated in a way where the middle school students are actively thinking about science without being prompted, then the next generation of scientific professionals has real potential.

B.9 Limitations

This case study was limited to a single resident engineer's experiences in the fall semester of one public middle school classroom. While the case study shows significant promise in encouraging scientific thought in eighth grade students, the scalability and sustainability of the program would be in question. However, Symbi is actively seeking ways in which to assimilate and disseminate these lesson plans for use by others. This would involve providing teachers the materials to confidently present these topics to students in ways that students will respond in similar fashion. Placing a resident engineer/scientist in the classroom is not always practical. And although the classroom would no longer benefit from the resident engineer/scientist as a mentor to the classroom for which students obtain a better appreciation for the profession, it is the authors' feeling that when a teacher is confident in offering the engineering concepts to the classroom, the classroom as a whole can gain substantial academic improvements and individual interest in the classroom. In this example, the resident engineer's work provided the support for the teacher to confidently present the material to the classroom in a way that emphasized engineering concepts.

B.10 References

[1] U.S. Department of Education. Institute of Education Sciences, National Center for Education Statistics. Nation's report card 2009.

[2] U.S. Department of Education, Institute of Education Sciences, National Center for Education Statistics, National Assessment of Educational Progress (NAEP), 2009 Science Assessment

[3] N. Tran, and M. Nathan. *Pre-College Engineering Studies: An Investigation of the Relationship between Pre-College Engineering Studies and Student Achievement in Science and Mathematics.* Journal of Engineering Education. 2010. 143-157.

[4] Business Roundtable. *Tapping America's Potential: The Education for Innovation Initiative.* Washington DC. Business Roundtable. 2005.

[5] Steve Spangler Science. *Twist in Time – Laminar Flow.* Retrieved from http://www.stevespanglerscience.com/science-video/twist-in-time 2013.

[6] Iowa Department of Education, Basic Educational Data Survey, Bureau of Information and Analysis Services, Fall 2011.

[7] U.S. Department of Education, Institute of Education Sciences, National Center for Education Statistics, State Education Data Profiles, 2009-2010.

[8] R. Bybee. *What is STEM Education?* Science. Vol. 329. 2010. 996.

[9] C. Rogers, M. Portsmore. *Bringing Engineering to Elementary School.* Journal of STEM Education. Vol 5. Iss. 3 and 4. P. 17-28. 2004.

[10] H. Kim. *Inquiry-Based Science and Technology Enrichment Program: Grean Earth Enhanced with Inquiry and Technology.* Journcal of Science Education Technology. 2011. 20:803-814.

[11] Talton, E. L., and Simpson, R. D. (1986). *Relationships of attitude towards self, family, and school with attitude toward science among adolescents*. Science Education 70: 365–374.

[12] Keeves, J. P. *The home, the school, and achievement in mathematics and science*. Science Education 1975. 59: 439–460.

[13] P. Cantrell, G. Pekcan, A. Itani, and N. Velasquez-Bryant. *The Effects of Engineering Modules on Student Learning in Middle School Science Classrooms.* Journal of Engineering Education. 2006. 301-309.

[14] G. Nicholls, H. Wolfe, M. Besterfield-Sacre, and L. Shuman. *Predicting STEM Degree Outcomes Based on Eighth Grade Data and Standard Test Scores.* Journal of Engineering Education. 2010. 209-222.